

THESIS

METHOD COMPARISON FOR ANALYSIS OF LNAPL NATURAL SOURCE ZONE
DEPLETION USING CO₂ FLUXES

Submitted by

Melissa Kay Tracy

Department of Civil and Environmental Engineering

In partial fulfillment of the requirements

For the Degree of Master of Science

Colorado State University

Fort Collins, Colorado

Spring 2015

Master's Committee:

Advisor: Tom Sale

Jens Blotevogel

Greg Butters

Copyright by Melissa Kay Tracy 2015

All Rights Reserved

ABSTRACT

METHOD COMPARISON FOR ANALYSIS OF LNAPL NATURAL SOURCE ZONE DEPLETION USING CO₂ FLUXES

Accidental releases of subsurface petroleum hydrocarbons, widely referred to as Light Non-Aqueous Phase Liquids (LNAPLs), are a common occurrence in the industrial world. Given potential risks to human health and the environment, effective remediation approaches are needed to address impacts. Natural source zone depletion (NSZD) is a remedial approach gaining wide acceptance, wherein natural mechanisms in the subsurface act to deplete LNAPL in the source zone. Recent research indicates biodegradation of contaminant-related carbon results in a predominantly upward flux of carbon through the vadose zone. Building on this concept, three methods have recently emerged to quantify rates of NSZD using soil gas fluxes; these include the gradient, chamber, and trap methods. Unfortunately, side-by-side field applications of the methods have shown differing estimates of NSZD, leaving concerns about method comparability.

The primary objective of this thesis was to conduct a laboratory comparison of the gradient, chamber, and trap methods using uniform porous media, constant environmental conditions, and a known CO₂ flux (i.e., ideal conditions). Given these experimental conditions, challenges associated with field comparisons could be minimized and the fundamental accuracy of the methods could be resolved. Preliminary efforts were also made to understand the effect of surface wind on the accuracy of the methods.

A large-scale column (1.52 m high x 0.67 m ID) was filled with dry, homogenous, well-sorted fine sand. Known CO₂ fluxes were imposed through the bottom of the column spanning a range typical of contaminant-related CO₂ fluxes observed at field sites (3.3-15.2 μmol/m²/s). Results under ideal experimental conditions indicated that on average, the chamber and trap methods accurately captured the imposed flux to within ± 7% of the true value, and the gradient method underestimated the imposed flux to within 38% of the true value. Accuracy of the gradient method was largely dependent on estimates of effective diffusion coefficients. Consistent underestimation of the true flux using the gradient method was attributed to the method only quantifying diffusive gas transport. Considering the accuracy of measurements for other subsurface processes (e.g., hydraulic conductivity), the range of accuracy observed among all methods is not surprising.

Surface winds were simulated by placing a fan on top of the column; achieved wind speeds ranged from 2.2-5.4 m/s. Laboratory studies identified that all methods were adversely affected by wind; however, the magnitude of laboratory results may have been exaggerated relative to what would be expected at field sites due to the laboratory sand being dry. Wind speeds within the tested range caused the gradient method to further underestimate the true flux to within 44% of the true value. The chamber method underestimated the true flux by 45-47% and 78% for wind speeds ranging from 2.2-3.6 m/s and 4.5-5.4 m/s, respectively. Wind had the opposite effect on the trap method, causing overestimations of the true flux by 60% and 122% for wind speeds ranging from 2.2-3.6 m/s and 4.5-5.4 m/s, respectively.

Given similar results under ideal experimental conditions, wind and other environmental factors common to field conditions are suspected to be the primary cause of disagreement observed in side-by-side comparisons of the methods at field sites. Each method has advantages and limitations for field application. Method selection should be predominately driven by site-specific attributes, including environmental factors that may make one method more applicable over another for a given field site. Further consideration of all methods under environmental conditions may provide greater insight into potential biases and support additional recommendations for method selection.

Secondary objectives included efforts to test design features specific to the trap method to support continued method development and to advance a model to describe steady-state advective and diffusive transport of a compressible gas through porous media. Results from trap modification studies suggested certain design features of the trap method may have affected the accuracy of measurements. Additional research and method development for the trap method could be undertaken to resolve issues raised in this thesis.

Results from modeling efforts suggested gas transport was primarily diffusion driven, accounting for approximately 58-79% of transport, depending on estimates of the effective diffusion coefficient. Analytical modeling did not indicate an appreciable difference in advective and diffusive contributions to gas transport as the imposed flux was varied; however, measured concentration gradients counterintuitively indicated the advective contribution to transport increased as the imposed flux decreased.

ACKNOWLEDGEMENTS

This thesis would not have been possible without the support and guidance of the following:

- Dr. Tom Sale for providing me with this great opportunity for personal and professional growth, for serving as my advisor, and for his support and patience through the many challenges this project faced over the last two years.
- Dr. Jens Blotevogel and Dr. Greg Butters for serving on my committee.
- Dr. Natasha Sihota and Dr. Uli Mayer at Chevron and the University of British Columbia, respectively, for their support with the LI-COR equipment.
- Dr. Dave McWhorter for his assistance with the analytical modeling.
- ERC Shop staff Junior Garza and Bart Rust for their help building a leak proof column.
- Dr. Ann Hess with the CSU Graybill Statistical Laboratory for her guidance with experimental design and statistical analysis.
- Mark Lyverse at Chevron for his continued support and knowledge.
- Ben McAlexander at TriHydro for providing literature and insight into field comparisons.
- Tom Palaia at CH2M Hill for sharing field data and insight.
- Gary Dick, Hannah Smith, Wes Tulli, Kevin Saller, Christina Ankrom, and Nolan Platt for laboratory support.
- The 2013-2015 CCH “Graduate Crew” for providing comic relief and much needed study/research breaks. I wouldn’t have made it without you all.
- My family for their continued support and encouragement throughout this long journey.

Funding for this work was provided by:

- Chevron

TABLE OF CONTENTS

ABSTRACT.....	ii
ACKNOWLEDGEMENTS.....	v
TABLE OF CONTENTS.....	vi
LIST OF TABLES.....	ix
LIST OF FIGURES.....	xi
1. INTRODUCTION.....	1
1.1 Natural Source Zone Depletion of LNAPL.....	1
1.2 Objectives.....	3
1.3 Organization and Content.....	3
2. LITERATURE REVIEW.....	4
2.1 Significance of NSZD.....	4
2.2 LNAPL Conceptual Site Model.....	5
2.3 NSZD Loss Mechanisms.....	7
2.3.1 Overview and Phase Partitioning.....	7
2.3.2 Saturated Zone Biodegradation.....	10
2.3.3 Vadose Zone Biodegradation.....	12
2.4 Environmental Factors Affecting Mechanisms and Measurement of NSZD.....	14
2.4.1 Wind.....	15
2.4.2 Temperature.....	16
2.4.3 Moisture.....	17
2.4.4 Barometric Pumping.....	18
2.4.5 Artificial Surfaces and Low Permeability Lenses.....	18
2.5 Quantification of NSZD Using Soil Gas Fluxes.....	19
2.5.1 Gradient Method.....	20
2.5.2 Chamber Method.....	25
2.5.3 Trap Method.....	29
2.6 Method Comparisons to Date.....	33
3. EXPERIMENTAL METHODS.....	34
3.1 Method Comparison under Ideal Conditions.....	34
3.1.1 Large-Scale Column Setup and CO ₂ Delivery System.....	34
3.1.2 CO ₂ Measurement Methods.....	37
3.1.2.1 Gradient Method.....	37
3.1.2.2 Chamber Method.....	39
3.1.3.3 Trap Method.....	40
3.2 Method Comparison under Simulated Windy Conditions.....	42
3.3 Trap Modification Studies.....	45
3.3.1 Mass of Absorbent in Bottom Element.....	45
3.3.2 CO ₂ Breakthrough to Top Absorbent Element.....	47
3.3.3 Height of Bottom Absorption Element above Soil Surface.....	48

4. MODELING	50
4.1 Model Derivation	50
4.2 Diffusive and Advective Contributions to Transport.....	54
5. RESULTS AND DISCUSSION.....	57
5.1 Methods Comparisons under Ideal Conditions	57
5.1.1 Gradient Method	58
5.1.2 Chamber Method	61
5.1.3 Trap Method.....	64
5.1.4 Method Comparisons	66
5.2 Methods Comparisons under Simulated Windy Conditions	68
5.2.1 Gradient Method	69
5.2.2 Chamber Method	71
5.2.3 Trap Method.....	74
5.3 Trap Modification Studies.....	76
5.3.1 Mass of Absorbent in Bottom Element.....	76
5.3.2 CO ₂ Breakthrough to Top Absorbent Element	77
5.3.3 Height of Bottom Absorption Element above Soil Surface.....	78
5.4 Modeling	80
5.4.1 Model versus Experimental Data.....	80
5.4.1.1 Model versus Experimental Data under Ideal Conditions	81
5.4.1.2 Model versus Experimental Data under Windy Conditions	84
5.4.2 Diffusive and Advective Contributions to Transport.....	86
5.4.2.1 Diffusive and Advective Contributions to Transport under Ideal Conditions	86
5.4.2.2 Diffusive and Advective Contributions to Transport under Windy Conditions ...	88
5.5 Summary of Results	90
6. CONCLUSIONS.....	93
6.1 Main Objectives and Primary Conclusions	93
6.2 Detailed Results.....	94
6.2.1 Laboratory Method Comparisons under Ideal Conditions.....	94
6.2.2 Laboratory Method Comparisons under Windy Conditions.....	95
6.2.3 Trap Modification Studies	96
6.2.4 Modeling	96
6.3 Recommendations for Method Selection	97
6.4 Recommendations for Future Work.....	97
6.4.1 Subsurface Pressure Gradients.....	98
6.4.2 Effects of Environmental Factors on Methods	98
6.4.3 Further Trap Development.....	98
6.4.4 Modeling of Chamber and Trap Methods.....	99
6.4.5 Thermal Fluxes as an Indicator of NSZD	99
7. REFERENCES	100

8. APPENDIX A: COLUMN DESIGN DATA.....	105
8.1 Grain Size Distribution of Column Fill.....	105
8.2 Moisture Content of Fine Sand	105
8.3 Porosity of Column Fill Material	106
8.4 Ambient Pressure in Hydraulics Laboratory.....	106
9. APPENDIX B: EXPERIMENTAL DATA FROM METHODS COMPARISONS	107
9.1 Summary of Imposed Fluxes	107
9.2 Summary of Gradient Data	110
9.2.1 In-Situ Effective Diffusion Coefficient Data.....	115
9.2.3 Gas Chromatography Calibration Curves	116
9.2.4 Integrity of Gas Sampling Syringes	117
9.3 Summary of Chamber Method Data	119
9.4 Summary of Trap Method Data	120
9.4.1 Chemistry of Gravimetric Acid Analysis	122
10. APPENDIX C: EXPERIMENTAL DATA FROM TRAP MODIFICATION STUDIES...	123
11. APPENDIX D: SAMPLE CALCULATIONS	124
11.1 Porosity and Moisture Content of Fill Material	124
11.2 Open System Imposed Flux Calculation.....	125
11.3 Percent CO ₂ to CO ₂ Flux (Gradient Analysis).....	126
11.4 Mass CO ₂ to Efflux CO ₂ (Trap Analysis)	127
12. APPENDIX E: STATISTICS.....	129
12.1 Confidence Intervals for Individual Methods vs Ideal Line (1:1).....	129
12.2 Method Comparison ANOVA Results.....	130

LIST OF TABLES

Table 1. Data needed for gradient method.....	21
Table 2. Summary of gradient method characteristics.....	24
Table 3. Summary of chamber method characteristics.....	28
Table 4. Summary of trap method characteristics	32
Table 5. Mass transport definitions for average velocity term of a multicomponent gas.....	51
Table 6. Summary statistics for gradient method under ideal conditions.....	59
Table 7. Summary statistics for chamber method under ideal conditions.....	62
Table 8. Summary statistics for trap method under ideal conditions.....	65
Table 9. Summary statistics for gradient method under windy conditions.....	69
Table 10. Summary statistics for chamber method under windy conditions.....	72
Table 11. Summary of trap method under windy conditions.....	74
Table 12. Potential CO ₂ breakthrough to top absorbent element.....	77
Table 13. Effective diffusion coefficients for air.....	81
Table 14. Diffusive and advective contributions to transport under ideal conditions using the Millington model to determine the effective diffusion coefficient for CO ₂	87
Table 15. Diffusive and advective contributions to transport under ideal conditions using the In-situ method to determine the effective diffusion coefficient for CO ₂	87
Table 16. Diffusive and advective contributions to transport under windy conditions using the Millington model to determine effective diffusion coefficient for CO ₂	88
Table 17. Diffusive and advective contributions to transport under windy conditions using the In-situ model to determine effective diffusion coefficient for CO ₂	89
Table 18. Relative merits of methods.....	91

Table 19. Moisture content of fine sand fill material.....	105
Table 20. Porosity test data for base gravel and fine sand fill material.	106
Table 21. Change in mass of CO ₂ cylinder for imposed test fluxes.	107
Table 22. Summary of imposed test fluxes.....	108
Table 23. Summary of soil gas sample data used with gradient method.	110
Table 24. Summary of triplicate results for gradient method.	114
Table 25. In-situ effective diffusion data.	115
Table 26. Data from LI-8100-104 Long-Term Survey Chamber.	119
Table 27. Data collection settings for LI-8100-104 Long-Term Survey Chamber.	119
Table 28. Results of gravimetric analysis for trap method	120
Table 29. Confidence intervals (CI) for individual methods based on best fit linear regression of average values.	129
Table 30. P-values for pairwise comparison of slopes between individual methods	130

LIST OF FIGURES

Figure 1. Conceptual evolution of an LNAPL release.....	5
Figure 2. Conceptual site model for a middle to late stage site	6
Figure 3. Conceptual model for natural depletion mechanisms in middle to late stage source zones	10
Figure 4. Environmental factors affecting mechanisms and measurement of NSZD.....	15
Figure 5. Conceptualization of gradient method.....	20
Figure 6. Conceptualization of chamber method.....	25
Figure 7. Chamber method data reduction output	27
Figure 8. Conceptualization of trap method	30
Figure 9. Schematic of column setup.....	35
Figure 10. Top view schematic of column showing locations for chamber method and triplicate trap placement.....	41
Figure 11. Schematic of experimental setup to test all methods under windy conditions.....	43
Figure 12. Schematic of modified trap with increased absorbent in bottom absorption element.	46
Figure 13. Conceptualization of CO ₂ breakthrough in deployed traps versus background trap...	47
Figure 14. Schematic of varying headspace heights in trap method.....	49
Figure 15. Physical basis for model.....	51
Figure 16. Triplicate results for gradient method under ideal conditions.....	58
Figure 17. Results from chamber method under ideal conditions	61
Figure 18. Triplicate results for trap method under ideal conditions.....	64
Figure 19. Comparison of average measured flux from all methods under ideal conditions	66

Figure 20. Average percent difference from imposed flux for each method under ideal conditions.....	67
Figure 21. Results from gradient method under windy conditions.....	69
Figure 22. Results from chamber method under windy conditions.....	71
Figure 23. Results from trap method under windy conditions.....	74
Figure 24. Triplicate results for mass of absorbent material in bottom trap element versus measured efflux.....	76
Figure 25. Height of bottom absorbent element from soil surface versus measured efflux	78
Figure 26. Experimental data versus model for imposed flux of $15.1 \pm 0.4 \mu\text{mol}/\text{m}^2/\text{s}$ under ideal conditions.....	82
Figure 27. Experimental data versus model for imposed flux of $10.7 \pm 0.2 \mu\text{mol}/\text{m}^2/\text{s}$ under ideal conditions.....	82
Figure 28. Experimental data versus model for imposed flux of $7.9 \pm 0.2 \mu\text{mol}/\text{m}^2/\text{s}$ under ideal conditions.....	83
Figure 29. Experimental data versus model for imposed flux of $3.3 \pm 0.1 \mu\text{mol}/\text{m}^2/\text{s}$ under ideal conditions.....	83
Figure 30. Experimental data versus model for imposed flux $8.7 \pm 0.2 \mu\text{mol}/\text{m}^2/\text{s}$ under no wind, base case conditions.....	84
Figure 31. Experimental data versus model for imposed flux $8.6 \pm 0.2 \mu\text{mol}/\text{m}^2/\text{s}$ under low wind conditions.....	85
Figure 32. Experimental data versus model for imposed flux $8.5 \pm 0.2 \mu\text{mol}/\text{m}^2/\text{s}$ under high wind conditions.....	85
Figure 33. Grain size distribution for base gravel and fine sand fill.....	105

Figure 34. Outdoor air pressure versus indoor air pressure in the laboratory testing facility.....	106
Figure 35, GC-TCD calibration curve for test #1, imposed flux $15.1 \mu\text{mol}/\text{m}^2/\text{s}$	116
Figure 36. GC-TCD calibration curve for test #2, imposed flux $10.7 \mu\text{mol}/\text{m}^2/\text{s}$	116
Figure 37. GC-TCD calibration curve for test #3, imposed flux $7.9 \mu\text{mol}/\text{m}^2/\text{s}$	116
Figure 38. GC-TCD calibration curve for test #4, imposed flux $3.3 \mu\text{mol}/\text{m}^2/\text{s}$	116
Figure 39. GC-TCD calibration curve for imposed wind tests.	117
Figure 40. GC-TCD calibration curve for CH_4 used with In-situ effective diffusion test	117
Figure 41. Results from syringe integrity test.....	118

1. INTRODUCTION

1.1 Natural Source Zone Depletion of LNAPL

Subsurface releases of petroleum hydrocarbon are a common occurrence in the industrial world. Petroleum liquids are composed of complex mixtures of organic compounds that are typically less dense than and immiscible with water and are widely referred to as Light Non-Aqueous Phase Liquids (LNAPLs). Where exposure scenarios exist, subsurface petroleum hydrocarbons can pose threats to human health and the environment. Given potential risks, effective remedies are needed to address LNAPL in source zones.

An LNAPL source zone is defined as soil, soil gas, and/or groundwater impacted by an LNAPL body (ITRC, 2009). Natural source zone depletion (NSZD) refers to natural mechanisms in the subsurface that act to deplete LNAPL in the source zone (ITRC, 2009). Critical natural loss mechanisms include biodegradation (aerobic and anaerobic), volatilization, and dissolution. Anaerobic biodegradation is often the most critical loss mechanism. Typically, anaerobic biodegradation involves common electron acceptors such as ferric iron, nitrate, sulfate, and manganese dioxide (Johnson et al., 2006). Given depletion of these electron acceptors, biodegradation can proceed via methanogenesis.

NSZD results in a predominantly vertical flux of contaminant-related carbon (Molins et al., 2010). Primary carbon products of biodegradation processes include carbon dioxide (CO₂) and methane (CH₄). Methane can be converted to CO₂ in the vadose zone by methanotrophic microorganisms, where oxygen is present, resulting in an upward flux of CO₂ that accounts for

both aerobic and anaerobic biodegradation processes. Consequently, soil gas fluxes through the vadose zone, particularly CO₂, can serve as a valuable tool for understanding LNAPL degradation processes and quantifying contaminant mass loss rates (Lahvis and Baehr, 1996; Lahvis et al., 1999; Chaplin et al., 2002; Lahvis et al., 2004; Amos et al., 2005; Lundegard and Johnson, 2006; Molins et al., 2010; Sihota et al., 2011; McCoy et al., 2014).

To date, three methods have been developed to quantify LNAPL loss rates based on soil gas fluxes. The concentration gradient method (gradient) uses vertical subsurface profiles of soil gas concentrations and estimates of effective diffusion coefficients to measure gas fluxes through the subsurface (Johnson et al., 2006; Lundegard and Johnson, 2006; ITRC, 2009). Consideration is given to inward fluxes of O₂ and/or outward fluxes of CO₂, CH₄, and volatile hydrocarbons. The dynamic closed chamber (chamber) (Sihota et al., 2011) and CO₂ Traps (trap) (McCoy et al., 2014) methods measure CO₂ efflux at grade.

All three methods are seeing widespread use at field sites. Unfortunately, side-by-side applications at field sites have shown differing estimates of NSZD (based on unpublished data at multiple field sites). Field comparisons are challenging due to subsurface heterogeneities, the inability to co-locate methods, time variant environmental factors and unknown true soil gas fluxes. Uncertainties among methods leave practitioners and regulators with choices regarding which method to employ. To date, no rigorous comparisons have been conducted that test all three methods against a known flux in a controlled environment.

1.2 Objectives

The primary objective of this thesis is to conduct a laboratory comparison of the gradient, chamber, and trap methods using uniform porous media, constant environmental conditions, and a known CO₂ flux (i.e., ideal conditions). This study provides absolute and relative performance comparisons of the methods, offering valuable insight into mechanisms that may be leading to inconsistencies with side-by-side comparisons of methods at field sites. Preliminary efforts are also made to understand the effect of surface wind on the performance of the measurement methods. The results of this study will provide a basis for resolving the relative merits of the three methods, support guidelines for appropriate method selection at field sites, and provide insights regarding further work that could be conducted to improve current methods for resolving rates of NSZD.

1.3 Organization and Content

Chapter 2 provides a discussion of background concepts relevant to the content of this thesis. This includes a conceptual model for governing processes and a review of the three methods for quantifying rates of NSZD using CO₂ fluxes. Chapter 3 summarizes laboratory experimental methods used to test each measurement method under ideal and simulated wind conditions. Experiments conducted to test specific design features of the trap method are also discussed. Chapter 4 includes modeling work relevant to the laboratory experiment. An analytical solution is presented that describes steady state vadose zone gas transport. Results and discussion from laboratory studies and modeling work are presented in Chapter 5, including a summary of the merits and limitations of all three methods. Lastly, conclusions and recommendations for additional work are presented in Chapter 6. Supplementary work is presented in appendices.

2. LITERATURE REVIEW

This chapter introduces a conceptual model for governing processes and a review of the three methods for quantifying rates of NSZD using gas fluxes. Section 2.1 introduces the significance of NSZD as a remedial action. A conceptual site model for the evolution of an LNAPL site is presented in Section 2.2. Contaminant loss mechanisms associated with NSZD are examined in Section 2.3. Section 2.4 explores environmental factors that can affect rates and measurement of NSZD. Section 2.5 discusses the quantification of NSZD using soil gas fluxes. Three methods used to quantify NSZD using CO₂ fluxes are presented. Finally, Section 2.6 presents previous method comparison efforts and identifies the need for additional studies.

2.1 Significance of NSZD

Losses due to NSZD are occurring at rates that rival active remedies (McCoy et al., 2014). Several studies have estimated natural losses due to NSZD on the order of hundreds of gallons to thousands of gallons of LNAPL/acre/year (Lundegard and Johnson, 2006; Sihota et al., 2011; McCoy et al., 2014). Losses in this range are significant because they demonstrate the ability of NSZD to act as a stand-alone remedial action if the risk of contaminant migration is low. NSZD can also be used as a benchmark for comparing the relative merits of more active remedies (Skinner, 2013). Furthermore, natural losses have been shown to control the stability of dissolved plumes (Wiedemeier et al., 1999) and LNAPL bodies (Mahler et al., 2012). NSZD holds several advantages over more active remedies, including having the capacity to inherently deal with subsurface heterogeneities and the ability to address residual LNAPL saturations active

remedial systems cannot recover (ITRC, 2009). NSZD may also prove to be a more sustainable remedial option given minimal site disturbance and potential for cost savings (US EPA, 1999).

2.2 LNAPL Conceptual Site Model

A source zone refers to the entire LNAPL body, either in a mobile or discontinuous state, which can act as a long-lived source of secondary impacts to adjacent soil and groundwater (ITRC, 2009). Characteristics of LNAPL distribution within a source zone are dependent on site age. Figure 1 illustrates a conceptual model for the evolution of an LNAPL source zone.

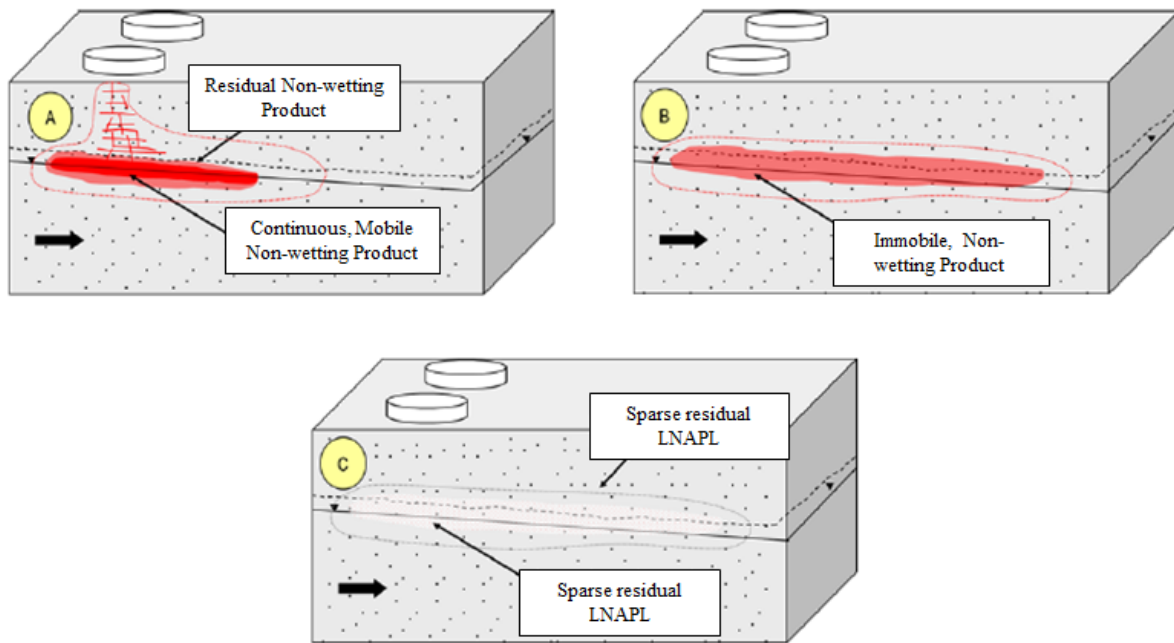


Figure 1. Conceptual evolution of an LNAPL release (following McCoy, 2012). A) Early stage. B) Middle stage. C) Late stage.

At an early stage site, during or immediately following a release, the source zone consists of a continuous, mobile body of non-wetting LNAPL that can expand and migrate. At middle stages, expansion is offset by natural losses and the LNAPL body becomes stable or shrinking.

Active recovery efforts are limited by the low relative permeability of the LNAPL, rendering it hydraulically immobile (Payne et al., 2008). At late stages, natural losses have removed the bulk of LNAPL and the remaining contaminant exists as sparse residual LNAPL.

Many existing LNAPL impacted sites are in the middle stage of site evolution. The relative abundance of middle stage sites compared to early stage sites is attributed to improved industrial practices, active depletion remedies, and ongoing NSZD. Figure 2 depicts a detailed conceptual site model for a middle stage site, highlighting key factors that pertain to this thesis.

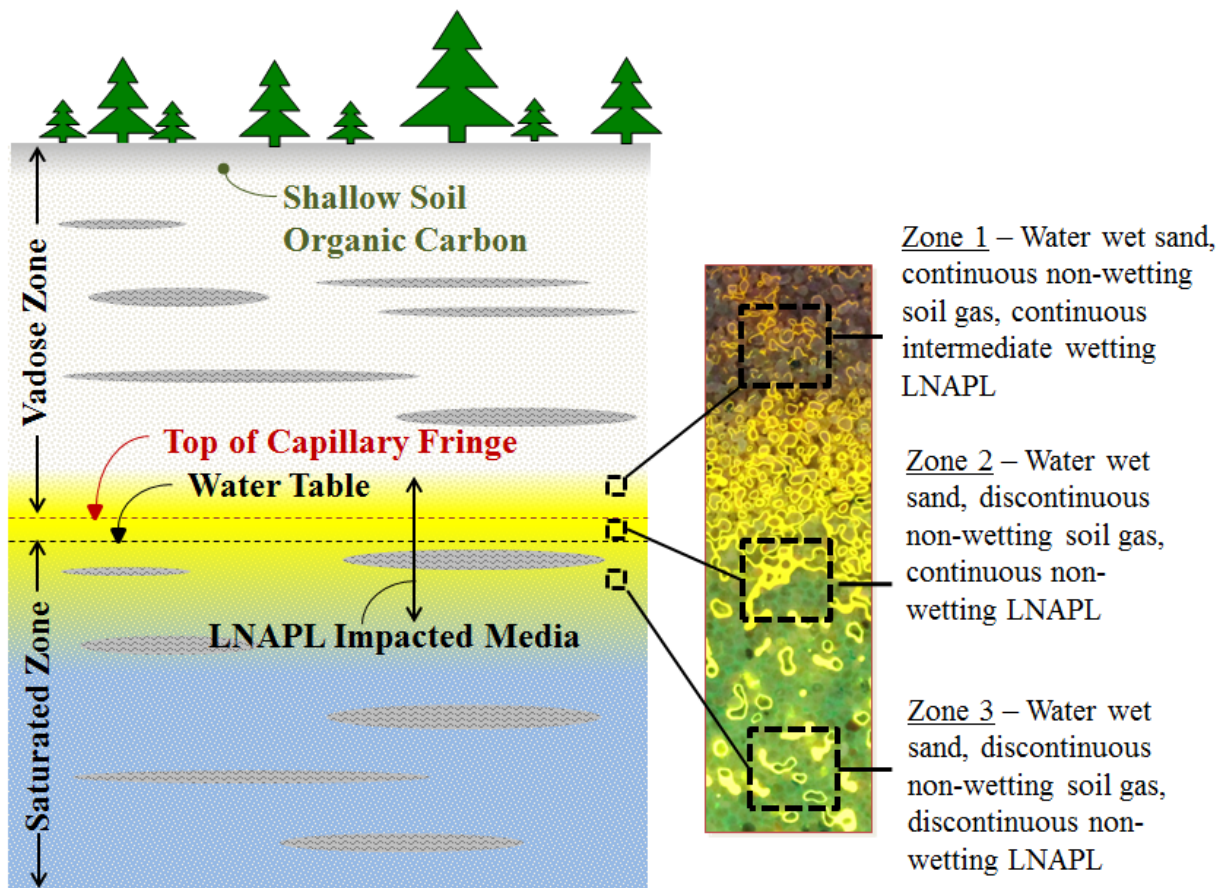


Figure 2. Conceptual site model for a middle to late stage site. LNAPL impacted media is depicted in yellow. Photographic image from Skinner, 2013.

As shown in Figure 2, LNAPL can exist in the source zone as a continuous intermediate wetting phase fluid above the capillary fringe (zone 1), as a continuous non-wetting phase fluid about the capillary fringe (zone 2), and as a discontinuous non-wetting phase fluid below the water table (zone 3). Also illustrated is shallow soil organic carbon that serves as an additional source of carbon (modern) above the source zone.

2.3 NSZD Loss Mechanisms

2.3.1 Overview and Phase Partitioning

NSZD is the result of processes that act to either physically redistribute (non-destructive mechanism) or biologically degrade (destructive mechanism) LNAPL components (Washington State Department of Ecology, 2005). Non-destructive mechanisms include dissolution to groundwater, volatilization to the vadose zone and sorption to matrix solids. Microbial mediated biodegradation is considered a destructive mechanism because contaminants are broken down and partially or completely mineralized into CH₄ or CO₂, respectively.

Contaminant mass within the source zone can exist in four phases; 1) LNAPL, 2) aqueous, 3) sorbed and 4) gas. Partitioning from LNAPL to aqueous, sorbed, and gas phases is dictated by mass transfer principles. Dissolution to the aqueous phase is controlled by the effective solubility (S_i^e) of the LNAPL constituent and the mole fraction of the constituent (X_i) in the LNAPL (ITRC, 2009),

$$S_i^e = X_i S_i \quad (1)$$

where S_i is the solubility of the constituent in its pure phase. The mole fractions of constituents in LNAPL change with time (Schwarzenbach et al., 2003). Initially, the more water-soluble constituents are preferentially dissolved. This leads to higher mole fractions of less-soluble constituents as the LNAPL ages. The dissolved concentration of an LNAPL constituent in water ($C_{i,w}$) is given by (Schwarzenbach et al., 2003):

$$C_{i,w} = \frac{C_{i \text{ mix}}}{K_{i \text{ mix},w}} \quad (2)$$

where $C_{i \text{ mix}}$ is the concentration of the constituent in the LNAPL mixture and $K_{i \text{ mix},w}$ is the LNAPL mixture-water partitioning coefficient.

The concentration of a sorbed constituent ($C_{i,s}$) is a function of the dissolved concentration ($C_{i,w}$) and the soil-water partitioning coefficient (K_d). The relationship between the sorbed and dissolved concentrations of a constituent at a constant temperature is referred to as an adsorption isotherm. Adsorption isotherms can be linear or non-linear. Commonly, a linear model is used to express sorbed phase concentrations (Schwarzenbach et al., 2003):

$$C_{i,s} = K_d C_{i,w} = K_{oc} f_{oc} C_{i,w} \quad (3)$$

where K_{oc} is the soil-organic carbon partitioning coefficient and f_{oc} is the organic carbon content of the soil.

Volatilization of LNAPL into hydrocarbon vapors is described using Raoult's Law,

$$p_i = X_i p_i^* \quad (4)$$

where p_i is the partial pressure of the LNAPL constituent and p_i^* is the partial pressure of the pure constituent. The concentration of hydrocarbon vapors ($C_{i,v}$) is given by (Schwarzenbach et al., 2003):

$$C_{i,v} = C_{i,mix} K_{i,v,mix} \quad (5)$$

where $C_{i,mix}$ is the concentration of the constituent in the LNAPL mixture and $K_{i,v,mix}$ is the vapor-LNAPL mixture partitioning coefficient.

It is generally assumed that biodegradation reactions occur within the aqueous phase; similarly, it is generally assumed that biodegradation of sorbed phase occurs when constituents repartition into the aqueous phase. Biodegradation of volatiles occurs when hydrocarbon vapors partition into pore water. This process is governed by Henry's law:

$$C_{i,w} = \frac{p_i}{K_{i,H}} \quad (6)$$

where $K_{i,H}$ is the dimensional Henry's law constant for the LNAPL constituent. Aqueous phase constituents are prone to aerobic and/or anaerobic biodegradation depending on electron acceptors available within the soil and water (ITRC, 2009). Biodegradation can sustain phase partitioning by reducing the aqueous phase concentrations, preventing equilibrium from being reached. Building on Amos et al. (2005) and Irianni-Renno (2013), Figure 3 summarizes

biodegradation processes. Processes within each of the four regions presented in Figure 3 are discussed in more detail in the following sections.

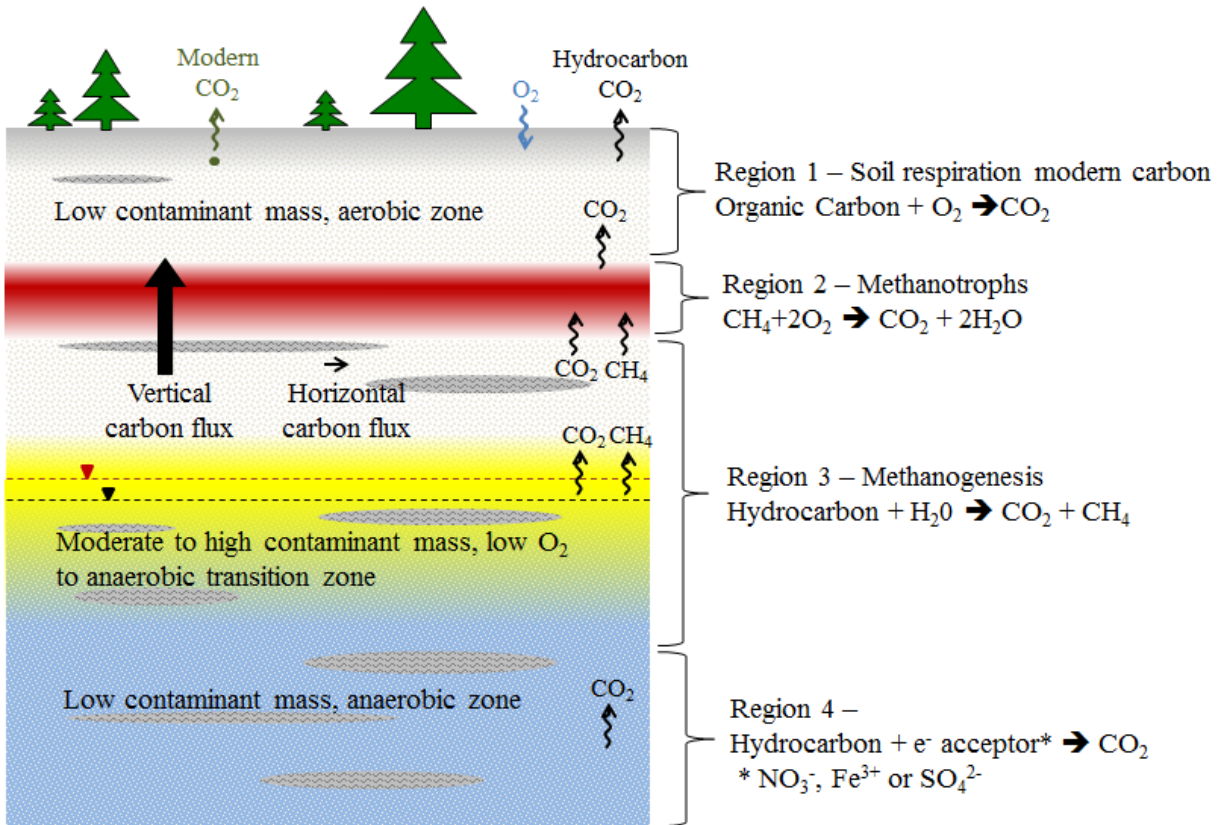
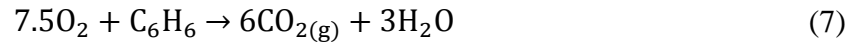


Figure 3. Conceptual model for natural depletion mechanisms in middle to late stage source zones (following Amos et al. (2005) and Irianni-Renno (2013)). LNAPL impacted media is depicted in yellow. The flux of contaminant-related carbon is predominantly in the vertical direction. General reactions for each region are listed on the right.

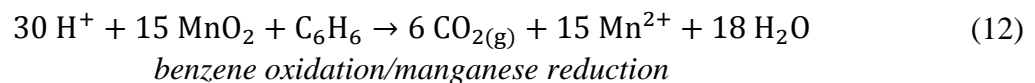
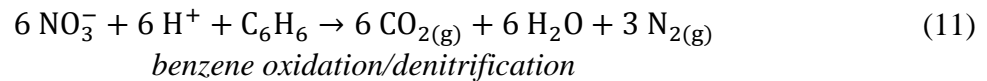
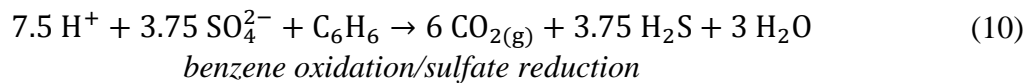
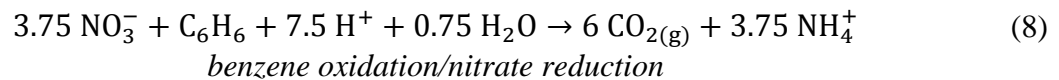
2.3.2 Saturated Zone Biodegradation

Biodegradation of aqueous phase constituents occurs primarily in regions 3-4. Region 4 lies entirely below the water table and biodegradation is limited by low contaminant mass and the

availability of common electron acceptors. In environments where the groundwater is aerobic, oxygen serves as the primary electron acceptor. Equation 7 demonstrates the aerobic oxidation of an LNAPL using benzene as an example (US EPA, 1998).

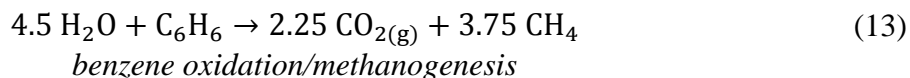


However, in most cases, region 4 is anaerobic and commonly available electron acceptors are nitrate (NO_3^-), iron oxide-hydroxide ($\text{Fe}(\text{OH})_3$) or sulfate (SO_4^{2-}), depending on geologic characteristics. Manganese dioxide (MnO_2) may also act as an electron acceptor, though it is less commonly encountered. Equations 8-12 demonstrate anaerobic oxidation of LNAPL again using benzene as an example (US EPA, 1998).



Region 3 encompasses the areas directly below the water table, in the capillary fringe, and just above the capillary fringe. The region is anaerobic and characterized by methanogenesis. Given depletion of commonly available electron acceptors (Equations 8-12), contaminants are degraded by methanogenic microorganisms. This process is of critical importance because methanogenic

degradation can be sustained within the core of the source zone in the absence of more thermodynamically favorable electron acceptors. Equation 13 demonstrates the methanogenic degradation of benzene (US EPA, 1998).



The production of CO₂ and CH₄ in all of the biodegradation reactions listed above can lead to saturated solutions and the formation of gas bubbles (see Region 3 in Figure 3) (Amos et al., 2005). Ebullition of gas bubbles occurs when buoyancy forces overcome capillary forces. Recent research suggest substantial amounts of gaseous CO₂ and CH₄ in the vadose zone originate from ebullition of dissolved gases from the saturated zone (Amos and Mayer, 2006a; Amos and Mayer 2006b).

2.3.3 Vadose Zone Biodegradation

Gaseous phase LNAPL constituents in the vadose zone partition into pore water and degrade. Degradation occurs primarily via methanogenic processes (Equation 13), resulting in the production of CO₂ and CH₄. Region 2 in Figure 3 represents the methane oxidation front. In this region, CH₄ produced in region 3 is oxidized and transformed into CO₂ by methanotrophic bacteria that utilize CH₄ as their sole carbon source. Based on work at a former refinery in Wyoming (Irianni-Renno, 2013), the top of region 2 fluctuates seasonally due to variations in the inward fluxes of O₂ and outward fluxes of CH₄.

Contaminant mass loss associated with volatilization coupled with biodegradation has been shown to be 2 orders of magnitude greater than mass loss associated with dissolution coupled with biodegradation (Lundegard and Johnson, 2006). A study by Molins et al. (2010) found that up to 98% of contaminant-related carbon exits at ground surface as CO₂. Thus, contaminant-related carbon flux occurs primarily in the vertical direction. These findings illustrate the critical role vertical gas phase transport of contaminant-related carbon plays on overall contaminant mass reduction in the source zone.

Total carbon fluxes are composed of contributions from contaminant-related carbon fluxes and natural soil respiration (modern carbon). Modern carbon fluxes result from the biodegradation of natural organic matter in shallow soil layers. To accurately capture gas phase carbon fluxes related solely to biodegradation of contaminants, fluxes due to natural soil respiration must be accounted for. This can be accomplished by the background subtraction method (Sihota et al., 2011):

$$J_{\text{Contaminant}} = J_{\text{Total}} - J_{\text{Background}} \quad (14)$$

where $J_{\text{Contaminant}}$ is the carbon flux related to contaminant biodegradation (moles contaminant carbon/area/time), J_{Total} is the total carbon flux (moles total carbon/area/time) and $J_{\text{Background}}$ is the background carbon flux due to soil respiration (moles modern carbon/area/time).

Alternatively, stable carbon and radiocarbon isotope analysis can be used to determine contaminant-related carbon fluxes (Coffin et al., 2008). Contaminant-related fluxes can be described in terms of a flux through the subsurface or an efflux from the subsurface to the atmosphere. Typical ranges of CO₂ effluxes above LNAPL-impacted sites have been documented to range from 2.2-21.2 μmol/m²/s (Sihota et al., 2011; McCoy et al., 2014).

Gas transport through the vadose zone results from advective and diffusive transport. Transient, 3-dimensional transport can be described by the following equation (modified from Molins and Mayer, 2007):

$$\frac{\partial}{\partial t} [S_g \phi C_g^i] + \nabla \cdot [\mathbf{q}_g C_g^i] - \nabla \cdot \mathbf{N}_{T,g}^i - Q_g^i = 0 \quad (15)$$

where t is time, S_g is gas phase saturation (volume gas/volume void), ϕ is total porosity (volume void/total volume), C_g^i is the total gaseous concentration of component i (moles/volume), \mathbf{q}_g is the gaseous phase Darcy flux vector for component i (length/time), $\mathbf{N}_{T,g}^i$ is the gaseous phase diffusive flux vector for component i (moles/volume), and Q_g^i is the external source and sink term for the gaseous phase boundary flux (moles/volume/time).

2.4 Environmental Factors Affecting Mechanisms and Measurement of NSZD

This section introduces environmental conditions that may affect rates of biodegradation, gas transport mechanisms in the vadose zone, and subsequent quantification of NSZD rates.

Environmental conditions addressed include (1) wind, (2) temperature, (3) moisture (soil and precipitation), (4) barometric pumping, and (5) artificial surfaces and low permeability lenses.

Figure 4 summarizes the environmental factors discussed below.

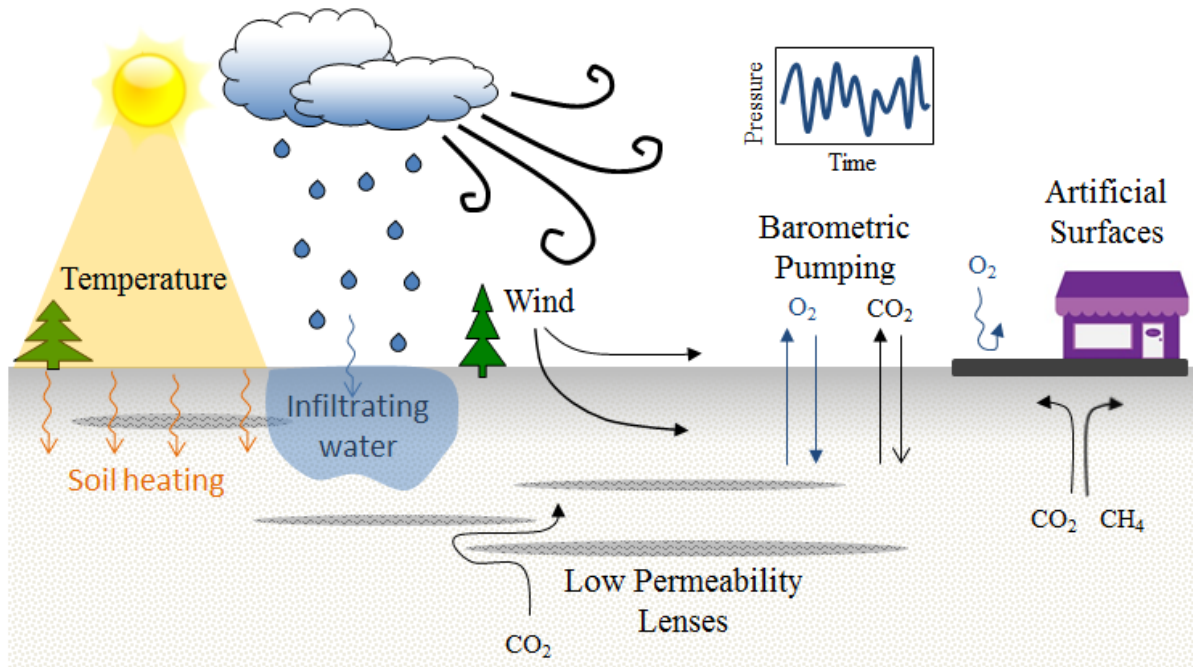


Figure 4. Environmental factors affecting mechanisms and measurement of NSZD.

2.4.1 Wind

Wind can affect subsurface processes and measurement methods by creating near surface pressure differentials, driving advective gas transport that would not occur in the absence of wind. Wind-induced pressure differentials can (1) directly affect gas efflux from the soil column or (2) act on the surficial measurement methods to induce a negative pressure within the measurement apparatus.

Wind-induced transport can account for a large portion of the total gas transport at grade (Poulsen and Moldrup, 2006). For example, a study of boreal forest soil respiration by Hirsch et al. (2003) found that CO_2 effluxes were higher in the presence of wind. Wind can also drive atmospheric gases such as oxygen into the soil column (Lundegard et al., 2008), sustaining

aerobic biodegradation and methane oxidation by methanotrophs. Wind-induced transport is more important for soils with higher moisture contents in which gas diffusivity is reduced (Poulsen and Møldrup, 2006). Furthermore, wind may have a lesser effect in finer soil textures where resistance to advective transport is large (Kimball and Lemon, 1971). Wind can also create lateral pressure differentials across surface objects. Lundegard et al. (2008) found that wind speeds greater than approximately 4 m/s were enough to induce a 60 Pa pressure differential between the windward and leeward sides of a building.

2.4.2 Temperature

Temperature can affect (1) natural and contaminant soil respiration rates, (2) gas diffusivity, and (3) aqueous solubility of gases. Natural soil respiration has been shown to be temperature dependent (Hirsch et al., 2003; Jassal et al., 2005), with higher respiration rates corresponding to higher soil temperatures. Furthermore, Zeman (2012) found aerobic LNAPL biodegradation was at an optimum between 22 and 30°C. These results suggest that gas effluxes above LNAPL source zones can vary with seasonal temperature fluctuations, both with respect to natural and contaminant soil respiration.

Gas diffusivity is also temperature dependent and will vary with temperature fluctuations.

Following Bird et al. (2002), temperature effects on gas diffusion can be accounted for using

Equation 16:

$$D_i = D_o \left(\frac{T}{T_o} \right)^b \quad (16)$$

where D_i is the temperature corrected gas diffusivity ($\text{length}^2/\text{time}$), D_o is gas diffusivity at a reference temperature ($\text{length}^2/\text{time}$), T is the temperature ($^{\circ}\text{K}$), T_o is the reference temperature (typically $298\text{ }^{\circ}\text{K}$), and b is a constant defined in the literature. Gas diffusivity will be greater at warmer temperatures than at colder temperatures. Thus, understanding subsurface temperatures is critical for understanding diffusive gas transport.

Furthermore, aqueous solubility of gases is temperature dependent (Schwarzenbach et al., 2003). As temperature increases, aqueous solubility of gases decreases. Conversely, aqueous solubility of gases is increased as temperature is decreased.

2.4.3 Moisture

Moisture can affect gas fluxes by (1) temporarily enhancing soil respiration, (2) displacing CO_2 -rich soil gas, and (3) reducing gas phase effective diffusion coefficients. Soil rewetting caused by a precipitation event can result in a temporary increase in microbial activity, followed by a subsequent decrease as the soil dries (Orchard and Cook, 1983). This may lead to temporary increases in total CO_2 efflux, particularly the contribution from natural soil respiration.

Enhanced microbial respiration and corresponding increases in CO_2 effluxes can be sustained for several days (Jassal et al., 2005). Infiltrating precipitation can also cause CO_2 rich soil gas to be displaced, primarily at shallow soil depths (Jassal et al., 2005). This may also lead to short-term increases in CO_2 efflux.

Conversely, CO_2 effluxes may be severely reduced by larger precipitation events. Gas transport is dominated by the air-filled pore space (diffusive transport) and relative permeability

(advective transport), both of which are highly sensitive to changes in soil moisture. Fully saturated surface soils can completely inhibit gas efflux. Reduced vertical gas transport may also lead to horizontal transport.

2.4.4 Barometric Pumping

Barometric pumping is the inward and outward movement of subsurface air that occurs due to changes in atmospheric pressure. A study by Wyatt et al. (1995) reported that soil gas effluxes increased during periods of depressed atmospheric pressure. Conversely, soil gas effluxes decreased during periods of high atmospheric pressure, and periods of stable atmospheric pressure were capable of halting gas migration. Furthermore, modeling suggests atmospheric air can migrate several meters into the subsurface in porous media with high gas permeability due to barometric pumping (Massman & Farrier, 1992). The inward transport of atmospheric air is critical because it supplies oxygen-rich air to the subsurface, supporting aerobic biodegradation and methane oxidation processes.

2.4.5 Artificial Surfaces and Low Permeability Lenses

Artificial surfaces (such as pavement) and low permeability clay or silt lenses can (1) inhibit vertical gas migration and (2) encourage horizontal gas transport. Inhibiting vertical transport can have substantial impacts on soil gas concentration profiles and transport. For example, Coffin et al. (2008) found that vertical concentrations of soil gases were not significantly different between deep and shallow monitoring points underneath an asphalt surface. These results illustrate that capping the soil with an artificial surface can lead to the build-up of soil gases by preventing atmospheric exchange, and minimize/eliminate apparent concentration

gradients of select gas species. Following Le Chatelier's principle, the build-up of reaction byproducts may also act to slow the forward rate of biodegradation reactions as chemical equilibrium is shifted.

Artificial surfaces can also limit inward oxygen transport, having negative implications for biodegradation and methane oxidation processes. Without oxygen replenishment, aerobic biodegradation and methane oxidation processes can be reduced or stopped altogether. As a result, vapor intrusion problems may exist in nearby structures and methane may be discharged to the atmosphere.

Additionally, near surface heterogeneities caused by low permeability lenses and artificial surfaces can cause horizontal pressure gradients to develop (Massmann and Farrier, 1992). Horizontal pressure gradients can drive lateral flow, altering gas transport mechanisms in the source zone.

2.5 Quantification of NSZD Using Soil Gas Fluxes

Three methods have recently emerged to quantify NSZD using soil gas fluxes, particularly CO₂. These methods build on the assumption that losses of contaminant-related carbon are manifested as vertical gas transport through the vadose zone. These methods include the gradient, chamber, and trap methods. Each method is discussed in detail below.

2.5.1 Gradient Method

The concentration gradient method (gradient) is based on vertical soil gas concentration profiles to quantify mass loss due to volatilization and biodegradation (Figure 5) (Johnson et al., 2006).

Gas concentration profiles can be measured using nested gas probes or multi-level samplers.

The gradient method provides an instantaneous snapshot of LNAPL loss rates based on soil gas distributions at the time of sampling. Consideration is given to inward fluxes of O₂ and/or outward fluxes of CO₂, CH₄, and volatile hydrocarbons (HC). Soil gas profiles are coupled with effective diffusion coefficients and used as inputs into Fick's First Law.

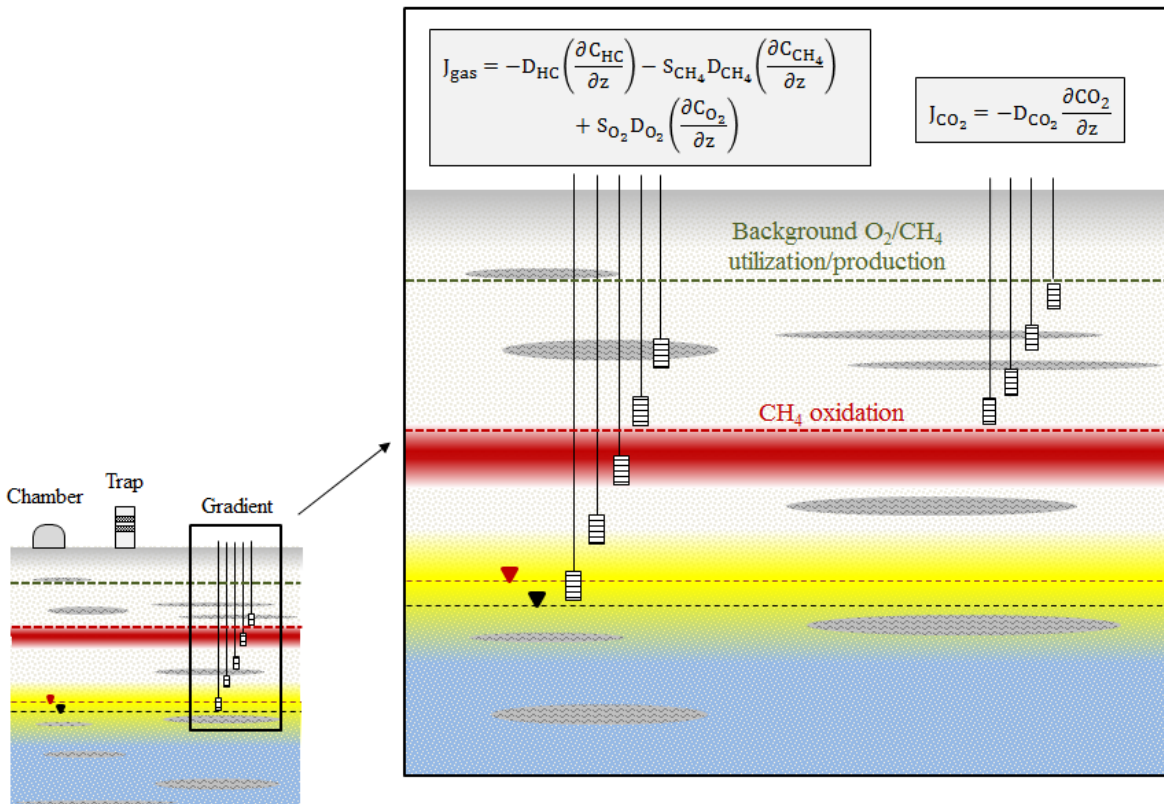


Figure 5. Conceptualization of gradient method (following Johnson et al., 2006). Measurements may include O₂, CH₄, CO₂, and HC concentration profiles. Measurements can be simplified if HC concentrations are negligible and measurements are made above the methane oxidation front.

Gas concentration profiles can be obtained using nested gas probes (shown) or a multi-level sampler.

The methodology was originally proposed by Johnson et al. (2006) and successfully demonstrated at a former oil field site by Lundegard and Johnson (2006). The gradient method is also endorsed by the ITRC (2009) for evaluating NSZD. Table 1 summarizes the data collection needed for the gradient method.

Table 1. Data needed for gradient method. Modified from Johnson et al., 2006

Data Needed	Significance
Hydrocarbon (HC) concentration profiles	Decreasing hydrocarbon concentrations in the direction away from the source zone is evidence of volatilization
O ₂ concentration profile	Decreasing oxygen concentrations in the direction towards the source zone is evidence of aerobic biodegradation of hydrocarbons
CO ₂ concentration profile	Decreasing carbon dioxide concentrations in the direction away from the source zone is evidence of aerobic biodegradation of hydrocarbons
CH ₄ concentration profile	Increasing methane concentrations in the direction towards the source zone is evidence of anaerobic biodegradation of hydrocarbons
Effective gas phase diffusion coefficients	Required to calculate gaseous phase loss rates; can be estimated using moisture content and porosity or measured in-situ

The rate of steady state, homogeneous, one-dimensional gas transport can be obtained from simplifications of Equation 15. Gas transport can be expressed as a mass flux, J_{gas} (mass/time/length²) (based on Johnson et al., 2006):

$$J_{\text{gas}} = -D_{\text{HC}} \left(\frac{\partial C_{\text{HC}}}{\partial z} \right) - S_{\text{CH}_4} D_{\text{CH}_4} \left(\frac{\partial C_{\text{CH}_4}}{\partial z} \right) + S_{\text{O}_2} D_{\text{O}_2} \left(\frac{\partial C_{\text{O}_2}}{\partial z} \right) \quad (17)$$

where D_{HC} is the effective gas phase diffusion of hydrocarbons at the depth of measurement (length²/time), $\partial C_{\text{HC}}/\partial z$ is the vertical concentration gradient of hydrocarbon gas ([mass-

HC/volume-gas]/length), S_{CH_4} is the stoichiometric coefficient for anaerobic conversion of hydrocarbon to methane (mass-HC/mass-methane), D_{CH_4} is the effective gas phase diffusion of methane at the depth of measurement (length²/time), $\partial C_{CH_4}/\partial z$ is the vertical concentration gradient of methane gas ([mass-CH₄/volume-gas]/length), S_{O_2} is the stoichiometric coefficient for the aerobic oxidation of hydrocarbons and methane (mass-hydrocarbon/mass-O₂), D_{O_2} is the effective gas phase diffusion of oxygen at the depth of measurement (length²/time) and $\partial C_{O_2}/\partial z$ is the vertical concentration gradient of oxygen ([mass-O₂/volume-vapor]/length).

If reactions and volatilization are assumed negligible, the rate of NSZD can also be expressed as a mass flux using CO₂ concentration gradients (J_{CO_2}):

$$J_{CO_2} = -D_{CO_2} \frac{\partial CO_2}{\partial z} \quad (18)$$

where D_{CO_2} is the effective gas phase diffusion of carbon dioxide at the depth of measurement (length²/time) and $\partial C_{CO_2}/\partial z$ is the vertical concentration gradient of carbon dioxide gas (mass-CO₂/volume-gas]/length). This method is valid for more mature sites where volatilization is negligible and all reactions are either aerobic (i.e., no methane production) or soil gas concentrations are measured above the zone of methane oxidation.

As noted in Table 1, the effective gas phase diffusion of soil gas constituents is a necessary component for the gradient method. One method for estimating effective vapor phase diffusion is using an in-situ “push-pull” method, herein referred to as the In-situ method (Johnson et al., 1998). In this method, a conservative tracer of known concentration and volume is injected into

a subsurface sampling port. After allowing a period of time to pass (minutes to hours), a sample of soil gas is extracted from the same sampling port and the fraction of tracer recovered is used to estimate the effective diffusion of the tracer gas (D_t). Using a simple ratio, the effective diffusion of the desired gas phase constituent (D_i) can be calculated:

$$D_i = D_t \left(\frac{D_{air,i}}{D_{air,t}} \right) \quad (19)$$

where $D_{air,i}$ is the free air diffusion coefficient of the gas phase constituent and $D_{air,t}$ is the free air diffusion of the tracer gas.

Another method to calculate the effective diffusion coefficient for a gas phase constituent is to use numerical equations that rely on estimates of total porosity and air-filled porosity (e.g., Penman, 1940; Millington, 1959; Moldrup et al., 2000). The Millington (1959) model is commonly used in literature to estimate the effective diffusion coefficient of a gas in dry porous media:

$$D_i = D_m \phi^{4/3} \quad (20)$$

where D_m is the molecular diffusivity of the gas phase constituent in air and ϕ is the total porosity (assumed to be completely air-filled). This approach provides a simple approximation if the soil is dry and total porosity is known and can be assumed constant throughout the soil column.

Equation 20 can be modified to account for porous media containing multiple fluid phases:

$$D_i = D_m S_g^{10/3} \phi^{4/3} \quad (21)$$

where S_g is the gas phase saturation.

Table 2 summarizes characteristics of the gradient method relevant to quantifying NSZD.

Statements about each characteristic are based on theory of the method, findings observed in the literature, and opinions of the author.

Table 2. Summary of gradient method characteristics.

Characteristic	Evaluation
Intrusiveness of method	Intrusive. Subsurface sampling required.
Period of measurement	Instantaneous
Time to results	Weeks. Time includes sample analysis and data reduction.
Level of effort required	High. Requires installation of sampling systems, collection of gas samples, determination of effective diffusion coefficients, and data reduction ^[a] .
NSZD mechanism(s) measured	Volatilization and biodegradation ^[a] . Measuring Ar and N ₂ can give insight into mass loss processes ^[b] . Hydrocarbon concentrations give insight into volatilization rates.
Transport process quantified	Diffusive ^[a]
Correction for natural soil respiration	Depends on location of gas sampling ports. Measurements can be made below depth of background O ₂ utilization and CH ₄ production, eliminating need to correct for natural soil respiration ^[a] .
Influence of barometric pumping	Method provides instantaneous snapshot of subsurface gas profiles which may be subject to barometric pumping ^[c] .
Influence of surface wind	Depends on soil texture and moisture content ^[c, d] . Surface wind may affect subsurface gas distributions if soil texture is relatively coarse and moisture content is relatively high.
Influence of precipitation and/or soil moisture	Effective diffusion coefficients are highly sensitive to changes in soil moisture. Method is not well suited for shallow aquifer applications due to difficulties estimating effective diffusion coefficients near the water table and capillary fringe ^[a, c] .
Influence of artificial surfaces/heterogeneities	Effective diffusion coefficients are highly sensitive to changes in soil moisture and texture caused by subsurface heterogeneities. Artificial surfaces may lead to accumulation of select gas species, leading to small apparent concentration gradients ^[e] .

^[a] Johnson et al., 2006, ^[b] Amos et al., 2005, ^[c] Maier and Schack-Kirchner, 2014,

^[d] Poulson and Møldrup, 2006, ^[e] Coffin et al., 2008. Statements without references are based on general knowledge pertaining to the method and opinions of the author.

2.5.2 Chamber Method

The dynamic closed chamber method (chamber) consists of a soil gas chamber placed on a PVC collar at grade to measure total CO₂ efflux using an infrared gas analyzer (IRGA) (LI-COR, 2010). Figure 6 illustrates the use of the chamber method over an LNAPL source zone.

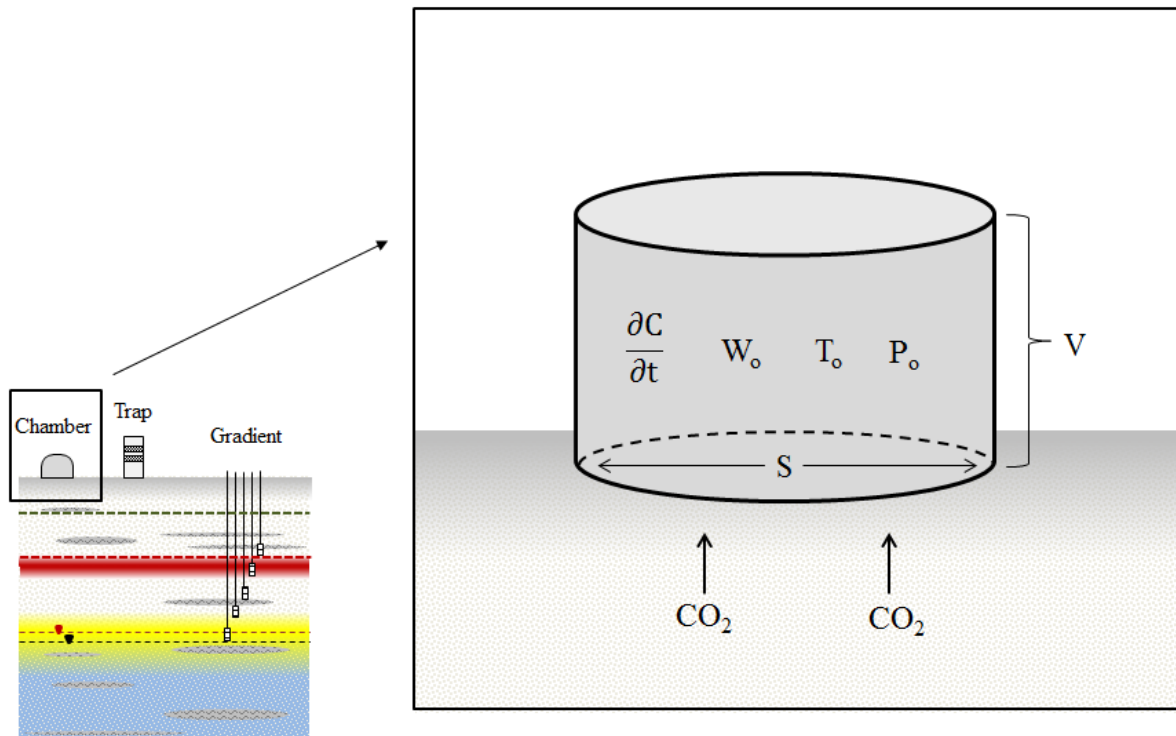


Figure 6. Conceptualization of chamber method. The change in CO₂ concentration with time is measured using an infrared gas analyzer (IRGA).

The chamber is typically placed over the soil surface for 90 to 120 seconds (LI-COR, 2010). As CO₂ in the chamber headspace increases, the absorption of infrared light increases. The reduction in the transmission of infrared light through the chamber is then used to calculate CO₂ concentration (Thomas and Haider, 2013). A survey chamber allows for instantaneous results,

whereas a long-term chamber provides sequential measurements of CO₂ efflux through time at a given location.

The rate of CO₂ increase in the chamber headspace is measured and fit to Equation 22 (LI-COR, 2010) using either a linear and exponential regression:

$$C(t) = C_x + (C_o - C_x)e^{-a(t-t_o)} \quad (22)$$

where $C(t)$ is the instantaneous water-corrected chamber CO₂ mole fraction ($\mu\text{mol CO}_2/\text{mol air}$), C_x is a parameter defining the concentration asymptote ($\mu\text{mol CO}_2/\text{mol air}$), C_o is the initial value of $C(t)$ when the chamber closed ($\mu\text{mol CO}_2/\text{mol air}$), a is a parameter defining the curvature of the fit (s^{-1}), t is time (s) and t_o is the initial time the chamber closed (s). The exponential regression is designed to correct for alterations on the natural diffusion gradient (chamber effects) noted in previous chamber studies (Davidson et al., 2002).

Using the regression with the best fit parameters (R^2 and coefficient of variation), the change in CO₂ concentration with respect to time is used as an input to Equation 23 (LI-COR, 2010) to calculate CO₂ efflux:

$$J_{\text{chamber}} = \frac{10VP_o \left(1 - \frac{W_o}{1000}\right) \partial C}{RS(T_o + 273.15) \partial t} \quad (23)$$

where J_{chamber} is the efflux of CO₂ ($\mu\text{mol}/\text{m}^2/\text{s}$), V is volume of the chamber headspace (cm^3), P_o is the initial atmospheric pressure (kPa), W_o is the initial water vapor mole fraction (mmol/mol), S is the soil surface area (cm^2), T_o is the initial air temperature ($^{\circ}\text{C}$), and $\partial C/\partial t$ is the initial rate

of change in water-corrected CO₂ mole fraction (μmol/m). Figure 7 shows a screenshot from the LI-COR Biosciences data reduction software (Fileviewer 3.1.1).

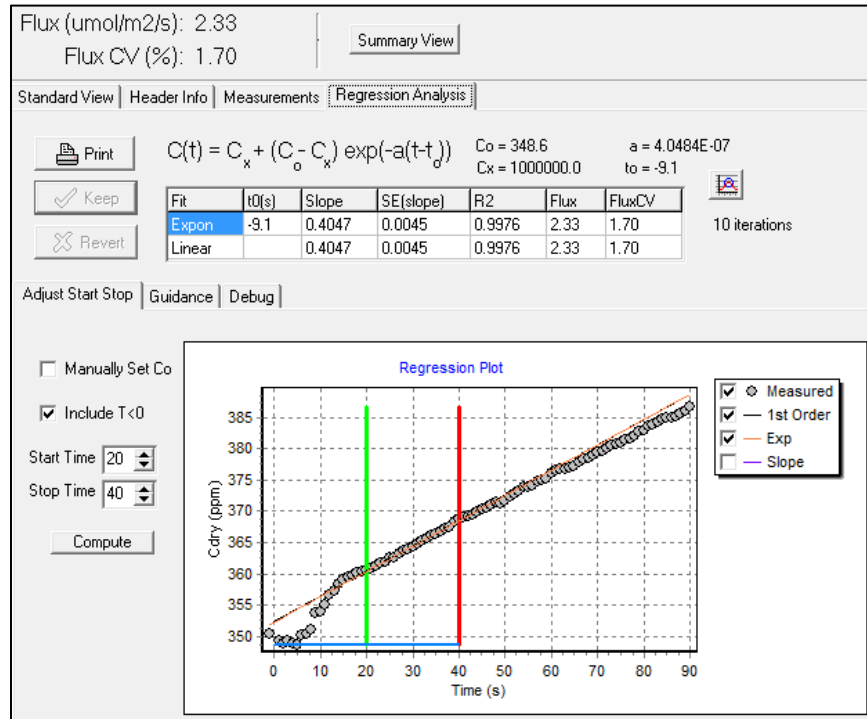


Figure 7. Chamber method data reduction output. CO₂ concentration vs. time is shown, along with exponential and linear fits to Equation 22. Green and red vertical bars represent time interval of data used in the regression analysis. In this example, both fits converge on the same CO₂ flux value. Non-linear CO₂ concentration vs. time may indicate a poor seal between the chamber and soil collar.

Soil CO₂ chambers have long been used in the fields of agronomy and forestry to quantify microbial respiration, root activity, and natural carbon cycles from various soil environments (e.g., Nay et al., 1994; Kabwe et al., 2002; Jassal et al., 2005; Sullivan et al., 2010). The chamber method was first used quantify CO₂ effluxes associated with petroleum hydrocarbon degradation in a proof-of-concept study by Sihota et al. (2011).

Table 3 summarizes characteristics of the chamber method in quantifying NSZD. Statements about each characteristic are based on theory of the method, findings observed in the literature, and opinions of the author.

Table 3. Summary of chamber method characteristics.

Characteristic	Evaluation
Intrusiveness of method	Minimal. System is deployed at ground surface and soil collar is inserted centimeters into the soil ^[a] .
Period of measurement	Instantaneous or long-term depending on equipment
Time to results	Real time field values
Level of effort required	Moderate. Requires training for proper use. Method is easy to transport and capable of making multiple measurements in a short time period.
NSZD mechanism(s) measured	Biodegradation, assuming CH ₄ oxidation ^[b]
Transport process quantified	Advective and diffusive ^[b]
Correction for natural soil respiration	Required. Can be corrected for using stable carbon and radiocarbon isotope analysis ^[c] or background correction method ^[d] . Isotope analysis requires collection of gas samples in the field.
Influence of barometric pumping	Depends on period of measurement. Survey measurements provide an instantaneous snapshot of CO ₂ efflux which may be subject to barometric pumping ^[e] . Long-term measurements provide insight into variations caused by changes in atmospheric pressure.
Influence of surface wind	Potential influence. Surface winds across the chamber body may cause pressure differentials to develop ^[f] , altering gas flow in and around the chamber. Research is ongoing to determine effect of wind.
Influence of precipitation and/or soil moisture	Fully saturated soils can shut down soil gas efflux, making measurements impossible following precipitation events.
Influence of artificial surfaces/heterogeneities	Method cannot be used on artificial surfaces. Subsurface heterogeneities may affect measurements if soil collar is inserted through a lower permeability material, creating a preferential pathway for gas flow that would not occur naturally.

^[a] LI-COR, 2010, ^[b] Molins et al., 2010, ^[c] Coffin et al., 2008, ^[d] Sihota et al., 2011, ^[e] Wyatt et al., 1995, ^[f] Lundegard et al., 2008. Statements without references are based on general knowledge pertaining to the method and opinions of the author.

2.5.3 Trap Method

The CO₂ Trap method (trap) consists of two soda lime absorbent elements that convert gaseous CO₂ into solid phase carbonates (Zimbron et al., 2013; McCoy et al., 2014). Absorption elements are placed inside a vertical 10 cm ID PVC pipe at grade. The bottom absorption element is designed to capture CO₂ efflux from the soil column. The top absorption element intercepts atmospheric CO₂ and prevents it from reaching the bottom absorption element. The trap is placed on a PVC receiver inserted up to 18 cm into the ground. The trap and receiver are covered with a larger, thin-walled 15 cm ID PVC pipe with several holes drilled in it that acts as a rain cover to protect the absorbent from precipitation. Figure 8 illustrates the use of a trap to measure CO₂ effluxes over an LNAPL source zone.

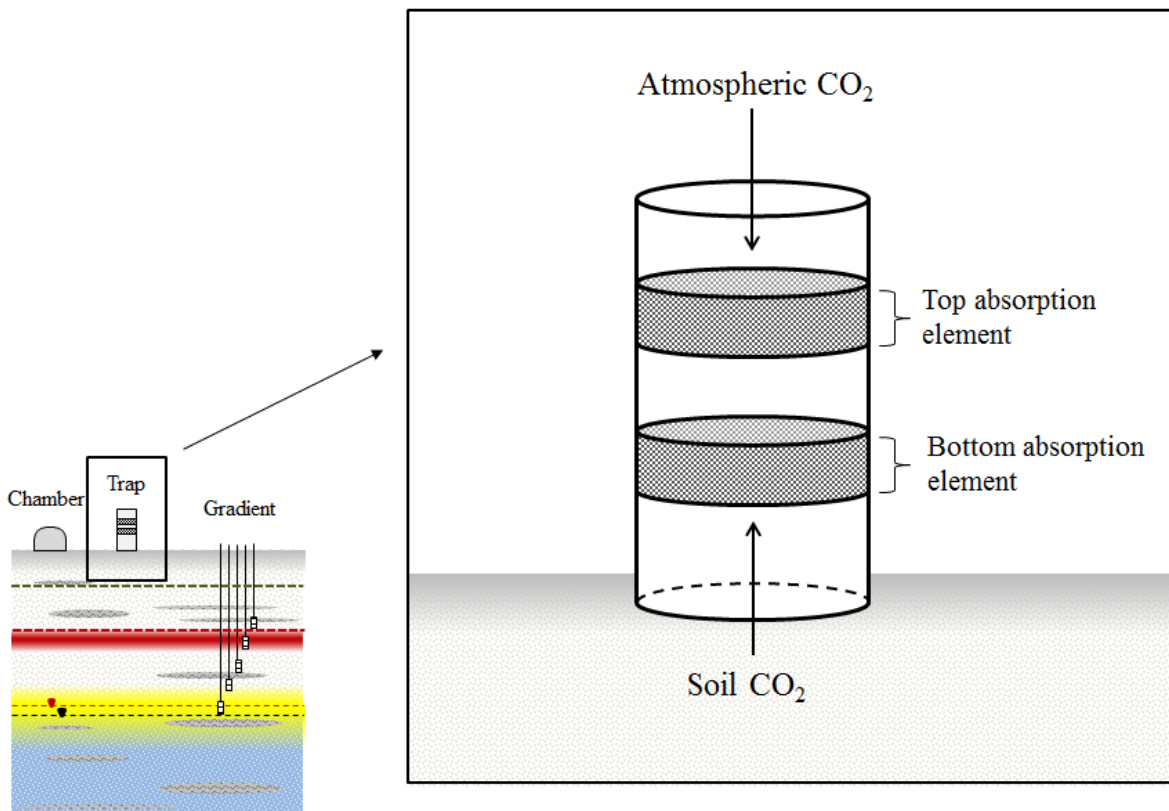


Figure 8. Conceptualization of trap method. Soil CO₂ is captured by the bottom absorption element and atmospheric CO₂ is intercepted by the top absorption element. Note, rain cover is not shown.

Traps are typically deployed at a field site for 2-4 weeks. Deployment duration is limited by the maximum absorption capacity of the soda lime (30% by weight). At field sites with higher expected CO₂ effluxes, traps should be deployed for shorter durations to avoid oversaturating the soda lime. Field sites with lower expected CO₂ effluxes may require longer deployment durations so that an appreciable amount of CO₂ can be captured. After traps have been deployed for a sufficient amount of time, they are retrieved and sent off for analysis to quantify the mass of CO₂ captured.

A travel blank is used to account for CO₂ absorption that occurs during trap construction and analysis. The background mass of CO₂ is subtracted from the total mass captured by the traps in the field (Equation 24).

$$\text{contaminant carbon mass} = \text{total carbon mass} - \text{background carbon mass} \quad (24)$$

CO₂ efflux is determined by dividing the mass of CO₂ captured in the bottom absorption element by the cross-sectional area of the absorbent element and the deployment duration:

$$J_{\text{trap}} = \frac{m_{\text{CO}_2}}{A_{\text{trap}} t} \quad (25)$$

where J_{trap} is the efflux of CO₂ (μmol/m²/s), m_{CO_2} is the mass of CO₂ captured in the bottom absorption element (μmol), A_{trap} is the cross-sectional area of the trap (m²), and t is the deployment duration (s).

Alkali absorption by soda lime has been used for decades in static closed chambers to quantify CO₂ effluxes from natural soil environments. Despite an apparent shift away from the static closed chamber method, using soda lime is appealing because it provides time-integrated estimates of CO₂ effluxes. Traps containing soda lime were first used to quantify CO₂ effluxes associated with an LNAPL source zone in a proof-of-concept study by McCoy et al. (2014).

Table 4 summarizes characteristics of the trap method for quantifying NSZD. Statements about each characteristic are based on theory of the method, findings observed in the literature, and opinions of the author.

Table 4. Summary of trap method characteristics

Characteristic	Evaluation
Intrusiveness of method	Minimal. System is deployed at ground surface and trap receiver is inserted up to 18 centimeters into the soil ^[a] .
Period of measurement	Time averaged integral value ^[b, f] .
Time to results	Weeks. Time is required for trap deployment, sample analysis, and data reduction ^[a, b, f] .
Level of effort required	Low. Placement of traps at field sites requires minimal effort. Traps are sent to an independent lab for analysis.
NSZD mechanism(s) measured	Biodegradation, assuming CH ₄ oxidation ^[c]
Transport process quantified	Advective and diffusive ^[c, f]
Correction for natural soil respiration	Required. Can be corrected for using stable carbon and radiocarbon isotope analysis ^[d] or background correction method ^[e] . Gas samples for isotope analysis can be obtained during trap analysis ^[a] .
Influence of barometric pumping	Method is an integral measurement designed to capture variation due to barometric pumping ^[f] .
Influence of surface wind	Potential influence. Surface winds may cause a negative pressure differential to develop inside of trap and/or rain cover and affect CO ₂ efflux via a Venturi-like effect. Research is ongoing to determine effect of wind.
Influence of precipitation and/or soil moisture	Rain cover may prevent wetting of underlying soil ^[b] , causing rain shadow in which preferential flow can develop. Research is ongoing to determine effect of precipitation on trap measurements.
Influence of artificial surfaces/heterogeneities	Method cannot be used on artificial surfaces. Subsurface heterogeneities may affect measurements if trap receiver is inserted through a lower permeability material, creating a preferential pathway for gas flow that does not occur naturally.

^[a] McCoy, 2012, ^[b] Zimbron et al., 2013, ^[c] Molins et al., 2010, ^[d] Coffin et al., 2008, ^[e] Sihota et al., 2011

^[f] McCoy et al., 2014. Statements without references are based on general knowledge pertaining to the method and opinions of the author.

2.6 Method Comparisons to Date

Comparison studies provide valuable insight into the accuracy and relative performance of the methods for measuring soil gas fluxes. Side-by-side comparisons of all methods have been conducted at multiple field sites, but have shown differing estimates of NSZD rates (based on unpublished data at multiple field sites). Per discussion with practitioners and regulators, concerns exist regarding method comparability in light of observed differences. Field comparisons are challenging due to subsurface heterogeneities, the inability to co-locate methods, time variant environmental factors and unknown true soil gas fluxes. Furthermore, comparisons from side-by-side applications at field sites only provide insight into the relative performance of methods because the true underlying flux is unknown.

Some laboratory studies have been conducted using a known imposed flux (Kabwe et al., 2002; Nay et al., 1994; Martin et al., 2004), but the focus was primarily on comparisons between the static closed chamber (using soda lime absorption) and dynamic closed chamber (i.e., chamber) methods. The gradient method has been found to produce reasonable results, but is limited mainly by uncertainties in estimating effective diffusion coefficients (Maier and Schack-Kirchner, 2014). No published comparisons have been made using traps because the method is the most recent to emerge. Thus, the relative and absolute performance of the gradient, chamber and trap methods for evaluating rates of NSZD is still largely unresolved.

3. EXPERIMENTAL METHODS

Large-scale laboratory column studies were conducted to compare the gradient, chamber, and trap methods. This chapter presents the experimental methods for these studies. Section 3.1 summarizes methods used to test the performance of the measurement methods under ideal experimental conditions. Section 3.2 presents methods used to test the measurement methods under simulated wind conditions. Experiments conducted to address select design features of the trap method are discussed in Section 3.3.

3.1 Method Comparison under Ideal Conditions

This section describes a large-scale laboratory study used to test the performance of the gradient, chamber, and trap methods using uniform porous media, constant environmental conditions, and known imposed CO₂ fluxes (i.e., ideal conditions). First, the large-scale column setup and CO₂ delivery system are presented. Second, deployment and analytical methods related to each of the measurement methods are discussed.

3.1.1 Large-Scale Column Setup and CO₂ Delivery System

Figure 9 presents the experimental setup. A 1.52 m tall by 0.67 m ID polyvinyl chloride (PVC) column was filled with fine sand (20-40 Colorado Silica Sand, Premier Silica) using a gravel diffuser. The sand was underlain by a coarse gravel layer 0.10 m thick that acted as a CO₂ mixing chamber. The sand and gravel layers were separated by a layer of geocomposite (Synotec, Tenflow II 1010) to prevent the sand from settling into the gravel. Sand samples were tested

ex-situ for water content and porosity. Average volumetric water content and porosity of the fine sand were determined to be 0.003 and 0.40, respectively. The column was located in a climate-controlled hydraulic laboratory facility. Seven multi-level soil gas sampling ports were installed in the column. Gas sampling ports were constructed of 3 mm O.D. Tygon[®] tubing and installed through Swagelok[®] compression fittings. Sampling ports extended 0.20 m into the column.

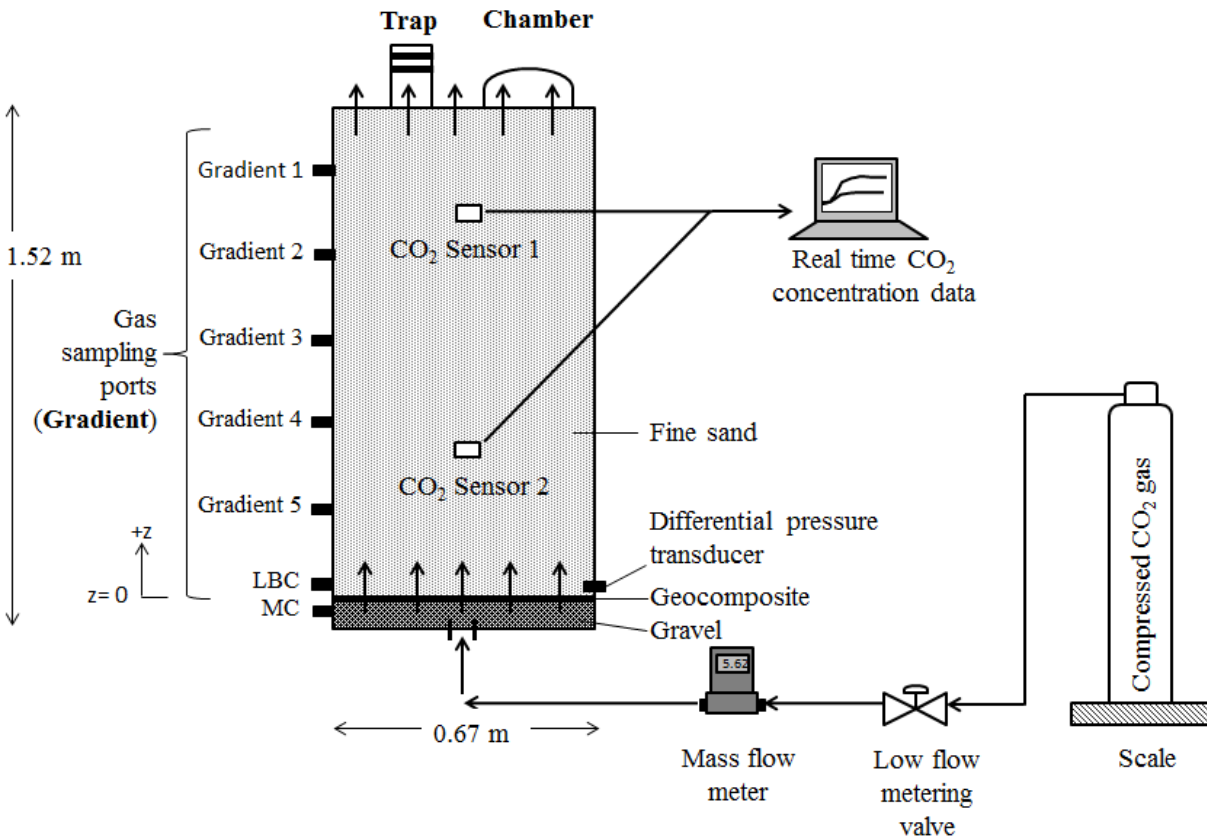


Figure 9. Schematic of column setup. LBC = lower boundary condition sampling port; MC = gravel mixing chamber sampling port.

Two continuous sensors (K-33 BLG, SE-0027) were installed to monitor real time CO₂ concentrations and determine when steady state conditions had been reached. Pressure differentials across the height of the fine sand were measured using a differential pressure transducer (OMEGA Engineering, PX277-0.1D5V).

Bone dry CO₂ gas (Airgas, Inc., CD BD200) was metered with a low-flow metering valve (Swagelok, B-SS2) and a mass flow meter (Aalborg, GFM17A-VBL6-A0). The CO₂ was delivered to the base of the column through 3 mm O.D. copper tubing. Swagelok[®] compression fittings were used throughout the system. All fittings and sampling ports were leak tested by capping and pressurizing the column to 13.8 kPa for 72 hours. No quantifiable loss in pressure was observed over this time period.

Four fluxes were imposed, spanning a range typical of contaminant-related CO₂ fluxes observed at field sites (3.3-15.2 μmol/m²/s) (Sihota et al., 2011; McCoy et al., 2014). Gas flow rates were adjusted between each trial and CO₂ concentrations in the column were allowed to reach steady state before measurement methods were employed. Gas flux rates (μmol/m²/s) were calculated using the mean gas flow rate given by the mass flow meter (minimum 16 observations), the column cross-sectional area (0.36 m²), and the mean CO₂ density. CO₂ density was calculated using mean ambient air temperature (measured using a Solinst Barologger Gold, 3001) and barometric pressure (measured at Christman Field Weather Station, Fort Collins, CO) values for the duration of each trial. Imposed CO₂ fluxes were independently verified using a scale (Cole-Parmer, EW-11119-87). Independent verification of gas fluxes was calculated using the change in mass of compressed CO₂ cylinder, the column cross-sectional area, and duration of a given flow rate.

3.1.2 CO₂ Measurement Methods

3.1.2.1 Gradient Method

Following Lundegard and Johnson (2006), gas samples were collected at each sampling depth by purging two tubing volumes of gas (0.8 mL), followed by the collection of a 5 mL sample in a gastight BD syringe capped with a Luer Lock[®] fitting. Sample collection started at the bottom of the column and progressed towards the top. Total sample volume accounted for approximately 0.02% of the total column pore volume. Given the small sample volume, sampling is assumed to have had a negligible effect on steady state conditions. Samples were analyzed within 2 hours of collection using a HP 5890 Series II gas chromatograph equipped with a thermal conductivity detector. 50- μ L samples were analyzed in triplicate for percent CO₂ using an Alltech Hayesep[®] Q 80/100 column (8' x 1/8" x 0.085" SS) with helium as the carrier gas and a constant oven temperature of 40°C. Calibrations were performed before each imposed flux trial.

For each imposed flux, a total of three sampling events occurred. Each sampling event consisted of pulling samples from all 7 sampling ports. Sampling events were spaced at the beginning, middle, and end of each period of fixed flux and extractions were made at approximately the same time each day. Percent CO₂ was converted into molar concentration ($\mu\text{mol}/\text{m}^3$) using average ambient temperature and pressure values for the imposed flux trial in conjunction with the Ideal Gas Law. CO₂ flux through the column was estimated using Fick's First Law, neglecting advection and reactions:

$$J_{\text{Gradient}} = -D_{\text{CO}_2} \frac{C_{\text{atm}} - C_z}{\Delta z} \quad (26)$$

where J_{Gradient} is the flux of CO_2 ($\mu\text{mol}/\text{m}^2/\text{s}$), D_{CO_2} is the effective diffusion coefficient of CO_2 in the column, C_{atm} is atmospheric CO_2 concentration (defined as 400 ppm), C_z is the CO_2 concentration at a given depth, and z is the distance between the ground surface and sampling depth (m). For all calculations, z was defined as the lower boundary condition sampling port. Given linear CO_2 concentration profiles throughout the column, any set of sampling ports could have been used.

Effective diffusion coefficients for CO_2 in the fine sand were determined following the analytical Millington model (1959) and experimentally using the In-situ tracer method (Johnson et al., 1998). Following common field practices, both methods were used to calculate D_{CO_2} to compare the effect of different methods for obtaining gas-phase diffusivity on measured flux.

For the Millington model, water content was assumed negligible, the gas-filled porosity (ϕ_g) was assumed equal to the total porosity ($\phi = 0.40$), and total porosity was assumed to be constant throughout the column. These assumptions were consistent with measured values for the fine sand in the column. The molecular diffusion coefficient of CO_2 in air (D_m) was defined as $1.60 \times 10^{-5} \text{ m}^2/\text{s}$ for $T = 20^\circ\text{C}$ (Haynes, 2015), which is representative of the average ambient temperature of the laboratory testing facility. Effective diffusion of CO_2 in the porous media was defined as $4.72 \times 10^{-6} \text{ m}^2/\text{s}$ using the Millington equation for dry media (Millington, 1959):

$$D_{\text{CO}_2} = D_m \phi_g^{4/3} \quad (27)$$

For the In-situ method, 100 mL of a known concentration of CH₄ (80%, balanced with N₂) was injected into a gas sampling port. Methane was assumed to be an inert tracer under the test conditions (i.e., dry with no biological reactions). After 15 to 60 min, 100 mL of soil gas were extracted and the remaining CH₄ concentration was determined in triplicate analysis by gas chromatography. Following protocol described in Johnson et al. (1998), the fraction of CH₄ mass recovered was used to determine an effective diffusion coefficient for methane (D_{CH_4}).

The effective diffusion coefficient for CO₂ was determined by multiplying D_{CH_4} by the ratio of the molecular diffusion of CO₂ to CH₄. The molecular diffusion of CH₄ was defined as $2.10 \times 10^{-5} \text{ m}^2/\text{s}$ for $T = 20^\circ\text{C}$ (Haynes, 2015). This process was repeated for sampling ports 1 through 5 and an average value of $3.45 \times 10^{-6} \text{ m}^2/\text{s}$ was calculated for the fine sand and assumed representative of the entire column.

3.1.2.2 Chamber Method

Chamber measurements were conducted using a long-term chamber (LI-COR Biosciences Inc., LI-8100-104) following methods of Sihota et al. (2011). A 21.3 cm O.D. PVC collar was inserted to a depth of 6 cm. A minimum of 24 hours elapsed prior to data collection to allow CO₂ efflux to re-stabilize following collar insertion. Chamber measurements were taken every 30 min for the duration of each imposed flux trial. Prior to continuous data collection, sample data was taken to ensure an air-tight seal was made between the chamber and PVC collar during measurements. To minimize chamber effects on the diffusion gradient, measurements were

limited to 1.5 min. To ensure steady mixing in the chamber, the first 20 seconds of data from each measurement were discarded.

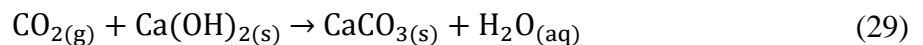
Measured CO₂ effluxes were calculated using the manufacturer supplied software (Fileviewer 3.1.1). The rate of change in CO₂ concentration with respect to time in the chamber headspace was fit to both a linear and exponential model. CO₂ efflux was calculated for each model using the following equation:

$$J_{\text{Chamber}} = \frac{10VP_o \left(1 - \frac{W_o}{1000}\right) \partial C}{RS(T_o + 273.15) \partial t} \quad (28)$$

where J_{Chamber} is the flux of CO₂ (μmol/m²/s), V is volume of the chamber headspace (cm³), P_o is the initial atmospheric pressure (kPa), W_o is the initial water vapor mole fraction (mmol/mol), S is the soil surface area (cm²), T_o is the initial air temperature (°C), and $\partial C/\partial t$ is the initial rate of change in water-corrected CO₂ mole fraction (μmol/m).

3.1.3.3 Trap Method

Following McCoy et al. (2014), traps were constructed from 10 cm I.D. schedule 40 PVC pipes fitted with rubber O-rings to create air-tight seals between upper and lower trap elements. Each trap had two passive CO₂ absorption elements each containing 50.0 g of soda lime material (W.R. Grace, Sodasorb[®] HP-6/12). CO₂ capture by the soda lime is described by the following reaction:



Traps were deployed in triplicate on 10 cm ID PVC receivers 30 cm long installed to a depth of 17.8 cm below grade. For each imposed CO₂ flux, the trap deployment period was based on the time necessary to achieve approximately 5% CO₂ saturation by weight (g CO₂/g soda lime), assuming 0% initial saturation and linear absorption. For each set of traps deployed, one travel blank was included to account for background CO₂ absorption due to ambient air exposure during trap construction, disassembly, and analytical processes. The trap and chamber methods were simultaneously deployed for each test flux. Figure 10 shows the orientation of the traps and chamber on the top of the column.

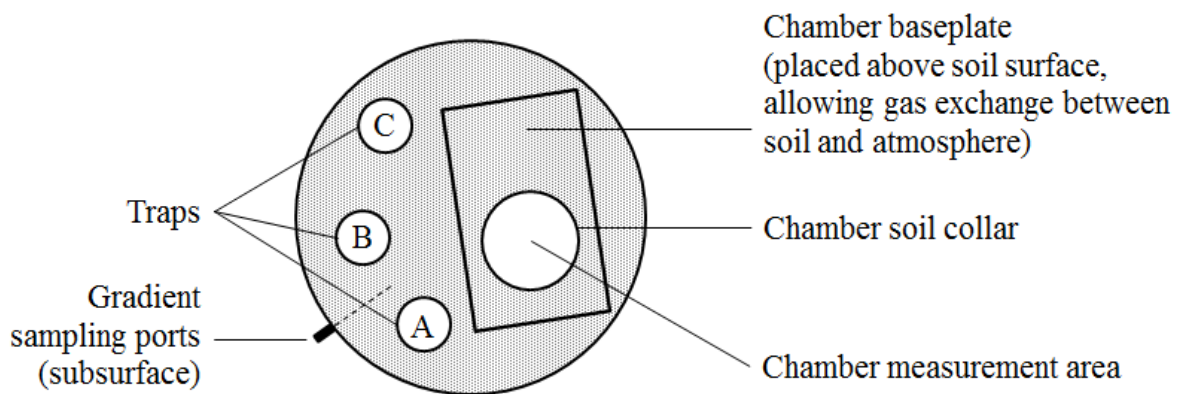


Figure 10. Top view schematic of column showing locations for chamber method and triplicate trap placement.

After deployment, traps were disassembled in the laboratory to recover the soda lime absorbent material. The absorbent material was vacuum-dried in a room temperature desiccator for a minimum of 48 hours to remove H₂O formed during the absorption reaction. Dried absorbent samples were homogenized by grinding and 5 g aliquots were analyzed in triplicate for CO₂

using gravimetric analysis (Bauer et al., 1972). CO₂ was desorbed from the soda lime using 6 N HCl solution and is described by the following reaction:



Measured CO₂ effluxes for the trap method (J_{Trap}) were calculated by dividing the background corrected CO₂ mass recovered (m_{CO_2}) by the cross-sectional area of the trap (A_{trap} , $8.1 \times 10^{-3} \text{ m}^2$) and duration of deployment (t).

$$J_{\text{Trap}} = \frac{m_{\text{CO}_2}}{A_{\text{trap}}t} \quad (31)$$

3.2 Method Comparison under Simulated Windy Conditions

This section describes modifications to the large-scale laboratory study used to test the performance of the gradient, chamber, and trap methods under simulated wind conditions.

Figure 11 shows the modified experimental setup. The same column and fill material described in Section 3.1.1 were used and a 3-speed, 50.8 cm box fan (Galaxy, B20100) was installed near the top of the column to simulate surface wind. The box fan was positioned equidistant from the trap and chamber to ensure both measurement methods were subjected to the same range of wind speeds.

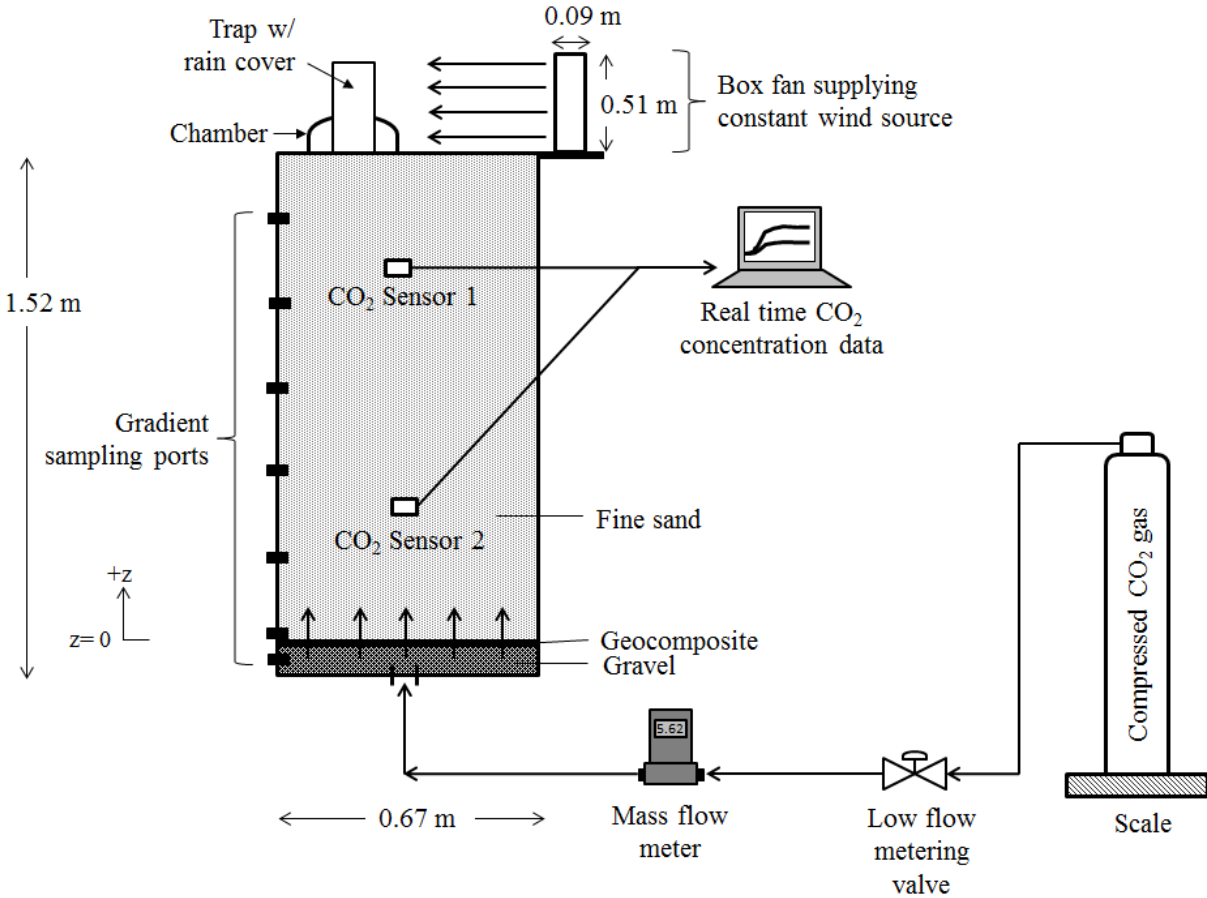


Figure 11. Schematic of experimental setup to test all methods under windy conditions.

Three trials, each consisting of a different constant wind speed, were conducted. Tested wind speeds were approximately 0 m/s (base case), 2.2-3.6 m/s, and 4.5-5.4 m/s measured at the surficial methods with a handheld wind meter (Ambient Weather, WM-2). For all three trials, the imposed flux remained constant (approximately $8.6 \pm 0.2 \mu\text{mol}/\text{m}^2/\text{s}$) and was calculated using methods described in Section 3.1.1. All three methods were deployed as described in Section 3.1 with the exception of the trap method.

For this experiment, only one trap was used and a rain cover was installed over the trap. Space limitations on top of the column with the rain cover in place prevented multiple traps from being

deployed. Results from one measurement were assumed to be representative due to consistent variations in measured fluxes observed with triplicate trap placement under ideal experimental conditions. The rain cover was 55.9 cm tall and had 16-1.6 cm diameter holes drilled in it for venting.

Pressure differentials were measured in the trap receiver to determine if the tested wind speeds created a measureable pressure difference between ambient air and the trap headspace. To detect pressure differentials, the trap receiver was connected to a differential pressure transducer (OMEGA Engineering, PX277-0.1D5V) using 3 mm O.D. copper tubing installed through a Swagelok[®] compression fitting located between the soil surface and bottom absorbent element.

For a given wind speed, all methods were deployed simultaneously for a duration of approximately 9 days to allow the trap to reach 5% CO₂ saturation by weight. Gradient method samples were collected three times over each imposed wind speed. Chamber measurements were recorded every 30 min for the 9 day duration.

3.3 Trap Modification Studies

This section describes modifications that were made to the trap method to test specific trap design features. Section 3.3.1 describes an experiment in which the mass of soda lime absorbent in the bottom trap element was increased. Section 3.3.2 discusses an experiment designed to detect and quantify breakthrough of soil CO₂ from the bottom absorbent element to the top absorbent element. Section 3.3.3 addresses the effect of the height of the bottom absorbent element above the soil surface on measured efflux.

3.3.1 Mass of Absorbent in Bottom Element

The mass of absorbent material in the traps may affect the accuracy of CO₂ efflux measurements by altering the absorption kinetics (e.g., number of reaction sites and retention time through absorbent layer). To test the effect of absorbent mass on measured flux, two sets of traps (3 traps per set) were constructed with differing masses of absorbent. Figure 12 illustrates a trap configuration with increased absorbent mass.

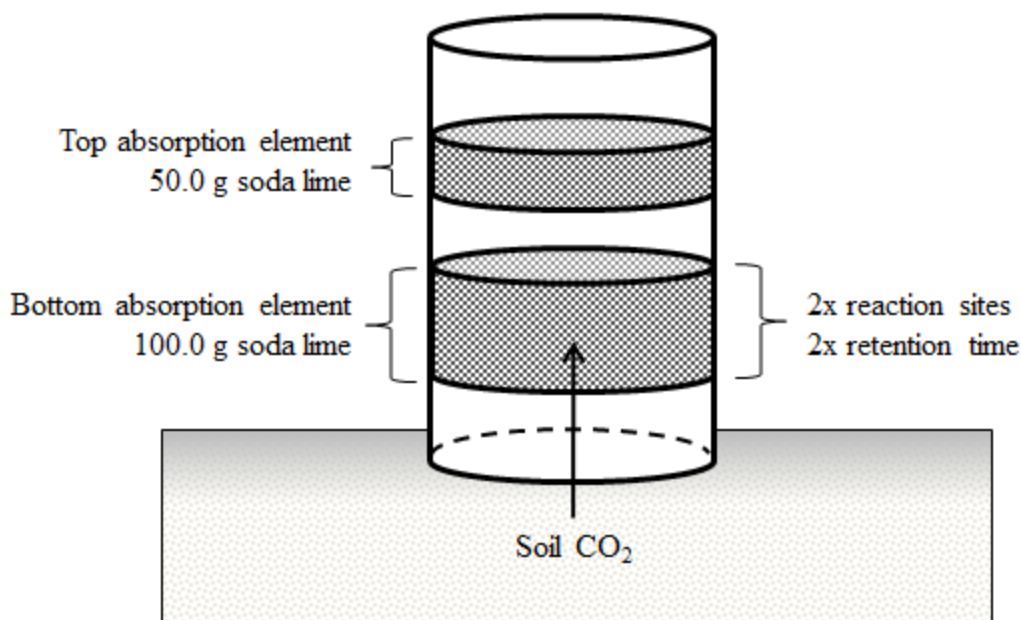


Figure 12. Schematic of modified trap with increased absorbent in bottom absorption element.

In the first set, 50.0 g of absorbent (W.R. Grace, Sodasorb[®] HP-6/12) was placed in both the top and bottom trap elements. This trap arrangement is herein referred to as the standard. In the second set, 100.0 g of the absorbent material was placed in the bottom trap element and 50.0 g of absorbent material was placed in the top trap element. In this capacity, the traps with the 100.0 g absorbent material had twice the number of reaction sites and retention time compared to the standard.

Each set of traps were tested under the same imposed flux conditions ($10.5 \pm 0.4 \mu\text{mol}/\text{m}^2/\text{s}$) and were deployed for varying amounts of time necessary to achieve approximately 5% CO₂ saturation by weight. All traps were inserted 6 cm into the soil column, leaving 26 cm of headspace between the bottom absorbent element and soil surface. Upon retrieval, traps were analyzed as described in Section 3.1.3.3.

3.3.2 CO₂ Breakthrough to Top Absorbent Element

A test was conducted to determine if CO₂ breakthrough occurred in the traps due to incomplete absorption by the bottom trap element. An additional trap with no underlying imposed CO₂ flux, herein referred to as the background trap, was deployed to measure CO₂ absorption in the top trap element due solely to absorption of atmospheric CO₂. The background trap was used to compare CO₂ mass captured by the top element to CO₂ mass captured by the top element in traps having an underlying imposed flux. In this capacity, CO₂ mass captured in excess of the background top absorption element could be attributed to breakthrough of soil CO₂ from the bottom absorption element. Figure 13 illustrates the concept of CO₂ breakthrough.

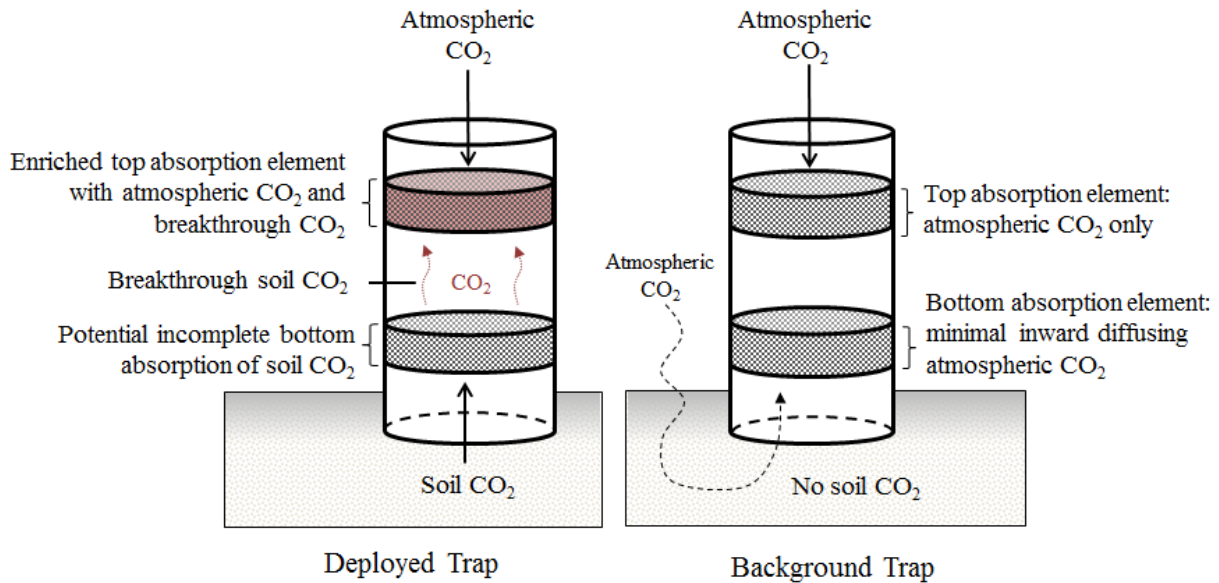


Figure 13. Conceptualization of CO₂ breakthrough in deployed traps versus background trap, assuming incomplete absorption by the bottom element.

This test was conducted under a range of the four imposed fluxes associated with the main experiment described in Section 3.1. Traps were constructed with 50.0 g soda lime in each of the top and bottom absorption elements and were deployed for varying lengths needed to achieve approximately 5% CO₂ saturation by weight. For each imposed flux, three traps were placed on top of the large column and one trap was placed on an 18.9 L bucket containing the same fine sand as the column but with no imposed CO₂ flux. The bucket was placed in the same laboratory facility next to the large column. Traps were analyzed in triplicate using gravimetric analysis described in Section 3.1.3.3.

3.3.3 Height of Bottom Absorption Element above Soil Surface

To determine if the height of the bottom absorption element above the soil surface has an effect on the accuracy of measured efflux, three different headspace heights were tested under an imposed flux of $10.5 \pm 0.4 \mu\text{mol}/\text{m}^2/\text{s}$. Headspace refers to the void space in the traps between the soil surface and bottom absorption element. One trap for each headspace height was deployed; tested headspace heights were 2.0 cm, 15.5 cm, and 26.0 cm above the soil surface (Figure 14).

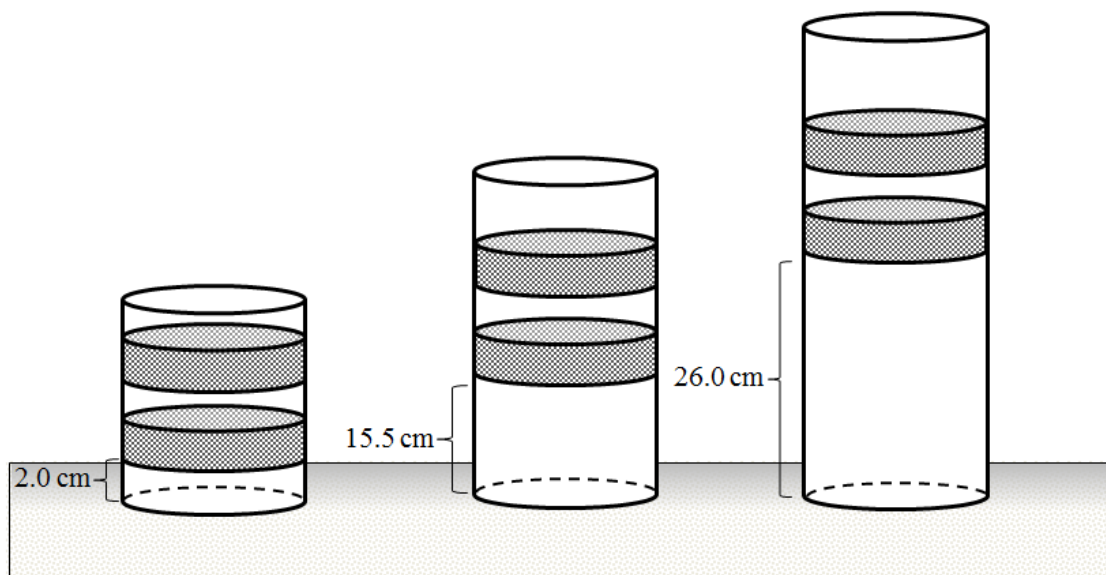


Figure 14. Schematic of varying headspace heights in trap method.

All traps were constructed with 50.0 g of soda lime in each of the top and bottom absorption elements. Traps were deployed for 8 days, allowing the traps to reach approximately 5% CO₂ saturation by weight. Upon retrieval, traps were analyzed in triplicate using gravimetric analysis described in Section 3.1.3.3.

4. MODELING

This chapter introduces an analytical model for calculating the concentration of CO₂ as a function of depth using compressible, advective-diffusive gas transport under steady state conditions. Section 4.1 presents the derivation of the model. Section 4.2 discusses the use of the model to determine the relative contributions of advective and diffusive components of gas transport.

4.1 Model Derivation

Steady state, one dimensional advective-diffusive transport of a species i in multicomponent gas through homogeneous, isotropic, porous media is described by Equation 32, assuming z increases positively in the direction of transport (Bird et al., 2002):

$$J_i = -D_i \frac{dC_i}{dz} + C_i v \quad (32)$$

where J_i is the mass flux (mass/time/area), D_i is the effective diffusion (length²/time), dC_i/dz is the vertical concentration gradient (mass/volume/time), C_i is the concentration (mass/volume), and v is the average velocity of the multicomponent gas (length/time). The average velocity of the multicomponent gas can be defined by the mass, molar, or volume average velocity (Table 5). The diffusive component of transport is given by $-D_i \frac{dC_i}{dz}$ and the advective component of transport is given by $C_i v$.

Table 5. Mass transport definitions for average velocity term of a multicomponent gas.
Modified from Bird et al., 2002.

Definition	1-D Equation	Variables
Mass	$v = \sum_{i=1}^n \omega_i v_i$	$\omega = \rho_i / \rho_T =$ mass fraction of species i $\rho_T =$ total mass concentration of all species
Molar	$v = \sum_{i=1}^n x_i v_i$	$x = C_i / C_T =$ mole fraction of species i $C_T =$ total mole concentration of all species
Volume	$v = \sum_{i=1}^n C_i v_i \bar{V}$	$\bar{V} =$ partial molar volume of species i $v_i =$ velocity of species i

Figure 15 illustrates the physical basis used in the model.

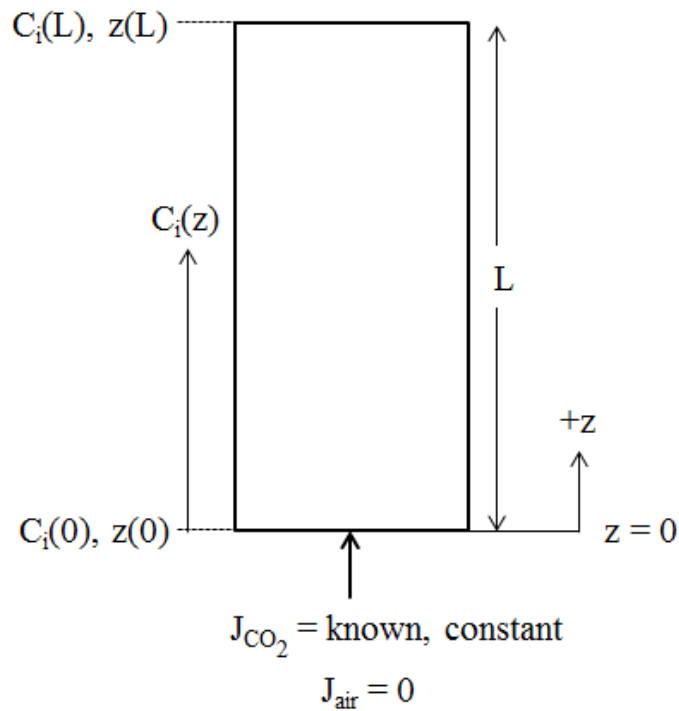


Figure 15. Physical basis for model. A known mass flux of CO_2 is imposed through the bottom of the column. The flux of air is zero.

In the case of the column experiment, the multicomponent gas consists of two gas species, air and CO₂. At steady state, air is the stagnant species and its concentration profile in the column is dependent on the constant flux of CO₂ (J_{CO_2}). For the model, air is defined as a single component composed of N₂, O₂, and other trace gases found in the atmosphere. Using the stagnant species and defining velocity using the molar average velocity definition, Equation 32 can be written as:

$$J_{air} = -D_{air} \frac{dC_{air}}{dz} + C_{air} \left(\frac{C_{air}}{C_T} v_{air} + \frac{C_{CO_2}}{C_T} v_{CO_2} \right) \quad (33)$$

Simplifying based on the assumption that the mass flux (J_{air}) and species velocity (v_{air}) are zero in the stagnant species yields:

$$D_{air} \frac{dC_{air}}{dz} = C_{air} \left(\frac{C_{CO_2} v_{CO_2}}{C_T} \right) \quad (34)$$

Separating variables and assuming $C_{CO_2} v_{CO_2}$ can be defined as J_{CO_2} at the lower boundary condition $z=0$, Equation 34 can be written as:

$$C_T D_{air} \frac{dC_{air}}{C_{air}} = J_{CO_2} dz \quad (35)$$

To account for compressibility effects of the gas species, C_T can be written as follows using the Ideal Gas Law:

$$C_T = \frac{n}{V} = \frac{P_T}{RT} \quad (36)$$

where n is the number of moles, V is volume, P_T is total pressure, R is the ideal gas constant, and T is temperature (K).

Substituting Equation 36 into Equation 35 and assuming constant total pressure and temperature throughout the system gives the following:

$$\frac{P_T}{RT} D_{\text{air}} \frac{dC_{\text{air}}}{C_{\text{air}}} = J_{\text{CO}_2} dz \quad (37)$$

Each side can be integrated to solve for concentration of air as a function of depth, where b is a dummy variable of integration:

$$\frac{P_T}{RT} D_{\text{air}} \int_{C_{\text{air}}(0)}^{C_{\text{air}}(z)} \frac{1}{C_{\text{air}}} dC_{\text{air}} = J_{\text{CO}_2} \int_0^z db \quad (38)$$

$$\frac{P_T}{RT} D_{\text{air}} \ln \left(\frac{C_{\text{air}}(z)}{C_{\text{air}}(0)} \right) = J_{\text{CO}_2} * z \quad (39)$$

Solving for $C_{\text{air}}(z)$:

$$C_{\text{air}}(z) = C_{\text{air}}(0) \exp \left(\frac{J_{\text{CO}_2} RTz}{P_T D_{\text{air}}} \right) \quad (40)$$

The total concentration of both species as a function of depth is defined using the Ideal Gas Law, where:

$$C_T(z) = \frac{P_T}{RT} = C_{\text{air}}(z) + C_{\text{CO}_2}(z) \quad (41)$$

Solving for CO₂ concentration as a function of depth and substituting Equation 40 for C_{air}(z) results in the following expression:

$$C_{\text{CO}_2}(z) = \frac{P_T}{RT} - C_{\text{air}}(0) \exp\left(\frac{J_{\text{CO}_2} RT z}{P_T D_{\text{air}}}\right) \quad (42)$$

Equation 42 can be used to compare CO₂ concentrations obtained from experimental data to model predicted CO₂ concentration as a function of depth.

4.2 Diffusive and Advective Contributions to Transport

Equation 32 can be used to determine the relative contributions of diffusive and advective CO₂ transport in the test column. The diffusive contribution ($J_{\text{CO}_2\text{Diffusion}}$) is first calculated by isolating the diffusive transport term:

$$J_{\text{CO}_2\text{Diffusion}} = -D_{\text{CO}_2} \frac{dC_{\text{CO}_2}}{dz} \quad (43)$$

Equation 43 can be solved by plugging in Equation 42 for C_{CO_2} :

$$J_{CO_2\text{Diffusion}} = -D_{CO_2} \frac{d}{dz} \left[\frac{P_T}{RT} - C_{air}(0) \exp\left(\frac{J_{CO_2} RTz}{P_T D_{air}}\right) \right] \quad (44)$$

Differentiating with respect to z :

$$J_{CO_2\text{Diffusion}} = -D_{CO_2} \left[-C_{air}(0) * \frac{J_{CO_2} RT}{P_T D_{air}} * \exp\left(\frac{J_{CO_2} RTz}{P_T D_{air}}\right) \right] \quad (45)$$

Equation 45 provides a closed-form analytical solution for determining the diffusive flux.

Alternatively, Equation 43 can be solved using experimental data, where dC_{CO_2}/dz is the measured CO_2 concentration gradient from the gradient method #1 sampling port to the lower boundary condition (LBC) sampling port:

$$J_{CO_2\text{Diffusion}} = -D_{CO_2} \left[\frac{C_{\text{gradient}\#1} - C_{LBC}}{z_{\text{gradient}\#1} - z_{LBC}} \right] \quad (46)$$

Once the diffusive flux is determined, it is compared to the total known imposed flux (J_{CO_2}) to determine the relative contribution to transport:

$$\%diffusion = \frac{J_{CO_2\text{Diffusion}}}{J_{CO_2}} * 100\% \quad (47)$$

Using the known total imposed CO₂ flux (J_{CO_2}) and the diffusive flux ($J_{CO_2\text{Diffusion}}$), Equation 32 can be rearranged to solve for the portion of transport due to advection ($J_{CO_2\text{Advection}}$):

$$J_{CO_2\text{Advection}} = J_{CO_2} - J_{CO_2\text{Diffusion}} \quad (48)$$

The advective flux is then compared to the total known imposed flux to determine the relative contribution of advective transport:

$$\% \text{advection} = \frac{J_{CO_2\text{Advection}}}{J_{CO_2}} * 100\% \quad (49)$$

5. RESULTS AND DISCUSSION

This chapter presents results from the experiments described in Chapter 3 and application of the model advanced in Chapter 4. Section 5.1 contains results and discussion from methods comparisons under ideal conditions. Section 5.2 presents results and discussion from method comparisons under low (2.2-3.6 m/s) and high (4.5-5.4 m/s) range wind speeds. Section 5.3 summarizes results and discussion from trap modification studies. Results from modeling efforts are discussed in Section 5.4. Section 5.5 provides a summary of all results in the form of a method comparison table.

5.1 Methods Comparisons under Ideal Conditions

This section presents results and discussion from laboratory studies comparing the methods using uniform porous media, constant environmental conditions, and a known CO₂ flux (i.e., ideal conditions). First, the individual performance of each method relative to the imposed fluxes is discussed. Second, the performance of each method relative to the other methods is discussed. Detailed results from statistical tests can be found in Appendix E. It is important to note that the outcomes of the statistical tests described below are limited by small sample sizes. All statistical tests presented in Section 5.1 were performed in Deducer statistical software using averaged values of each method for a given imposed flux.

5.1.1 Gradient Method

Results from the gradient method relative to the imposed fluxes are shown in Figure 16.

Statistics for each variation of the gradient method using different estimates for the effective diffusion coefficient are presented in Table 6.

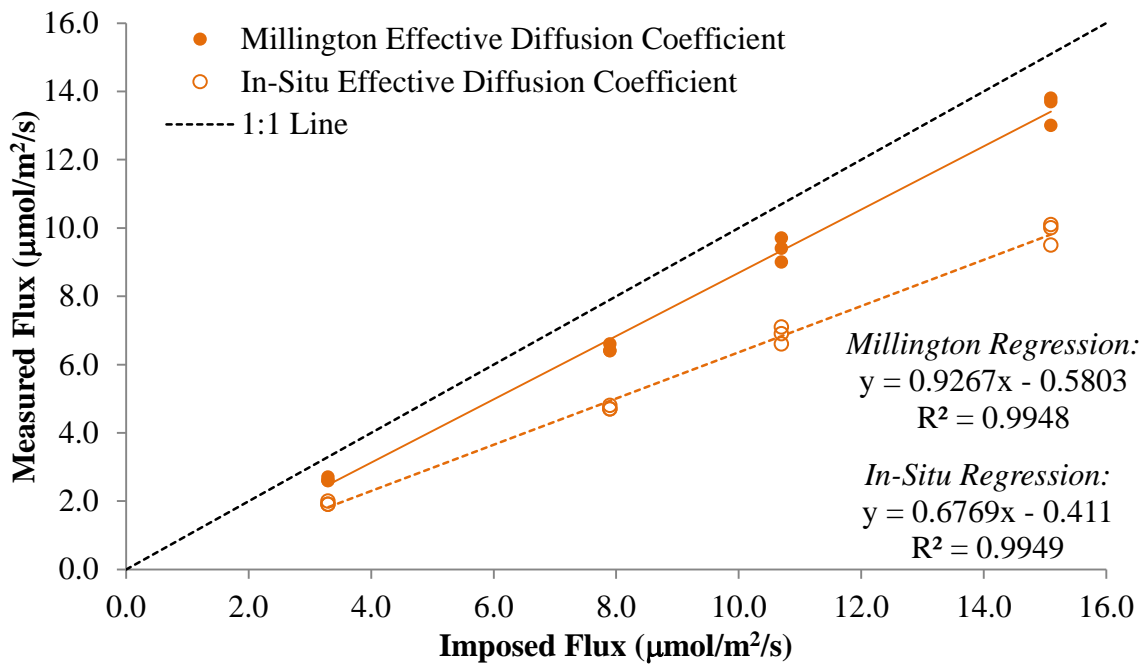


Figure 16. Triplicate results for gradient method under ideal conditions. Each individual point represents a single gradient measurement. Triplicate data is plotted for each imposed flux to illustrate variation within measurements. Standard deviations of the mean coinciding with triplicate data can be found in Table 6. Standard deviations of the imposed fluxes are not shown because they are small relative to the scale displayed. Standard deviations of the imposed fluxes can also be found in Table 6.

Table 6. Summary statistics for gradient method under ideal conditions.

Method for Calculating Effective Diffusion	Imposed Flux ($\mu\text{mol}/\text{m}^2/\text{s}$)	Average Measured Flux \pm Standard Deviation ($\mu\text{mol}/\text{m}^2/\text{s}$)	Average Difference from Imposed Flux (%)	Sample Size
Millington	15.1 ± 0.4	13.5 ± 0.4	-11	3
	10.7 ± 0.2	9.4 ± 0.4	-12	3
	7.9 ± 0.2	6.5 ± 0.1	-18	3
	3.3 ± 0.1	2.6 ± 0.1	-21	3
In-Situ	15.1 ± 0.4	9.9 ± 0.3	-34	3
	10.7 ± 0.2	6.9 ± 0.3	-36	3
	7.9 ± 0.2	4.7 ± 0.1	-41	3
	3.3 ± 0.1	1.9 ± 0.1	-42	3

For all cases, the gradient method systematically underestimated the imposed flux. Large differences were observed between the two methods for estimating the effective diffusion coefficient. The Millington method provided a more accurate prediction of the imposed flux than the In-situ method. The Millington method underestimated the imposed flux by 11-21%, whereas the In-situ method underestimated the imposed flux by 34-42%.

The Millington method is thought to have been a better predictor of the actual effective diffusion coefficient in the test column because the soil was dry and homogeneous. However, field applications of the Millington method in porous media containing mixed fluid phases are likely to produce more variation in effective diffusion estimates, leading to larger variations in measured soil gas fluxes. The accuracy of the In-situ method for estimating the effective diffusion coefficient may have been limited by assumptions in the methodology that were not valid in the test column. Following methods described in Johnson et al. (1998), the porous

media is assumed to be infinite in extent; however, the column was confined by walls that may have led to preferential flow of the tracer gas, complicating transport and quantification efforts.

Underestimations using the gradient method are primarily attributed to the method accounting for diffusive gas transport only. Interestingly, with both effective diffusion coefficient estimates, underestimations of the true flux increased as the imposed flux decreased (Table 6). These results were consistent with advective and diffusive transport contributions presented in Section 5.4 (Tables 16 and 17) using measured concentration gradients, which indicated the advective contribution to total gas transport increased as the imposed flux decreased. In this regard, the gradient method missed an increasing percentage of total CO₂ transport as the advective fraction increased.

The standard deviations about the means were minimal, ranging from ± 0.1 to ± 0.4 $\mu\text{mol}/\text{m}^2/\text{s}$. A 95% confidence interval calculated for the slope and intercept of the best fit line based on average values (n=4) of the gradient (Millington) method indicated that the slope was not significantly different from 1 and the intercept was not significantly different from zero. These results indicated the gradient (Millington) method accurately measured the imposed flux. A 95% confidence interval calculated for the slope and intercept of the best fit line based on average values (n=4) of the gradient (In-situ) method indicated that the intercept was not significantly different from 0, but the slope was significantly different from 1. These results indicated the gradient (In-situ) method did not accurately measure the imposed flux. These results also illustrate the importance of the effective diffusion coefficients on the accuracy of measured fluxes. Under field conditions, non-uniform soil properties (e.g., moisture and porosity) are

likely to lead to greater uncertainty regarding the accuracy of measured values with respect to the true values.

5.1.2 Chamber Method

Results from the chamber method relative to the imposed fluxes are shown in Figure 17.

Statistics for the chamber method using the linear and exponential regression models are presented in Table 7.

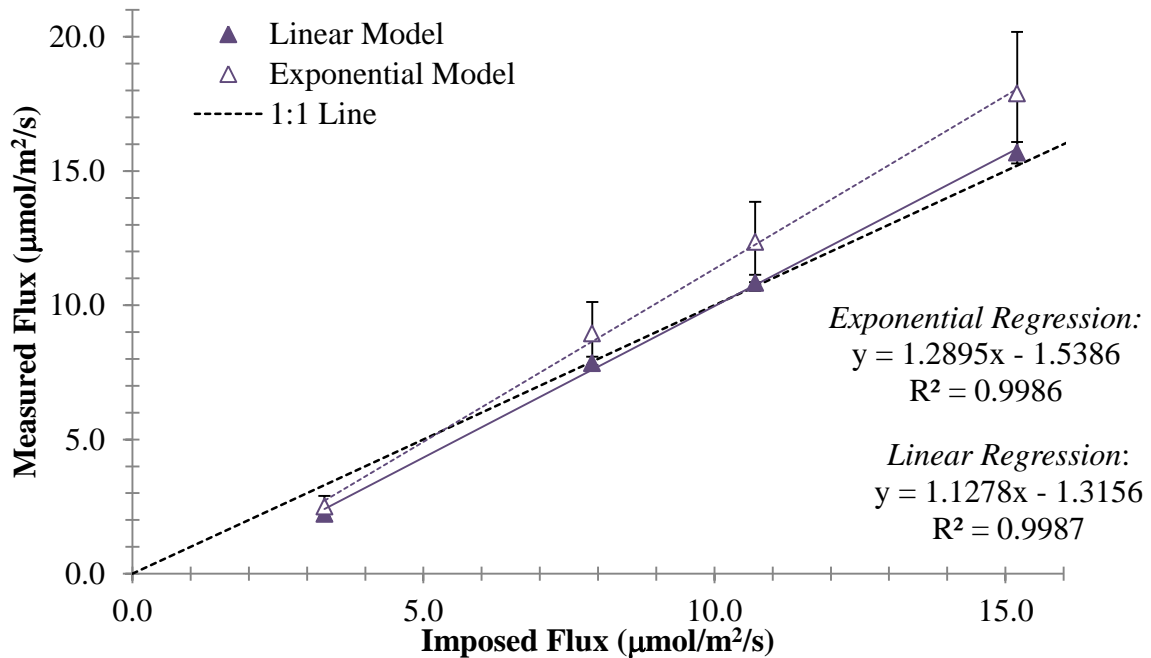


Figure 17. Results from chamber method under ideal conditions. Each point represents the mean value of all observations for a given imposed flux. Vertical bars represent standard deviation about the mean based on all samples measured for a given imposed flux. Standard deviations of the imposed fluxes are not shown because they are small relative to the scale displayed. Standard deviations of the imposed fluxes can also be found in Table 7.

Table 7. Summary statistics for chamber method under ideal conditions.

Regression Model	Imposed Flux ($\mu\text{mol}/\text{m}^2/\text{s}$)	Average Measured Efflux \pm Standard Deviation ($\mu\text{mol}/\text{m}^2/\text{s}$)	Average Difference from Imposed Flux (%)	Sample Size
Linear	15.2 \pm 0.7	15.7 \pm 0.4	+3	149
	10.7 \pm 0.2	10.8 \pm 0.3	+1	336
	7.9 \pm 0.2	7.8 \pm 0.2	-1	385
	3.3 \pm 0.1	2.2 \pm 0.1	-33	814
Exponential	15.2 \pm 0.4	17.9 \pm 2.3	+18	149
	10.7 \pm 0.2	12.4 \pm 1.5	+16	336
	7.9 \pm 0.2	8.9 \pm 1.2	+13	385
	3.3 \pm 0.1	2.5 \pm 0.4	-24	814

The chamber (linear) method showed no systematic bias. Standard deviations of the mean were minimal, ranging from ± 0.1 to $0.4 \mu\text{mol}/\text{m}^2/\text{s}$. A 95% confidence interval calculated for the slope and intercept of the best fit line using averaged values ($n=4$) of the chamber (linear) method indicated that the slope was significantly different from 1 and the intercept was significantly different than 0. These results indicated the chamber (linear) did not accurately measure the imposed flux at a statistically significant level. However, slope and intercept values fell just outside of the confidence intervals. Confidence intervals were narrow due to low standard deviations in the method. A large sample size was not a factor in the size of the confidence intervals because average values for each imposed flux were used ($n=4$).

The chamber (exponential) method overestimated the imposed flux for all test fluxes except the lowest ($3.3 \mu\text{mol}/\text{m}^2/\text{s}$). Standard deviations of the mean were much higher than observed with the chamber (linear) method, ranging from ± 0.4 to $2.3 \mu\text{mol}/\text{m}^2/\text{s}$. These were the highest among all methods. A 95% confidence interval calculated for the slope and intercept of the best fit line using averaged values ($n=4$) of the chamber (exponential) method indicated that the slope

was significantly different 1 and the intercept was significantly different from 0, also suggesting the chamber (exponential) method did not accurately measure the imposed fluxes at a statistically significant level.

The larger overestimations using the exponential regression model are attributed to the model correcting for alterations to the natural diffusion gradient that were likely not present in the column due to having a constant imposed flux. Overestimations by the exponential regression model may not be observed in the field or may be observed to a lesser extent. Additionally, differences in measured efflux between the two regression models was minimized by reducing the time interval over which the regression models were fit (refer to Figure 7).

5.1.3 Trap Method

The performance of the trap method relative to the imposed fluxes is shown in Figure 18.

Statistics for the trap method are presented in Table 8.

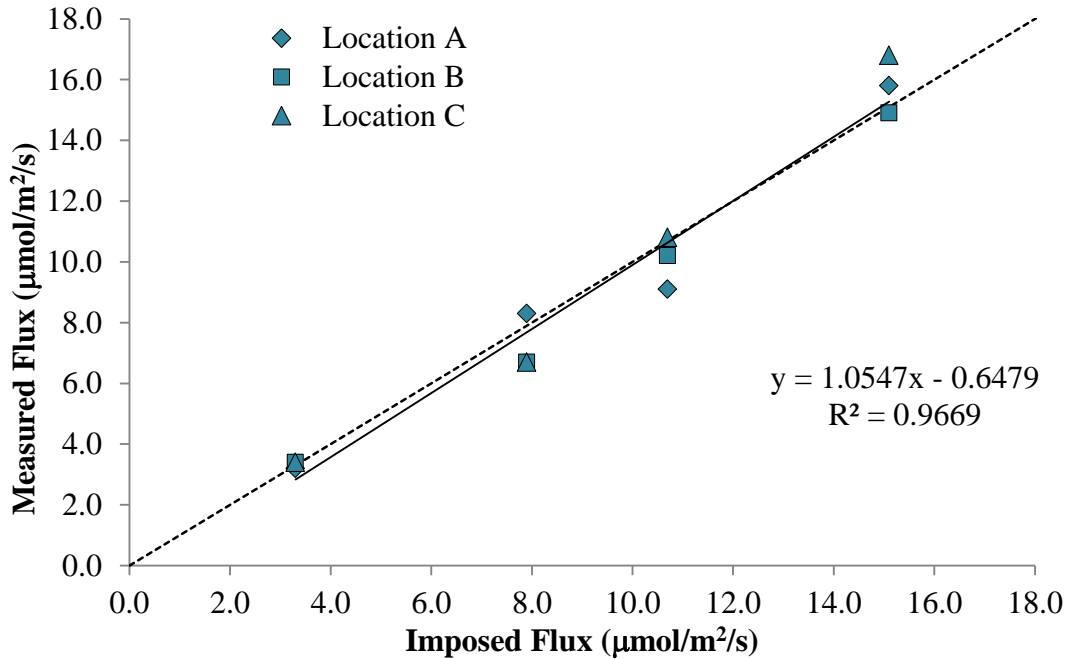


Figure 18. Triplicate results for trap method under ideal conditions. Each individual point represents a single trap measurement. Different symbols represent different trap locations on the column. Triplicate data is plotted for each imposed flux to illustrate variation within measurements and trap locations. Standard deviations of the mean coinciding with triplicate data can be found in Table 8. Standard deviations of the imposed fluxes are not shown because they are small relative to the scale displayed. Standard deviations of the imposed fluxes can also be found in Table 8.

Table 8. Summary statistics for trap method under ideal conditions. Results from individual traps are shown to illustrate no systematic bias between locations, indicative of uniform CO₂ flow through the column.

Imposed Flux (μmol/m ² /s)	Location on Column	Individual Measured Flux (μmol/m ² /s)	Average Measured Flux ± Standard Deviation (μmol/m ² /s)	Average Difference from Imposed Flux (%)	Sample Size
15.1 ± 0.4	A	15.8	15.8 ± 1.0	+5	3
	B	14.9			
	C	16.8			
10.7 ± 0.2	A	9.1	10.0 ± 0.9	-6	3
	B	10.2			
	C	10.8			
7.9 ± 0.2	A	8.3	7.2 ± 0.9	-8	3
	B	6.7			
	C	6.7			
3.3 ± 0.1	A	3.2	3.3 ± 0.1	+1	3
	B	3.4			
	C	3.4			

The trap method showed no systematic biases. The triplicate trap arrangement also showed no systematic bias, indicating flow through the column was uniform. A 95% confidence interval calculated for the slope and intercept of the best fit line using average values for each imposed flux indicated that the slope was not significantly different from 1 and the intercept was not significantly different from 0. These results suggested the trap method accurately measured the imposed flux. However, it is worth noting that the trap method had the largest confidence interval of all methods. Large confidence intervals were indicative of the relatively large and consistent observed standard deviations of the mean.

5.1.4 Method Comparisons

The average measured fluxes from each measurement method are plotted against the imposed fluxes in Figure 19.

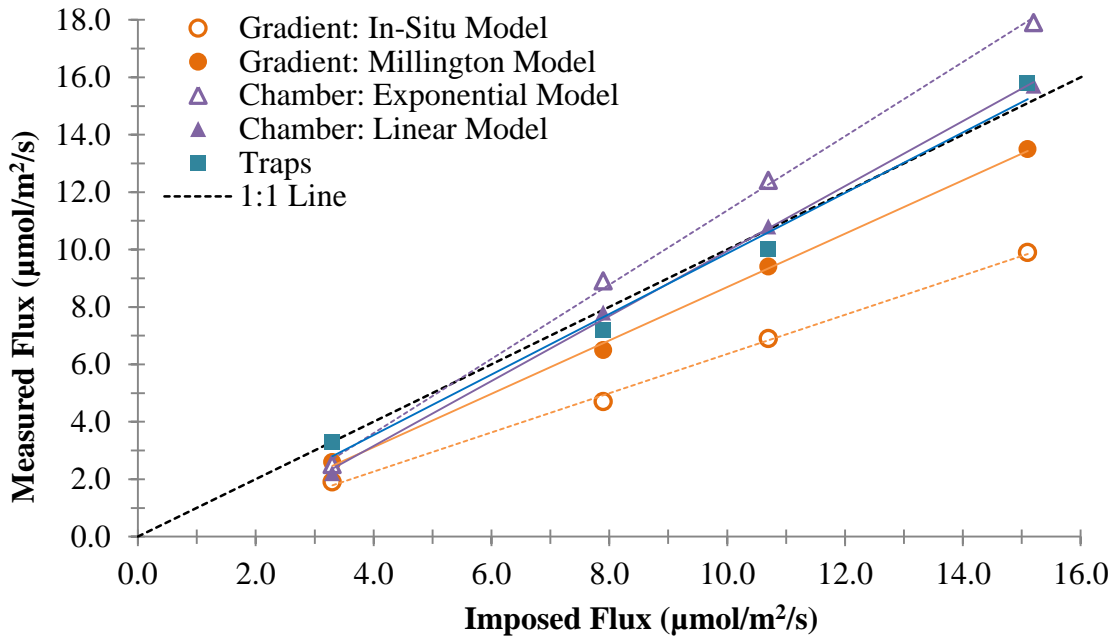


Figure 19. Comparison of average measured flux from all methods under ideal conditions.

An ANOVA test at a 95% confidence level indicated there were statistically significant differences among the slopes of the best fit linear regressions for each method. Therefore, overall rates of measuring CO_2 efflux between methods were not the same. Pairwise comparisons at 95% confidence level indicated there were not significant differences between the slopes of the gradient (Millington) and trap methods, and the chamber (linear) and trap methods. All other slope comparisons were significantly different. These results indicated the gradient, chamber, and trap methods were capable of quantitatively capturing the imposed flux at similar rates when the linear regression model was used for the chamber method and Millington

model was used for the gradient method. Further, these results once again highlight the importance of the effective diffusion coefficient on the accuracy of the gradient method. However, as previously noted, conclusions based on statistical testing should be taken with care due to small sample sizes. Many more data points are necessary to more accurately develop statistically significant relationships between the methods and imposed fluxes.

Figure 20 summarizes the overall average accuracy of each method for all imposed fluxes using the following equation:

$$\% \text{difference} = \frac{\text{measured flux} - \text{imposed flux}}{\text{imposed flux}} * 100\% \quad (50)$$

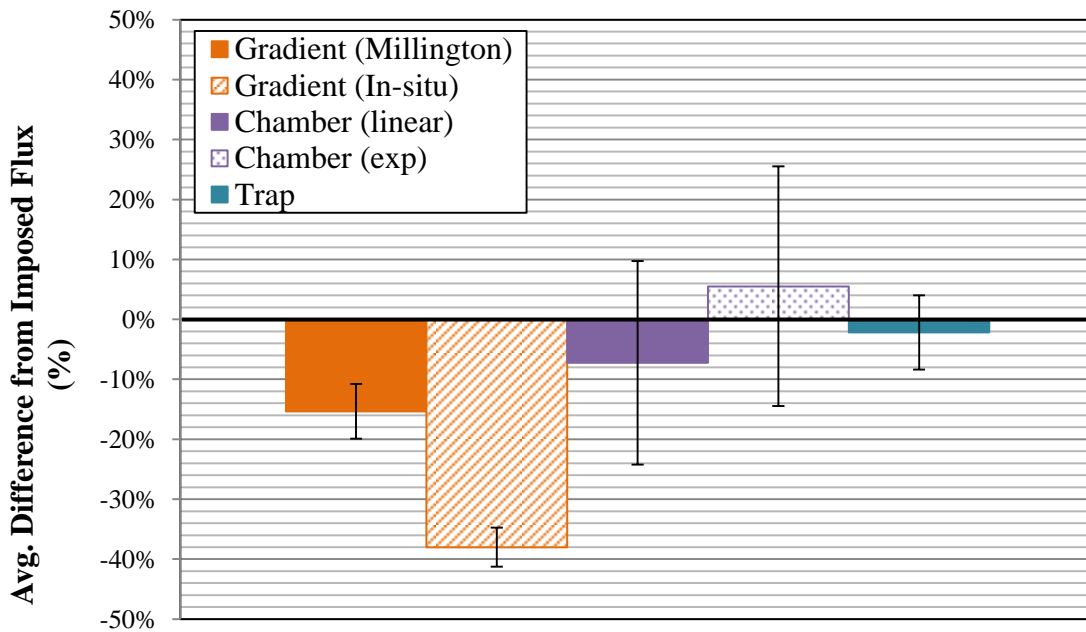


Figure 20. Average percent difference from imposed flux for each method under ideal conditions. Vertical bars represent the standard deviation of the mean for percent difference from imposed flux for each method.

Results viewed in this capacity may provide more relevant comparisons than statistical testing. For both the chamber and trap methods, the average measured fluxes were within $\pm 7\%$ of the imposed fluxes. The chamber method (both regression models) had the largest standard deviation of percent difference from the imposed fluxes. The gradient method consistently underestimated the true CO₂ flux by 15% to 38%, and the accuracy of measurements was largely dependent on the effective diffusion coefficient. Considering the accuracy of other subsurface measurements (e.g., hydraulic conductivity), the range of accuracy observed among all methods is not surprising.

5.2 Methods Comparisons under Simulated Windy Conditions

This section presents results and discussion from laboratory studies comparing the methods under imposed wind conditions. Tested wind speeds included a zero wind base case (0 m/s), low range (2.2-3.6 m/s), and high range (4.5-5.4 m/s). The inflowing rate of CO₂ remained constant for each imposed wind range; however, small variations in ambient temperature and pressure led to minor differences in the imposed flux. The imposed fluxes were 8.7 ± 0.2 , 8.6 ± 0.2 , and 8.5 ± 0.2 $\mu\text{mol}/\text{m}^2/\text{s}$ for the zero wind, low range, and high range tested wind speeds, respectively. Data presented in the following sections is presented in terms of percent difference from the imposed flux to account for the variation in imposed fluxes between tested wind speeds.

5.2.1 Gradient Method

The performance of the gradient method under simulated wind conditions is presented in Figure 21. Statistics for each wind speed and effective diffusion coefficient method are summarized in Table 9.

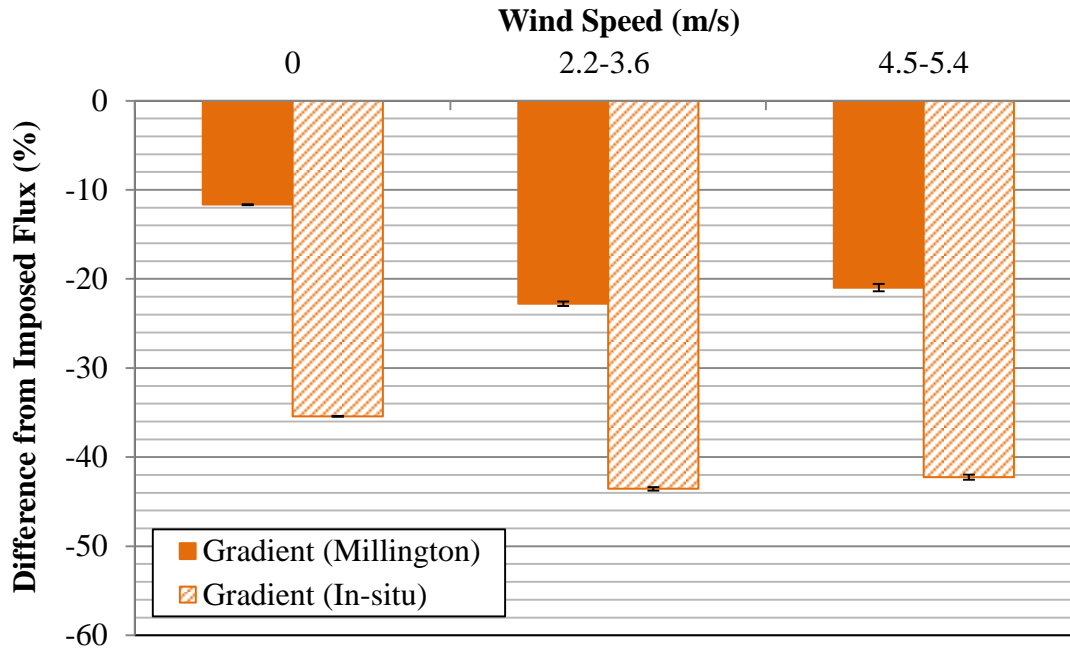


Figure 21. Results from gradient method under windy conditions. Percent difference of the average value from triplicate sampling from the imposed flux is plotted relative to wind speeds. Vertical bars represent standard deviation of the mean.

Table 9. Summary statistics for gradient method under windy conditions.

Method for Calculating Effective Diffusion Coefficient	Wind Speed	Imposed Flux ($\mu\text{mol}/\text{m}^2/\text{s}$)	Average Measured Efflux \pm Standard Deviation ($\mu\text{mol}/\text{m}^2/\text{s}$)	Average Difference from Imposed Flux (%)	Sample Size
Millington	Zero	8.7 ± 0.2	7.7 ± 0.1	-12	3
	Low	8.6 ± 0.2	6.6 ± 0.3	-23	3
	High	8.5 ± 0.2	6.7 ± 0.4	-21	3
In-situ	Zero	8.7 ± 0.2	5.6 ± 0.0	-35	3
	Low	8.6 ± 0.2	4.9 ± 0.2	-44	3
	High	8.5 ± 0.2	4.9 ± 0.3	-42	3

Figure 21 demonstrates that the gradient method was affected by wind conditions. In the absence of wind, the gradient method underestimated the imposed flux by 12% (Millington) to 35% (In-situ). These values were consistent with the results presented in Section 5.1.1. In the presence of the low range wind speeds (2.2-3.6 m/s), the gradient method underestimated the imposed flux by 23% (Millington) and 44% (In-situ). At the high range wind speeds (4.5-5.4 m/s), the gradient method underestimated the imposed flux by 21% (Millington) and 42% (In-situ).

One-tailed t-tests at a 95% confidence level indicated that the mean measured fluxes under both low and high range wind speeds were significantly less than the mean measured flux under the zero wind base case condition ($P=0.002$ and $P=0.015$ for Millington and In-situ, respectively). Furthermore, two-tailed t-tests at a 95% confidence level indicated there was no significant difference between the mean measured fluxes between the low and high range wind speeds ($P=0.858$ and $P=0.898$ for Millington and In-situ, respectively).

These results indicated that the presence of surface winds within the tested wind speed range, independent of wind speed, caused the gradient method to underestimate the true flux to a higher degree than under ideal conditions. Under field conditions, however, wind speed may have a greater effect on measurements due to non-uniform soil moisture and texture that would likely lead to the development of subsurface pressure gradients. Pressure gradients could result in advective transport not captured by the gradient method. Additionally, results from laboratory studies may have exaggerated the effect of wind on the gradient method; heterogeneities in soil

moisture and texture at field sites would provide resistance to advective transport that could mitigate the effects of wind.

5.2.2 Chamber Method

The performance of the chamber method under simulated wind conditions is presented in Figure 22. Statistics for each wind speed and regression model are summarized in Table 10.

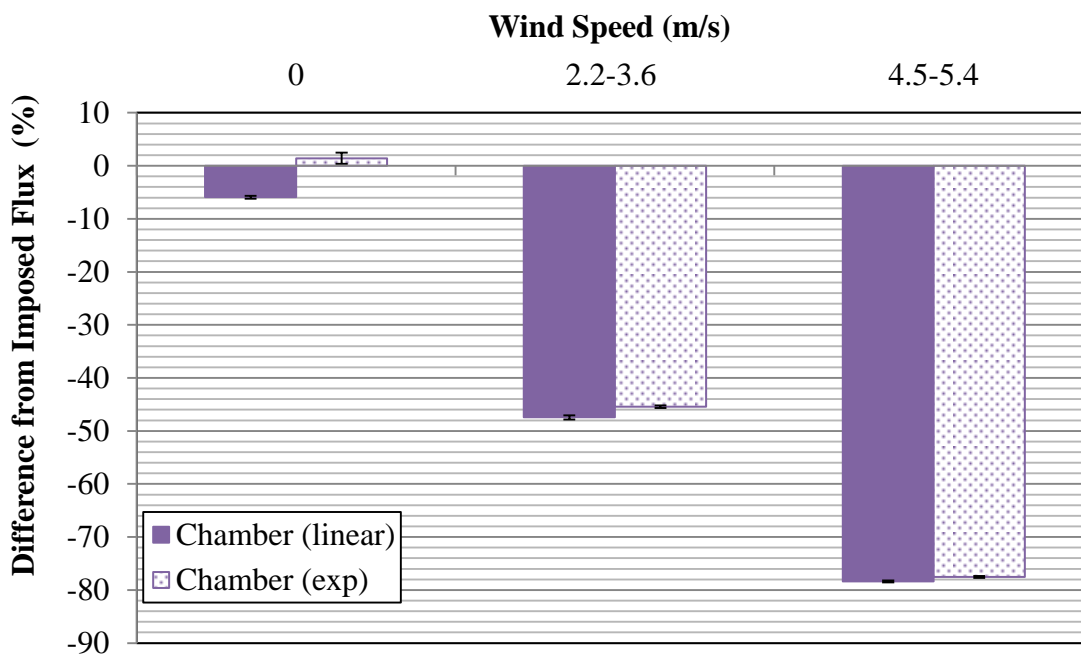


Figure 22. Results from chamber method under windy conditions. Percent difference of the average value from all samples from the imposed flux is plotted relative to wind speeds. Vertical bars represent standard deviation of the mean.

Table 10. Summary statistics for chamber method under windy conditions.

Regression Model	Wind Speed	Imposed Flux ($\mu\text{mol}/\text{m}^2/\text{s}$)	Average Measured Efflux \pm Standard Deviation ($\mu\text{mol}/\text{m}^2/\text{s}$)	Average Difference from Imposed Flux (%)	Sample Size
Linear	Zero	8.7 ± 0.2	8.2 ± 0.3	-6	462
	Low	8.6 ± 0.2	4.5 ± 0.4	-47	439
	High	8.5 ± 0.2	1.8 ± 0.2	-78	444
Exponential	Zero	8.7 ± 0.2	8.8 ± 1.0	+1	462
	Low	8.6 ± 0.2	4.7 ± 0.2	-45	439
	High	8.5 ± 0.2	1.9 ± 0.2	-78	444

Figure 22 demonstrates the chamber method was highly affected by surface winds. In the absence of winds, the chamber method underestimated the imposed flux by 6% with the linear regression model and overestimated the imposed flux by 1% with the exponential model. These results were consistent with those found in Section 5.1.2 under ideal conditions. In the presence of the low range wind speeds (2.2-3.6 m/s), the chamber method underestimated the imposed flux by 47% (linear) and 45% (exponential). At the high range wind speeds (4.5-5.4 m/s), the chamber method underestimated the imposed flux by 78% for both models.

Mechanisms explaining underestimation by the chamber method are not fully understood. A potential explanation is that wind caused lateral gas transport to occur within soil near the surface, causing CO_2 transport around the chamber instead of into the chamber. Results from laboratory studies may have been exaggerated due to the soil being dry. Heterogeneities in soil moisture and texture at field sites would provide additional resistance to advective transport that could mitigate the effects of lateral gas transport.

One-tailed t-tests at a 95% confidence level indicated that the mean measured fluxes under both low and high range wind speeds were significantly less than the mean measured flux under the zero wind base case condition ($P=0.000$ for both regressions). Furthermore, one-tailed t-tests indicated significant differences existed between the mean measured fluxes of the low range and high range wind speeds for both regression models ($P=0.000$ for both regressions). P-values were highly significant in all cases due to large sample sizes. These results indicated that surface winds within the tested range caused the chamber method to underestimate the true flux relative to ideal conditions. Additionally, the accuracy of the chamber method was dependent on wind speed; higher wind speeds resulted in larger underestimations of the true flux compared to lower wind speeds.

5.2.3 Trap Method

The performance of the trap method under windy conditions is presented in Figure 23 and Table 11.

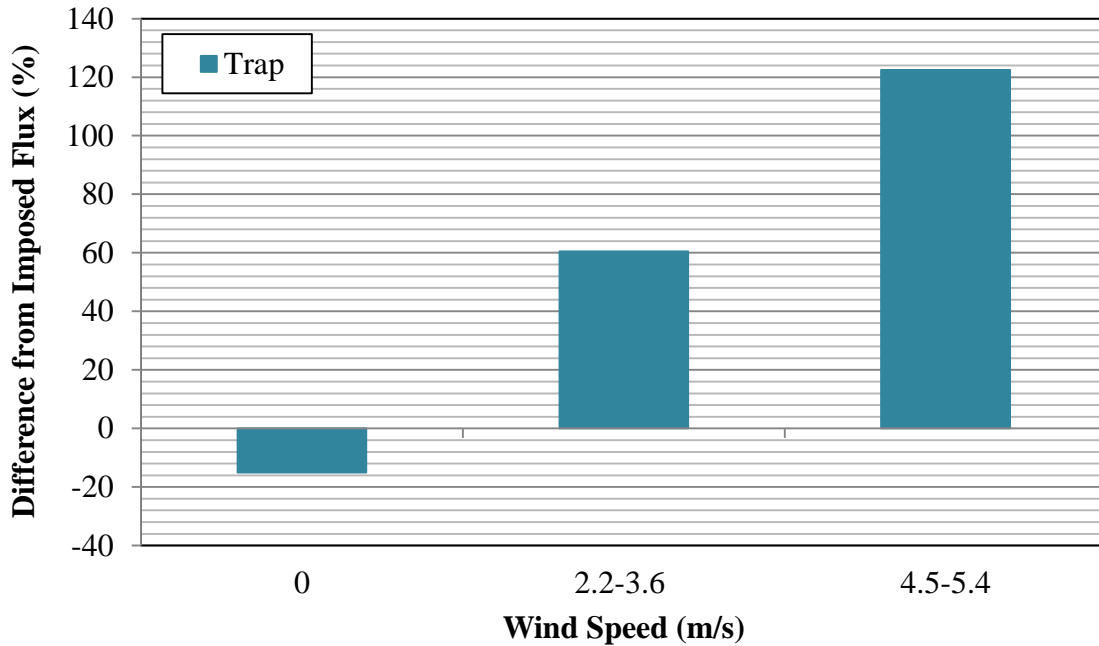


Figure 23. Results from trap method under windy conditions. Percent difference from the imposed flux is presented for a single trap value for each wind speed range.

Table 11. Summary of trap method under windy conditions.

Wind Speed	Imposed Flux ($\mu\text{mol}/\text{m}^2/\text{s}$)	Measured Efflux ($\mu\text{mol}/\text{m}^2/\text{s}$)	Difference from Imposed Flux (%)	Sample Size
Zero	8.7 ± 0.2	7.4	-15	1
Low	8.6 ± 0.2	13.8	+60	1
High	8.5 ± 0.2	18.9	+122	1

Figure 23 suggest the trap method was strongly affected by surface winds. In the absence of winds, the trap method underestimated the imposed flux by 15%. This was a larger underestimation than observed in Section 5.1.3 under ideal conditions. In the presence of the

low range wind speeds, the trap method overestimated the imposed flux by 60%. At the high range wind speeds, the trap method overestimated the imposed flux by 122%.

No quantifiable pressure differences were observed between the trap headspace and ambient air, although this may have been a limitation of the experimental design rather than an indication that no pressure differentials developed as a result of the wind. A working hypothesis is that the relatively large size of the rain cover may enhance the effect of wind on efflux measurements by acting as a blunt body object, creating drag and/or convective currents within the apparatus. Drag and convective currents may alter gas flow in and around the trap, affecting measurement accuracy. A lower profile rain cover may help to reduce these potential effects and improve accuracy of the trap method in windy conditions. Similar to the gradient and chamber methods, results from the trap method under windy conditions may have been exaggerated due to the soil being dry.

Statistical testing was not conducted on trap results because only one trap was tested due to space limitations on top of the column. These results represent an exploratory effort and further work is needed. Despite the preliminary nature of the results, Figure 23 suggests that surface winds within the tested wind speed range caused the trap method to overestimate the true flux relative to ideal conditions. Additionally, the accuracy of the trap method was apparently dependent on wind speed; higher wind speeds resulted in a much larger overestimate of the true flux compared to the lower range of wind speeds.

5.3 Trap Modification Studies

This section presents results and discussion from trap modification studies. Section 5.3.1 discusses the effect of increasing absorbent mass in the bottom trap element. Section 5.3.2 presents data related to tests for CO₂ breakthrough from the bottom trap element to the top trap element. Section 5.3.3 discusses the effect of the height of the bottom trap element from the soil surface on the accuracy of efflux measurements.

5.3.1 Mass of Absorbent in Bottom Element

The results of increasing the absorbent mass in the bottom trap element relative to the imposed flux are shown in Figure 24.

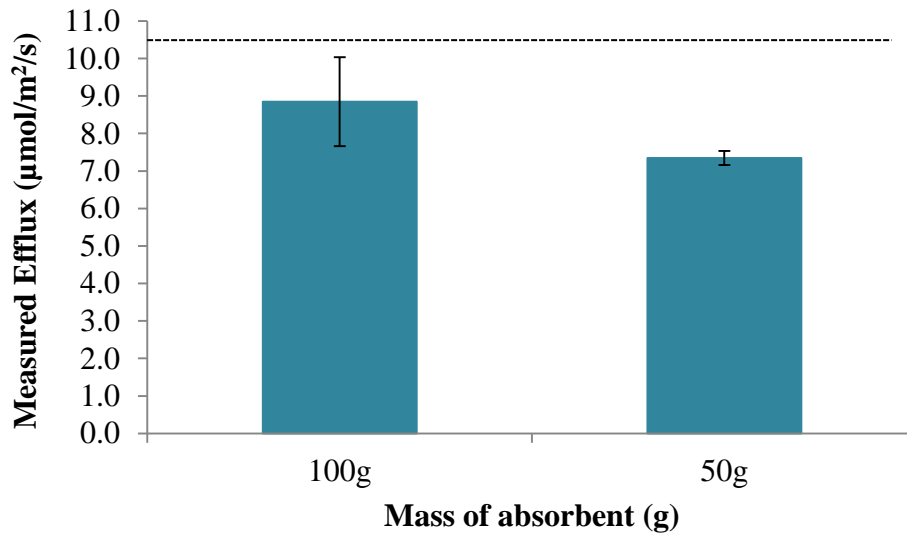


Figure 24. Triplicate results for mass of absorbent material in bottom trap element versus measured efflux. The black dashed line represents the imposed flux of $10.5 \pm 0.4 \mu\text{mol}/\text{m}^2/\text{s}$. Vertical bars represent standard deviation of the mean.

The dashed black line represents the imposed flux of $10.5 \pm 0.4 \mu\text{mol}/\text{m}^2/\text{s}$. The trap with 100.0 g absorbent in the bottom trap element measured an efflux of $8.8 \mu\text{mol}/\text{m}^2/\text{s}$, whereas the trap with 50.0 g absorbent in the bottom trap element measured an efflux of $7.3 \mu\text{mol}/\text{m}^2/\text{s}$. A two-tailed t-test at a 95% confidence level indicated there was no statistical difference between the measured effluxes (P two-tail = 0.157). However, it can be noted that both trap configurations measured effluxes less than the imposed flux.

5.3.2 CO₂ Breakthrough to Top Absorbent Element

The measured CO₂ fluxes from top absorbent elements in the background trap and traps deployed on the column are summarized in Table 12. The background trap value is from a single measurement. The value for deployed traps is an average of three individual traps.

Table 12. Potential CO₂ breakthrough to top absorbent element.

Imposed Flux ($\mu\text{mol}/\text{m}^2/\text{s}$)	Average Measured Flux from Deployed Bottom Trap Element ($\mu\text{mol}/\text{m}^2/\text{s}$)	Measured Flux from Background Trap Top Element ($\mu\text{mol}/\text{m}^2/\text{s}$)	Average Measured Flux from Deployed Traps Top Element ($\mu\text{mol}/\text{m}^2/\text{s}$)	Avg. Measured Top Element–Background ($\mu\text{mol}/\text{m}^2/\text{s}$)	Avg. Measured % Difference from Background (%)
15.1	15.8	2.4	2.8	0.4	+17
10.7	10.0	3.1	3.7	0.6	+19
7.9	7.2	4.0	4.8	0.8	+20
3.3	3.3	8.0	8.0	0.0	0

At the three highest imposed fluxes, the top absorbent elements on deployed traps captured 17-20% higher CO₂ fluxes than the background trap. At the lowest imposed flux, the top absorbent elements on deployed traps captured the same flux as the background trap. These results suggested CO₂ breakthrough from the bottom absorbent element to the top absorbent element may have occurred at higher range fluxes. However, it is important to note that this was a preliminary effort to understand if CO₂ breakthrough occurred and no statistical validation of results was conducted. Further studies are needed to gain better insight into the possibility of CO₂ breakthrough and implications for measurement accuracy.

5.3.3 Height of Bottom Absorption Element above Soil Surface

The effect of the height of the bottom absorbent element from the soil surface on the measured efflux is summarized in Figure 25.

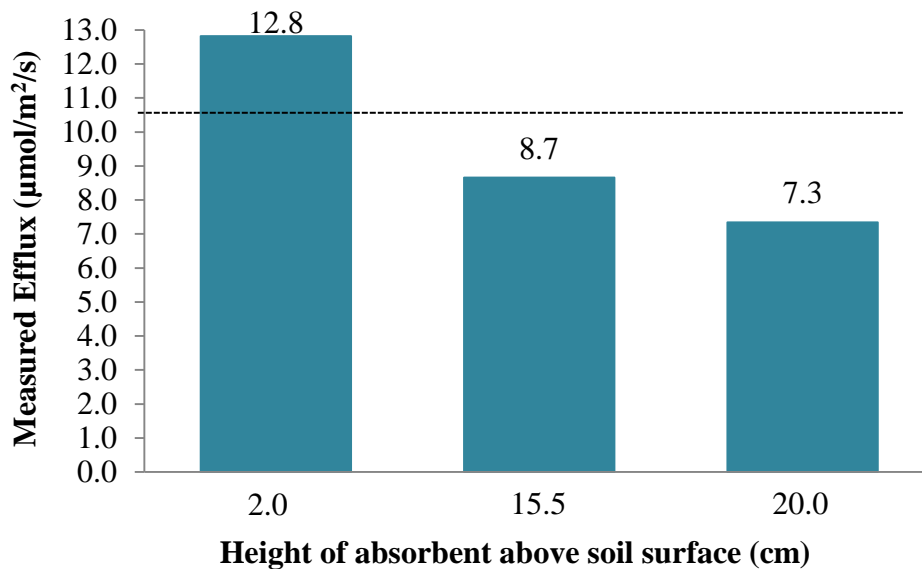


Figure 25. Height of bottom absorbent element from soil surface versus measured efflux. The black dashed line represents the imposed flux of $10.5 \pm 0.4 \mu\text{mol}/\text{m}^2/\text{s}$.

The imposed flux was $10.5 \pm 0.4 \mu\text{mol}/\text{m}^2/\text{s}$. Results indicated that when the absorbent was just above the soil surface (2.0 cm from soil surface, zero insertion depth), the measured efflux overestimated the imposed flux by 22%. At a height of 15.5 cm, corresponding to the recommended maximum insertion depth of 7 inches (17.8 cm) recommended by McCoy (2012), the measured efflux underestimated the imposed flux by 18%. At a height of 20.0 cm, corresponding to the same insertion depth as the chamber soil collar (6.0 cm), the imposed flux was underestimated by 30%. Statistical testing was not conducted to determine if each of the measured effluxes were significantly different from one another because each measured efflux is based off of a single trap measurement. However, Figure 25 suggests the height of the bottom absorbent element above the soil surface may have affected the accuracy of measured efflux. When the bottom absorbent element was closer to the soil surface, the measured efflux was greater than when the bottom absorbent element was further from the soil surface.

This experiment was conducted assuming CO_2 transport from the soil column to the trap absorption elements consisted of one-dimensional, vertical transport. Due to this assumption, the insertion depth was not standardized between traps. However, results suggested gas transport was not one-dimensional. For the trap placed 2.0 cm above the surface, the overestimation of the imposed flux can be explained by the bottom absorbent element absorbing CO_2 from surrounding areas not directly underneath the trap receiver. While a zero insertion depth scenario would not occur in field applications of the trap method, the results do suggest the insertion depth may play a role in the accuracy of the method. The presence of the trap receiver in the soil column is likely creating a boundary in which CO_2 transport is restricted to vertical transport only; variations in the insertion depth may influence the extent in which CO_2 transport

is restricted to vertical flow. Until further resolution regarding insertion depth and height of the bottom absorbent from the soil surface is achieved, it is recommended by the author that the trap receiver be inserted a depth of 7 inches as specified by McCoy (2012).

5.4 Modeling

Section 5.4.1 summarizes the performance of the model relative to experimental data. Results from ideal conditions are presented in Section 5.4.1.1 and results from windy conditions are presented in Section 5.4.1.2. Next, diffusive and advective contributions to transport are discussed in Section 5.4.2. Transport contributions under ideal conditions are first presented, followed by transport contributions under windy conditions.

5.4.1 Model versus Experimental Data

Equation 41 was used to compare CO₂ concentrations obtained from experimental data to model predicted CO₂ concentration as a function of depth. The effective diffusion coefficient for air was calculated using the same methods and assumptions described in Section 3.1.2.1. The molecular diffusion of air was defined as $2.02 \times 10^{-5} \text{ m}^2/\text{s}$ at T=20°C (Haynes, 2015), using an equimolar mixture of N₂ and O₂ as the reference system because a molecular diffusion coefficient for a molar mixture comparable to air was not found. Differences in molecular diffusion coefficients between the different molar mixtures were assumed negligible.

Table 13 summarizes the calculated effective diffusion coefficients for air that served as inputs for the model.

Table 13. Effective diffusion coefficients for air

Method	Effective Diffusion Coefficient for air at T=20°C (m²/s)
Millington	5.95 x 10 ⁻⁶
In-situ	4.40 x 10 ⁻⁶

5.4.1.1 Model versus Experimental Data under Ideal Conditions

Figures 26 through 29 present the model results given the conditions in the column and the effective diffusion coefficients in Table 13. The “Millington Model” refers to Equation 41 using the effective diffusion coefficient for air as determined by the Millington method. The “In-situ Model” refers to Equation 41 using the effective diffusion coefficient for air as determined by the In-situ tracer method. Each variation of the model was compared to average values of CO₂ concentration profiles that were measured under ideal experimental conditions described in Chapter 3.1.

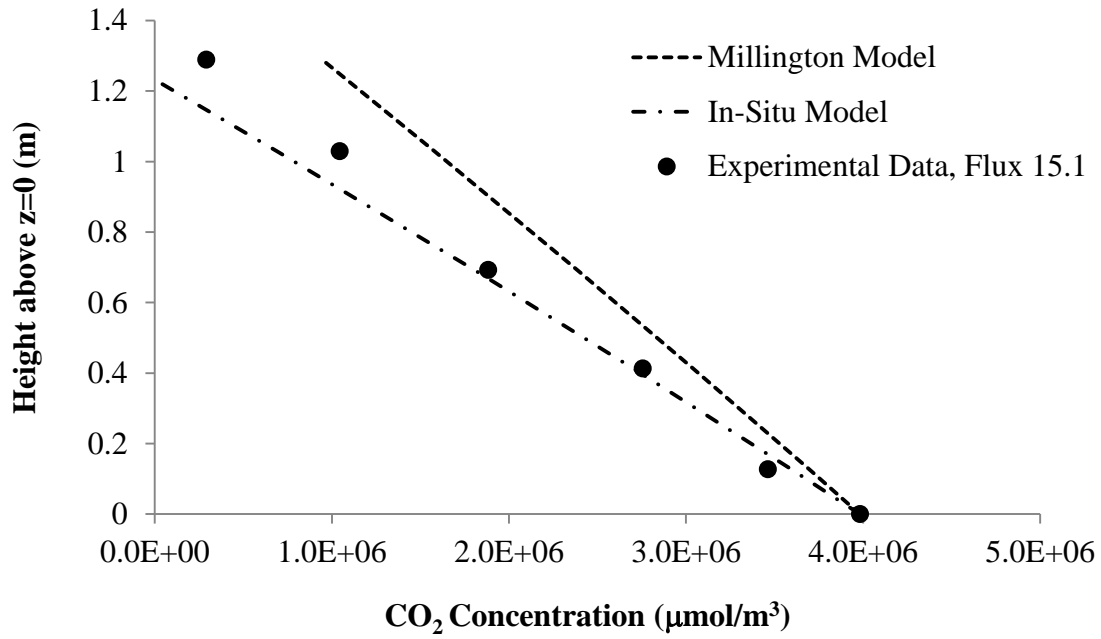


Figure 26. Experimental data versus model for imposed flux of $15.1 \pm 0.4 \mu\text{mol/m}^2/\text{s}$ under ideal conditions.

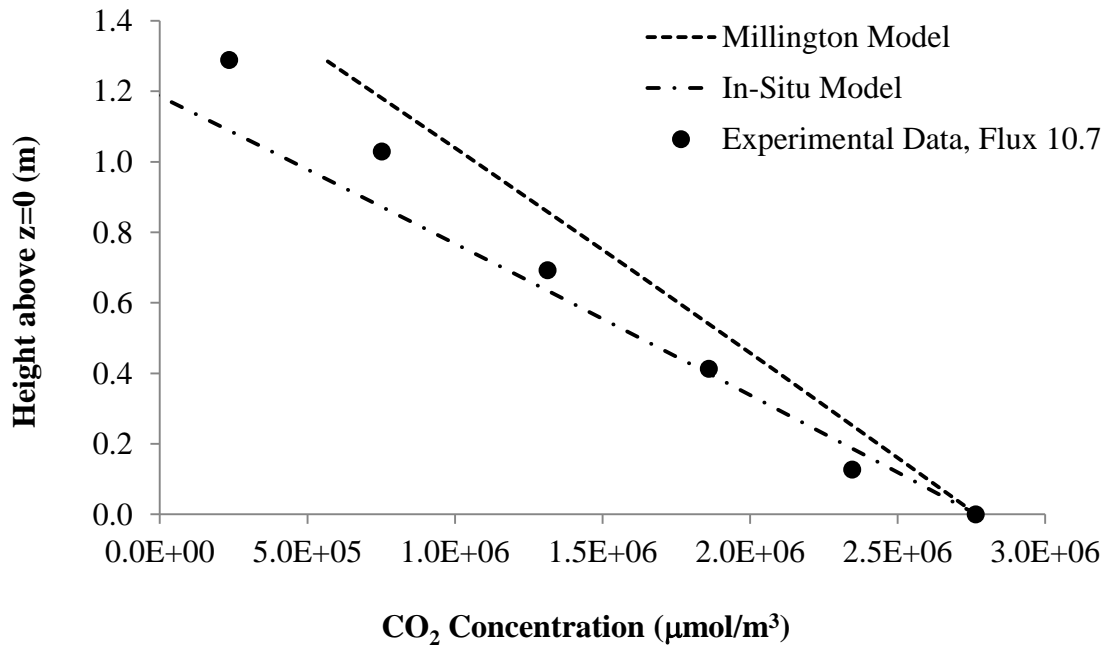


Figure 27. Experimental data versus model for imposed flux of $10.7 \pm 0.2 \mu\text{mol/m}^2/\text{s}$ under ideal conditions.

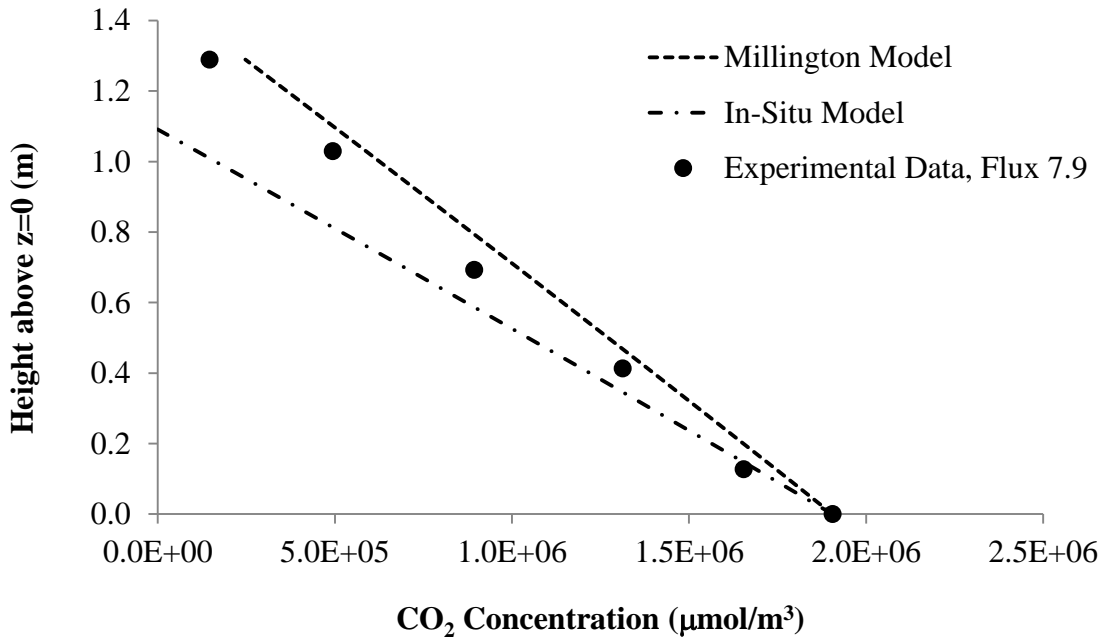


Figure 28. Experimental data versus model for imposed flux of $7.9 \pm 0.2 \mu\text{mol/m}^2/\text{s}$ under ideal conditions.

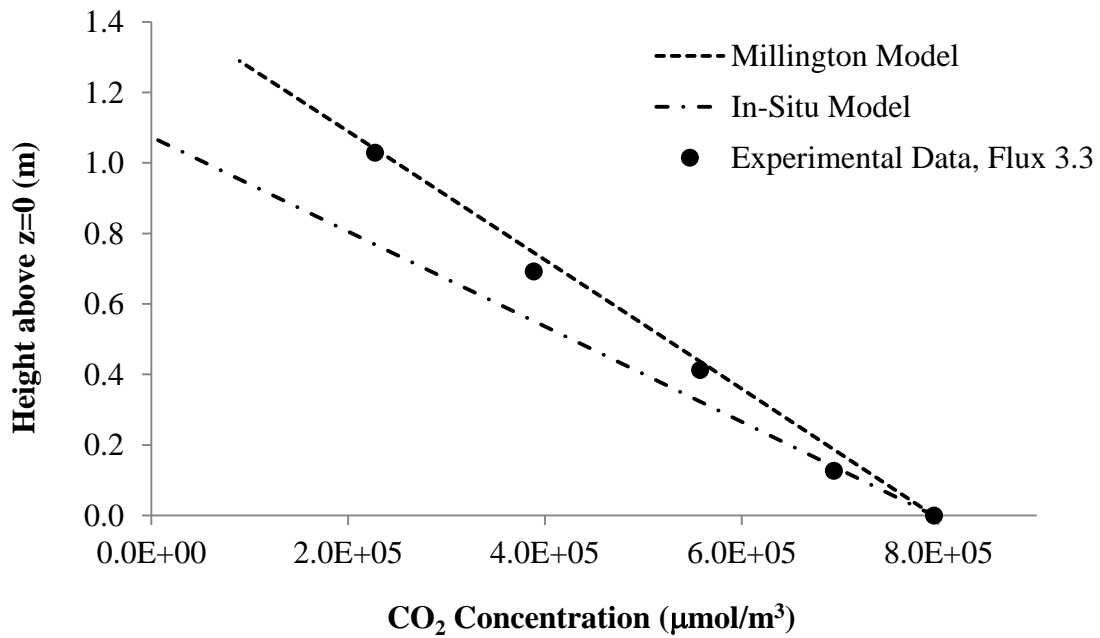


Figure 29. Experimental data versus model for imposed flux of $3.3 \pm 0.1 \mu\text{mol/m}^2/\text{s}$ under ideal conditions.

The data from each imposed CO₂ flux falls within model-predicted values. Initially, the experimental data more closely matched the Millington model. As the imposed CO₂ flux increased, the experimental data more closely matched the In-situ model. Differences between the experimental data and models illustrate challenges with accurately estimating an effective diffusion coefficient and quantifying CO₂ concentration profiles in the column.

5.4.1.2 Model versus Experimental Data under Windy Conditions

Figures 30 through 32 illustrate the performance of the model under windy conditions using each of the effective diffusion coefficients for air.

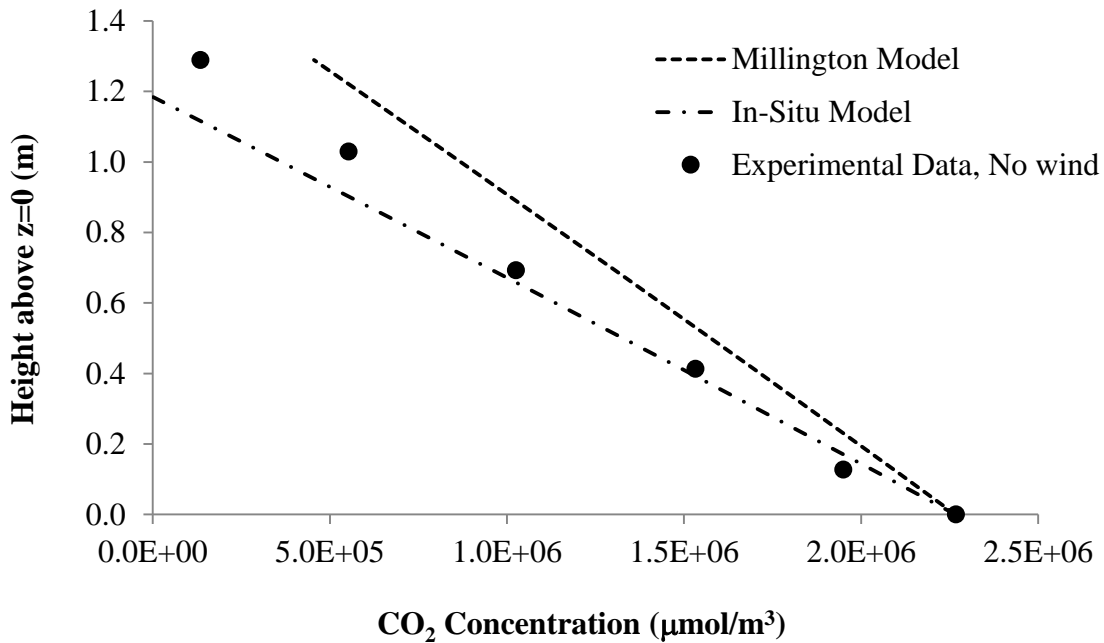


Figure 30. Experimental data versus model for imposed flux $8.7 \pm 0.2 \mu\text{mol}/\text{m}^2/\text{s}$ under no wind, base case conditions.

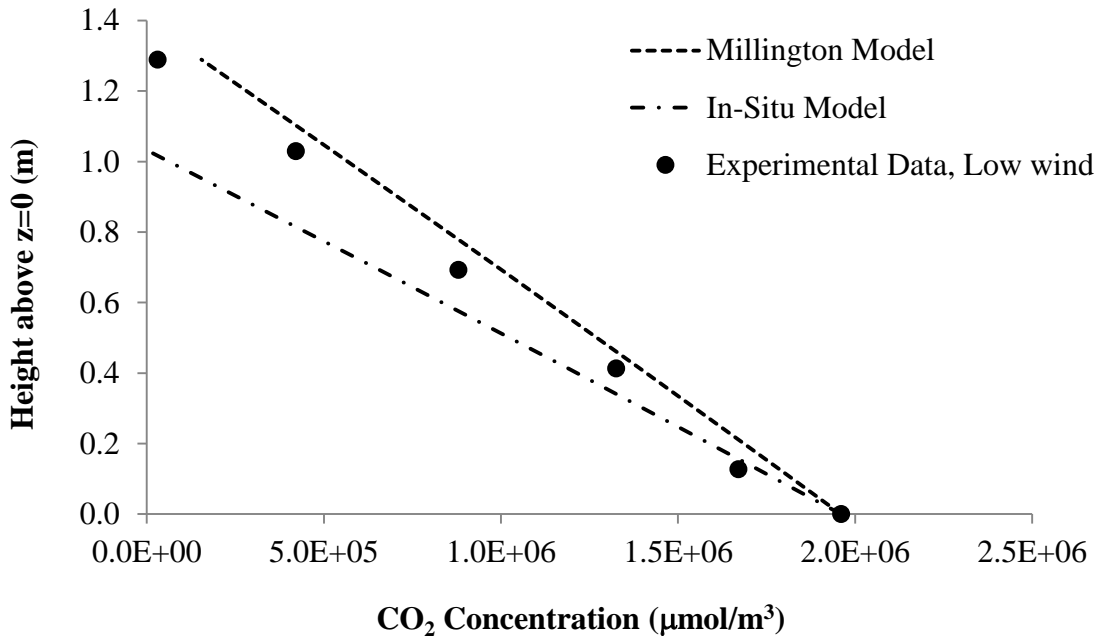


Figure 31. Experimental data versus model for imposed flux $8.6 \pm 0.2 \mu\text{mol}/\text{m}^2/\text{s}$ under low wind conditions.

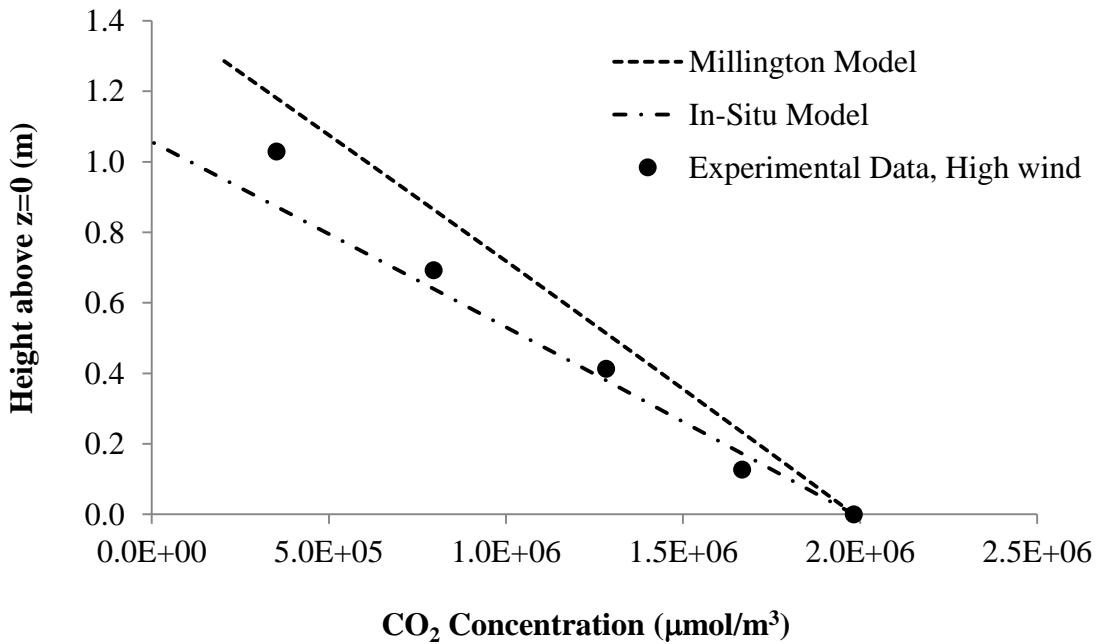


Figure 32. Experimental data versus model for imposed flux $8.5 \pm 0.2 \mu\text{mol}/\text{m}^2/\text{s}$ under high wind conditions.

The concentration vs. depth data from each imposed CO₂ flux closely matched the concentration versus depth profile predicted by each variation of the model; however, the model does not account for subsurface pressure differentials caused by surface winds. These results indicated that subsurface CO₂ concentration profiles were not noticeably affected by surface winds. Similar to results under ideal conditions, measured concentration data fell within model predicted concentration profiles. Differences between the experimental data and models once again illustrate challenges with accurately quantifying CO₂ concentrations and in determining an accurate effective diffusion coefficient.

5.4.2 Diffusive and Advective Contributions to Transport

Diffusive and advective transport processes are presented using both the closed-form analytical solution (Equation 44) and the measured concentration gradient (Equation 45) to calculate the diffusive component. In all scenarios using Equation 44, z was defined as the total column height (1.52 m).

5.4.2.1 Diffusive and Advective Contributions to Transport under Ideal Conditions

Table 14 summarizes the diffusive and advective contributions of CO₂ transport in the column experiment under ideal conditions using the Millington model for determining the effective diffusion coefficient for CO₂. Table 15 presents the same data but uses the In-situ method to determine the effective diffusion coefficient.

Table 14. Diffusive and advective contributions to transport under ideal conditions using the Millington model to determine the effective diffusion coefficient for CO₂.

Millington		Closed-form analytical solution		Measured concentration gradient	
Imposed CO ₂ Flux (μmol/m ² /s)	Test Condition	Diffusive (%)	Advective (%)	Diffusive (%)	Advective (%)
3.3	Ideal	79.4	20.6	79.1	20.9
7.9	Ideal	79.5	20.5	81.6	18.4
10.7	Ideal	79.0	21.0	86.6	13.4
15.1	Ideal	78.5	21.5	89.5	10.5

Table 15. Diffusive and advective contributions to transport under ideal conditions using the In-situ method to determine the effective diffusion coefficient for CO₂.

In-situ		Closed-form analytical solution		Measured concentration gradient	
Imposed CO ₂ Flux (μmol/m ² /s)	Test Condition	Diffusive (%)	Advective (%)	Diffusive (%)	Advective (%)
3.3	Ideal	58.0	42.0	57.8	42.2
7.9	Ideal	58.1	41.9	59.6	40.4
10.7	Ideal	57.7	42.3	63.3	36.7
15.1	Ideal	57.4	42.6	65.4	34.6

From Tables 14 and 15, the diffusive and advective contributions using the analytical solution showed little variation as the imposed flux was altered. Using the Millington model, the diffusive component decreased by 0.9% between the highest and lowest imposed fluxes. With the In-situ method, the diffusive component increased by 0.6% between the highest and lowest imposed fluxes. However, using the measured concentration gradient, an interesting pattern emerged. As the imposed flux was reduced, the advective contribution to transport increased. These results are counterintuitive to expected results. With the Millington model, the advective component increased by 10.4% between the highest and lowest imposed fluxes. Similarly, the advective component increased by 7.6% between the highest and lowest imposed fluxes using the In-situ method. Advection rates using the Millington model are similar to those modeled in

Molins et al. (2010) using CH₄ fluxes, suggesting the magnitude of advective flow through the column was reasonable with respect to gas transport processes at field sites.

Tables 14 and 15 also illustrate the importance of the effective diffusion coefficient on transport mechanisms. A larger estimate of the effective diffusion coefficient (as with the Millington model) will result in a larger contribution from diffusive transport. As the estimate for the effective diffusion coefficient decreases, the contribution from advective transport becomes more important.

5.4.2.2 Diffusive and Advective Contributions to Transport under Windy Conditions

Table 16 summarizes the diffusive and advective contributions of CO₂ transport in the column experiment under windy conditions using the Millington model for determining the effective diffusion coefficient for CO₂. Table 17 presents the same data but uses the In-situ method to determine the effective diffusion coefficient.

Table 16. Diffusive and advective contributions to transport under windy conditions using the Millington model to determine effective diffusion coefficient for CO₂.

Millington		Closed-form analytical solution		Measured concentration gradient	
Imposed CO₂ Flux (μmol/m²/s)	Test Condition	Diffusive (%)	Advective (%)	Diffusive (%)	Advective (%)
8.7	No wind	79.1	20.9	89.8	10.2
8.6	Low wind	79.7	20.3	82.2	17.8
8.5	High wind	79.6	20.4	88.0	12.0

Table 17. Diffusive and advective contributions to transport under windy conditions using the In-situ model to determine effective diffusion coefficient for CO₂.

In-situ		Closed-form analytical solution		Measured concentration gradient	
Imposed CO₂ Flux (μmol/m²/s)	Test Condition	Diffusive (%)	Advective (%)	Diffusive (%)	Advective (%)
8.7	No wind	57.8	42.2	65.6	34.4
8.6	Low wind	58.3	41.7	60.1	39.9
8.5	High wind	58.2	41.8	64.3	35.7

Tables 16 and 17 illustrate that diffusive and advective transport components were not affected by surface winds. These results agreed with conclusions reached in Section 5.4.1.2. It was hypothesized that surface winds would create pressure differentials, thereby increasing advective flow through the column. However, this was not observed in the data. Using the analytical solution, both methods for estimating the effective diffusion coefficient showed very little variation in transport components under all test conditions.

Data from measured concentration gradients showed only a 1.8% (Millington) and 1.3% (In-situ) increase in advective transport between the base case conditions with no wind and the highest imposed wind speed. The highest contribution from advective transport was observed under low imposed wind speeds. However, the estimate of advective transport at low wind speeds agreed with trends shown in Tables 14 and 15 in the absence of wind. Thus, wind had no observable effect on transport components. These results may be explained by the soil being completely dry; surface wind may have a greater effect on soils having higher moisture contents in which subsurface pressure gradients can develop.

5.5 Summary of Results

Table 18 summarizes the relative merits of each method. Table 18 is based on conclusions reached in this thesis, findings observed in the literature, discussion with field users, and the theory each method is founded on. Additionally, Table 18 is color coded to reflect opinions of the author with respect to each characteristic. Green indicates a positive attribute of the method or advantage over an alternate method(s). Yellow indicates a cautionary attribute the user should be aware of prior to selecting/using a method. Red indicates an attribute which may invalidate the use of a method in a particular field situation. White represents attributes in which current understanding is incomplete and more research is needed to reach appropriate conclusions.

All methods performed within a range of accuracy common to other subsurface measurements under ideal conditions; windy conditions caused more variation among methods. Given similar performance under ideal conditions, method selection should be based primarily on site-specific attributes, including environmental factors. Site specific attributes to consider include: depth to water table; the presence of artificial surfaces; the prevalence and magnitude of wind and precipitation; the complexity of subsurface soil texture; water quality and buffer capacity; the extent of limestone in the formation; and suspected NSZD mechanisms. Other considerations include site objectives and data needs.

Table 18. Relative merits of methods.

Characteristic	Method		
	Gradient	Chamber	Trap
Intrusiveness of method	Intrusive. Subsurface sampling required.	Minimal. System is deployed at ground surface and soil collar is inserted centimeters into the soil ^[e] .	Minimal. System is deployed at ground surface and trap receiver is inserted up to 18 centimeters into the soil ^[i] .
Period of measurement	Instantaneous	Instantaneous or long-term depending on equipment.	Time averaged integral value ^[j, k] .
Time to results	Weeks. Time includes sample analysis and data reduction.	Real time field values.	Weeks. Time is required for trap deployment, sample analysis, and data reduction ^[i, j, k] .
Level of effort required	High. Requires installation of sampling systems, collection of gas samples, determination of effective diffusion coefficients, and data reduction ^[a] .	Moderate. Requires training to use properly. Method is easy to transport and capable of making multiple measurements in a short time period.	Low. Placement of traps at field sites requires minimal effort. Traps are sent to an independent lab for analysis.
NSZD mechanism(s) measured	Volatilization and biodegradation ^[a] .	Biodegradation, assuming CH ₄ oxidation ^[f]	Biodegradation, assuming CH ₄ oxidation ^[f]
Transport process quantified	Diffusive ^[a]	Advective and diffusive ^[f]	Advective and diffusive ^[f, k]
Correction for natural soil respiration	Depends on location of gas sampling ports. Measurements can be made below depth of background O ₂ utilization and CH ₄ production, eliminating need to correct for natural soil respiration ^[a] .	Required. Can be corrected for using stable carbon and radiocarbon isotope analysis ^[d] or background correction method ^[g] . Isotope analysis requires collection of gas samples in the field.	Required. Can be corrected for using stable carbon and radiocarbon isotope analysis ^[d] or background correction method ^[g] . Gas samples for isotope analysis can be obtained during trap analysis ^[k] .
Influence of barometric pumping	Method provides instantaneous snapshot of subsurface gas profiles which may be subject to barometric pumping ^[b] .	Depends on period of measurement. Survey measurements provide an instantaneous snapshot of CO ₂ efflux which may be subject to barometric pumping ^[h] . Long-term measurements provide insight into variations caused by changes in atmospheric pressure.	Method is an integral measurement designed to capture variation due to barometric pumping ^[k] .

= Positive
 = Cautionary
 = Limitation
 = Incomplete understanding

	Method		
	Gradient	Chamber	Trap
Influence of surface wind	Low. Depends on soil texture and moisture content ^[b, c] . Surface wind may affect subsurface gas distributions if soil texture is relatively coarse and moisture content is relatively high.	Potential influence. Surface winds resulted in underestimations of the true flux in laboratory studies. Field studies are needed to fully understand effect of wind.	Potential influence. Surface winds resulted in overestimations of the true flux in laboratory studies. Field studies are needed to fully understand effect of wind.
Influence of precipitation and/or soil moisture	Method is not well suited for shallow aquifer applications due to difficulties estimating effective diffusion coefficients near the water table and capillary fringe. Effective diffusion coefficients are highly sensitive to changes in soil moisture ^[a, b] .	Fully saturated soils can shut down soil gas efflux, making measurements impossible following precipitation events.	Rain cover may prevent wetting of underlying soil ^[j] , causing rain shadow in which preferential flow can develop. More research is needed to determine effect of precipitation on trap measurements.
Influence of artificial surfaces/heterogeneities	Effective diffusion coefficients are highly sensitive to changes in soil moisture and texture caused by subsurface heterogeneities. Artificial surfaces may lead to accumulation of select gas species leading to small apparent concentration gradients ^[d] .	Method cannot be used on artificial surfaces. Subsurface heterogeneities may affect measurements if soil collar is inserted through a lower permeability material, creating a preferential pathway for gas flow that does not occur naturally.	Method cannot be used on artificial surfaces. Subsurface heterogeneities may affect measurements if trap receiver is inserted through a lower permeability material, creating a preferential pathway for gas flow that does not occur naturally.
Unique Niche	Capped sites	Site wide surveys	Longer term sampling

^[a] Johnson et al., 2006, ^[b] Maier and Schack-Kirchner, 2014, ^[c] Poulson and Møldrup, 2006, ^[d] Coffin et al., 2008, ^[e] LI-COR, 2010, ^[f] Molins et al., 2010, ^[g] Sihota et al., 2011, ^[h] Wyatt et al., 1995, ^[i] McCoy, 2012, ^[j] Zimbron et al., 2013, ^[k] McCoy et al., 2014. Statements without references are based on general knowledge pertaining to the method, discussion with field users, and opinions of the author.

6. CONCLUSIONS

6.1 Main Objectives and Primary Conclusions

The objective of this thesis was to conduct a laboratory comparison of the gradient, chamber, and trap methods using uniform porous media, constant environmental conditions, and a known CO₂ flux (i.e., ideal conditions). Preliminary efforts were also made to understand the effect of surface wind on the measurement methods. Overall goals of the thesis were to provide the relative merits of each method to support guidelines for appropriate method selection.

Secondary objectives included efforts to test design features specific to the trap method to support continued method development, and to advance a model to describe steady-state advective and diffusive gas transport through porous media.

Primary conclusions are that, under ideal conditions, the chamber and trap methods were in agreement and accurately measured the imposed flux within an acceptable range of uncertainty ($\pm 7\%$, on average). The gradient method consistently underestimated the imposed flux (up to 38%, on average). Considering the accuracy of measurements for other subsurface processes, the range of accuracy observed among all methods is not surprising.

All methods were adversely affected by wind. Given similar results under ideal conditions, wind and other environmental factors common to field conditions are suspected to be the primary cause of disagreement observed in side-by-side comparisons of the methods at field sites. Each method has advantages and limitations for field application. It is recommended that method selection be driven by site-specific attributes, including environmental factors that may make one

method more applicable over another for a given field site. Further consideration of all methods under environmental conditions may provide greater insight into potential biases and support additional recommendations for method selection. The following sections summarize results in more detail.

6.2 Detailed Results

6.2.1 Laboratory Method Comparisons under Ideal Conditions

Under ideal laboratory conditions, all methods were able to capture the true flux within a range of uncertainty common to subsurface measurements. The gradient method consistently underestimated the true flux. On average, estimates were 15-38% less than the imposed flux and varied with estimates of the effective diffusion coefficient. Consistent underestimations were attributed to the method only accounting for diffusive transport. The chamber method, on average, estimated the true flux to within $\pm 7\%$ and showed the largest standard deviations in the accuracy of measurement values compared to the other methods. The trap method, on average, estimated the true flux to within 2%.

Furthermore, ensuring the methods were properly used was a critical step in obtaining accurate results. For the gradient method, proper procedure included accurately quantifying CO₂ concentrations and obtaining a representative estimate of the effective diffusion coefficient. For the chamber method, critical steps included making sure a tight seal existed between the soil collar and chamber, as well as properly interpreting the data analysis outputs to ensure relative agreement between linear and exponential regression models. For the trap method, the height of

the bottom absorbent element from the soil surface and insertion depth of the receiver may affect measurements.

6.2.2 Laboratory Method Comparisons under Windy Conditions

Preliminary efforts indicated that all three methods were affected by surface winds within the tested wind speed range. It is important to note that wind speeds at field sites may commonly exceed the range of wind speeds used in laboratory experiments; however, the magnitude of laboratory results may have been exaggerated relative to what would be expected at field sites due to the laboratory sand being dry.

Wind caused the gradient method to further underestimate CO₂ flux, and measurements were within 44% of the imposed value. Underestimations were independent of wind speed, which was likely due to the laboratory soil being dry. Under field conditions, wind speed may have a greater effect on measurements due to non-uniform soil moisture and texture that could lead to development of subsurface pressure gradients.

With the chamber method, wind caused measurements to underestimate the true flux relative to ideal conditions. The accuracy of the chamber method was dependent on wind speed; the chamber method underestimated the true flux by 45-47% for the lower wind speed range (2.2-3.6 m/s) and by 78% for the higher wind speed range (4.5-5.4 m/s). The opposite behavior was observed with the trap method. Wind caused the traps to overestimate the true flux; the trap method overestimated the true flux by 60% for the lower wind speed range (2.2-3.6 m/s) and by 122% for the higher wind speed range (4.5-5.4 m/s). These results suggest wind may play a

critical role in explaining different rates of NSZD observed in field applications with respect to both method repeatability and method comparisons.

6.2.3 Trap Modification Studies

Preliminary efforts indicated the height of the bottom absorbent element above the soil surface (i.e. headspace) and insertion depth of the receiver may affect the accuracy of measurements. Relationships between insertion depth, headspace height, and measurement accuracy are not fully understood; additional testing may provide greater insight. Until further resolution is achieved, it is recommended by the author that the trap receiver be inserted to a depth of 7 inches, as specified by McCoy (2012). Additionally, results suggested breakthrough of soil CO₂ from the bottom absorbent element to the top absorbent element may have occurred at higher imposed fluxes. The mass of absorbent material in the bottom trap element was not found to affect the accuracy of measurements.

6.2.4 Modeling

An analytical model was presented to describe steady-state advective and diffusive gas transport through porous media. Agreement between experimental data and model-predicted CO₂ concentration profiles was sensitive to effective diffusion coefficient estimates and accurate quantification of measured concentration gradients. Application of the model to laboratory data indicated transport was diffusion dominated. Transport components were not affected by changing the imposed flux. However, measured concentration gradients indicated the advective contribution to transport increased as the imposed flux decreased. These results are counterintuitive to what would be expected.

6.3 Recommendations for Method Selection

The reader is referred to Table 19 (pg. 91-92) for a summary of current understanding of the merits and limitations of each method. Based on the similar performance of all methods under ideal conditions, wind and other environmental factors common to field conditions are suspected to be the primary cause of disagreement observed in side-by-side method comparisons at field sites. Each method has advantages and limitations and applicability of methods to field sites will vary. It is recommended that method selection be based primarily on site-specific attributes that may make one method more applicable than another for a particular field site. Careful evaluation of site attributes may reduce challenges and potential biases associated with environmental factors. Site specific attributes to consider include: depth to water table; the presence of artificial surfaces; the prevalence and magnitude of wind and precipitation; the complexity of subsurface soil texture; water quality and buffer capacity; the extent of limestone in the formation; and suspected NSZD mechanisms. Other considerations include site objectives and data needs.

6.4 Recommendations for Future Work

The following sections list recommendations for future work that build on conclusions reached in this thesis. Widespread use of all three methods is ongoing at field sites; the following ideas are not intended to represent limitations that must be overcome before the use of all methods can be continued. The following ideas are suggested purely as a means for obtaining greater insight into questions raised in this thesis.

6.4.1 Subsurface Pressure Gradients

Measurement of subsurface pressure gradients using a multi-level sampler may improve the gradient method by accounting for advective transport. This addition could provide better insight into transport mechanisms, resulting in more accurate estimates of subsurface gas fluxes and corresponding LNAPL loss rates.

6.4.2 Effects of Environmental Factors on Methods

Environmental factors are likely responsible for much of the inconsistencies observed in field applications of the methods. Preliminary efforts indicate wind affects the gradient, chamber, and trap methods in different ways. Additional testing is recommended using field soils to determine the effect of wind over a larger range of wind speeds and imposed CO₂ fluxes. Furthermore, the effects of precipitation, soil moisture, and barometric pumping on the accuracy of measurement methods are not fully understood. Given specific project needs, further studies may be warranted with respect to environmental factors, including wind.

6.4.3 Further Trap Development

Additional research and method development for the trap method could be undertaken to resolve issues raised in this thesis, including insertion depth of the receiver, headspace height, and potential design limitations such as the rain cover. A lower profile rain cover may help to reduce the effects of wind on the trap method and improve measurement accuracy. Further areas of development include understanding the effect of precipitation on trap measurements. A working hypothesis is that the trap receiver may prevent water from infiltrating the soil contained within

the receiver, thereby creating a preferential pathway for gas flow through the apparatus. The effect of convective currents on gas transport through the trap method as the result of wind and solar heating is also not fully understood and may warrant further study.

6.4.4 Modeling of Chamber and Trap Methods

At the time of this thesis, modeling studies are ongoing at the University of British Columbia led by Dr. Uli Mayer. It is hoped that modeling of the chamber and trap methods will provide insight into other variables that may affect the accuracy of surface measurement methods. Potential variables to test include: soil moisture content and precipitation; density of repacked soil in chamber soil collar and trap receiver apparatus; insertion of soil collar or receiver through heterogeneous media; and effect of absorbent saturation in trap method on measurement accuracy.

6.4.5 Thermal Fluxes as an Indicator of NSZD

Ongoing work by Colorado State University at the time of this thesis suggests that thermal fluxes from LNAPL bodies associated with NSZD can be used to estimate rates of NSZD. Thermal fluxes may overcome challenges associated with measuring gas fluxes. Once the method is more fully developed, thermal fluxes should be included as a method for quantifying rates of LNAPL NSZD and be ranked with the gradient, chamber, and trap methods.

7. REFERENCES

- Amos, R.T., K.U. Mayer, B.A. Bekins, G.N. Delin, and R.L. Williams. 2005. Use of dissolved and vapor-phase gases to investigate methanogenic degradation of petroleum hydrocarbon contamination in the subsurface. *Water Resources Research* 41, no. 2: W02001.
- Amos, R.T. and K.U. Mayer. 2006a. Investigating the role of gas bubble formation and entrapment in contaminated aquifers: Reactive transport modeling. *Journal of Contaminant Hydrology* 87, no. 1-2: 123-154.
- Amos R.T. and K.U. Mayer. 2006b. Investigating ebullition in a sand column using dissolved gas analysis and reactive transport modeling. *Environmental Science & Technology* 40, no. 17: 5361-5367.
- Bird, R.B., Stewart, W.E., and Lightfoot, E.N. 2002. *Transport Phenomena*. New York: John Wiley and Sons.
- Bauer, H.P., Beckett, P.H.T. and Bie, S.W., 1972. A rapid gravimetric method for estimating calcium carbonate in soils. *Plant and Soil* 37, no. 3: 689-690.
- Chaplin, B.P., G.N. Delin, R.J. Baker, and M.A. Lahvis. 2002. Long-term evolution of biodegradation and volatilization rates in a crude oil-contaminated aquifer. *Bioremediation Journal* 6, no. 3: 237-255.
- Coffin, R.B., J.W. Pohlman, K.S. Grabowski, D.L. Knies, R.E. Plummer, R.W. Magee, and T.J. Boyd. 2008. Radiocarbon and stable carbon isotope analysis to confirm petroleum natural attenuation in the vadose zone. *Environmental Forensics* 9, no. 1: 75-84.
- Davidson, E.A., K. Savage, L.V. Verchot, and R. Navarro. 2002. Minimizing artifacts and biases in chamber-based measurements of soil respiration. *Agricultural and Forest Meteorology* 113, no. 1-4: 21-37.
- Haynes, W.M. 2015. *CRC Handbook of Chemistry and Physics, 95th Edition*. Boca Raton, FL: Taylor & Francis Group, LLC.
- Hirsch, A.I., S.E. Trumbore, and M.L. Goulden. 2003. Direct measurement of the deep soil respiration accompanying seasonal thawing of a boreal forest soil. *Journal of Geophysical Research* 108, no. D3: WFX 2-1-WFX 2-10.
- ITRC. 2009. *Evaluating Natural Source Zone Depletion at Sites with LNAPL*. LNAPL-1. Washington, DC: Interstate Technology and Regulatory Council.

- Irianni-Renno, M. 2013. Biogeochemical characterization of a LNAPL body in support of STELA. Fort Collins, Colorado: Civil and Environmental Engineering, Colorado State University.
- Jassal, R., A. Black, M. Novak, K. Morgenstern, Z. Nestic, and D. Gaumont-Guay. 2005. Relationship between soil CO₂ concentrations and forest-floor CO₂ effluxes. *Agricultural and Forest Meteorology* 130, no. 3-4: 176-192.
- Johnson, P.C., C. Bruce, R.L. Johnson, and M.W. Kemblowski. 1998. In situ measurement of effective vapor-phase porous media diffusion coefficients. *Environmental Science & Technology* 32, no. 21: 3405-3409.
- Johnson, P., P. Lundegard, and Z. Liu. 2006. Source zone natural attenuation at petroleum hydrocarbon spill sites—I: Site-specific assessment approach. *Ground Water Monitoring & Remediation* 26, no. 4: 82-92.
- Kabwe, L.K., M.J. Hendry, G.W. Wilson, and J.R. Lawrence. 2002. Quantifying CO₂ fluxes from soil surfaces to the atmosphere. *Journal of Hydrology* 260, no. 1-4: 1-14.
- Kimball, B.A. and E.R. Lemon. 1971. Air turbulence effects upon soil gas exchange. *Soil Science Society of America Journal* 35, no. 1: 16-21.
- Lahvis, M.A. and A.L. Baehr. 1996. Estimation of rates of aerobic hydrocarbon biodegradation by simulation of gas transport in the unsaturated zone. *Water Resources Research* 32, no. 7: 2231-2249.
- Lahvis, M.A., A.L. Baehr, and R.J. Baker. 1999. Quantification of aerobic biodegradation and volatilization rates of gasoline hydrocarbons near the water table under natural attenuation conditions. *Water Resources Research* 35, no. 3: 753-765.
- Lahvis, M.A., A.L. Baehr, and R.J. Baker. 2004. Evaluation of volatilization as a natural attenuation pathway for MTBE. *Ground Water* 42, no. 2: 258-267.
- LI-COR. 2010. *LI-8100A Automated Soil CO₂ Flux System & LI-8150 Multiplexer Instruction Manual*. Lincoln, NE: LI-COR, Inc.
- Lundegard, P.D., and P.C. Johnson. 2006. Source zone natural attenuation at petroleum hydrocarbon spill sites—II: Application to a former oil field. *Ground Water Monitoring & Remediation* 26, no. 4: 93-106.
- Lundegard, P.D., P.C. Johnson, and P. Dahlen. 2008. Oxygen transport from the atmosphere to soil gas beneath a slab-on-grade foundation overlying petroleum-impacted soil. *Environmental Science & Technology* 42, no. 15: 5534-5540.

- Mahler, N., T. Sale, and M. Lyverse. 2012. A mass balance approach to resolving LNAPL stability. *Groundwater* 50, no. 6: 861-871.
- Maier, M. and H. Schack-Kirchner. 2014. Using the gradient method to determine soil gas flux: a review. *Agricultural and Forest Meteorology*, no. 192-193: 78-95.
- Martin, J.F., P.V. Bolstad, and J.M. Norman. 2004. A carbon dioxide flux generator for testing infrared gas analyzer-based soil respiration systems. *Soil Science Society of America Journal* 68, no. 2: 514-518.
- Massmann, J. and D.F. Farrier. 1992. Effects of atmospheric pressures on gas transport in the vadose zone. *Water Resources Research* 28, no. 3: 777-791.
- McCoy, K. 2012. Resolving natural losses of LNAPL using CO₂ traps. Fort Collins, Colorado: Civil and Environmental Engineering, Colorado State University.
- McCoy, K., Zimbron, J., Sale, T. and Lyverse, M. 2014. Measurement of natural losses of LNAPL using CO₂ traps. *Groundwater*. doi: 10.1111/gwat.12240
- Millington, R.J. 1959. Gas diffusion in porous media. *Science* 130, no. 3367: 100-102.
- Molins, S. and K.U. Mayer. 2007. Coupling between geochemical reactions and multicomponent gas and solute transport in unsaturated media: A reactive transport modeling study. *Water Resources Research* 43, no. 5: W05435.
- Molins, S., K.U. Mayer, R.T. Amos, and B.A. Bekins. 2010. Vadose zone attenuation of organic compounds at a crude oil spill site—Interactions between biogeochemical reactions and multicomponent gas transport. *Journal of Contaminant Hydrology* 112, no. 1-4: 15-29.
- Møldrup, P., T. Olesen, P. Schjønning, T. Yamaguchi, and D.E. Rolston. 2000. Predicting the gas diffusion coefficient in undisturbed soil from soil water characteristics. *Soil Science Society of America Journal* 64, no. 1: 94-100.
- Nay, M.S., K.G. Mattson, and B.T. Bormann. 1994. Biases of chamber methods for measuring soil CO₂ efflux demonstrated with a laboratory apparatus. *Ecology* 75, no. 8: 2460-2463.
- Orchard, V.A. and F.J. Cook. 1983. Relationship between soil respiration and soil moisture. *Soil Biology and Biochemistry* 15, no. 4: 447-453.
- Payne, F.C., J.A. Quinnan, S.T. Potter. 2008. *Remediation Hydraulics*. Boca Raton, FL: Taylor & Francis Group, LLC.
- Penman, H.L. 1940. Gas and vapor movements in the soil: I. The diffusion of vapors through porous solids. *The Journal of Agricultural Science* 30, no. 3: 437-462.

- Poulsen, T.G. and P. Møldrup. 2006. Evaluating effects of wind-induced pressure fluctuations on soil-atmosphere gas exchange at a landfill using stochastic modeling. *Waste Management & Research* 24, no. 5: 473-481.
- Schwarzenbach, R.P., P.M. Gschwend, D.M. Imboden. 2003. *Environmental Organic Chemistry*. New Jersey: John Wiley & Sons.
- Sihota, N.J., O. Singurindy, and K.U. Mayer. 2011. CO₂-efflux measurements for evaluating source zone natural attenuation rates in a petroleum hydrocarbon contaminated aquifer. *Environmental Science and Technology* 45, no. 2: 482-488.
- Skinner, A. 2013. LNAPL longevity as a function of remedial actions: tools for evaluating LNAPL remedies. Fort Collins, Colorado: Civil and Environmental Engineering, Colorado State University.
- Sullivan, B.W., S. Dore, T.E. Kolb, S.C. Hart, and M.C. Montes-Helu. 2010. Evaluation of methods for estimating soil carbon dioxide efflux across a gradient of forest disturbance. *Global Change Biology* 16, no. 9: 2449-2460.
- Thomas, S. and N.S. Haider. 2013. A study on basics of a gas analyzer. *International Journal of Advanced Research in Electrical, Electronics and Instrumentation Engineering* 2, no. 12: 6016-6025.
- US EPA. 1998. Technical protocol for evaluating natural attenuation of chlorinated solvents in ground water. EPA/600/R-98/128. Office of Research and Development, Washington, DC. <http://www.epa.gov/superfund/health/conmedia/gwdocs/protocol.htm>
- US EPA. 1999. Monitored natural attenuation of petroleum hydrocarbons. EPA/600/F-98/021, Office of Research and Development, Washington, DC. <http://www.epa.gov/nrmrl/gwerd/publications.html>
- Washington State Department of Ecology. 2005. Guidance on remediation of petroleum-contaminated ground water by natural attenuation. Publication no. 05-09-091. Toxics Cleanup Program, Olympia, WA. <https://fortress.wa.gov/ecy/publications/publications/0509091.pdf>
- Wiedemeier, T.H., H.S. Rifai, C.J. Newell, and J.T. Wilson. 1999. *Natural Attenuation of Fuels and Chlorinated Solvents in the Subsurface*. New York: John Wiley & Sons.
- Wyatt, D.E., D.M. Richers, and R.J. Pirkle. 1995. Barometric pumping effects on soil gas studies for geological and environmental characterization. *Environmental Geology* 25, no. 4: 243-250.
- Zeman, N. 2012. Thermally Enhanced Bioremediation of LNAPL. Fort Collins, Colorado: Civil and Environmental Engineering, Colorado State University.

Zimbron, J.A., T.C. Sale, M. Lyverse. 2013. Gas flux measurement using traps. Patent WO
2013 1020063 A1

8. APPENDIX A: COLUMN DESIGN DATA

Data in this appendix pertains to the design of the large column experiment, including properties of the fill material and pressure conditions in the testing facility.

8.1 Grain Size Distribution of Column Fill

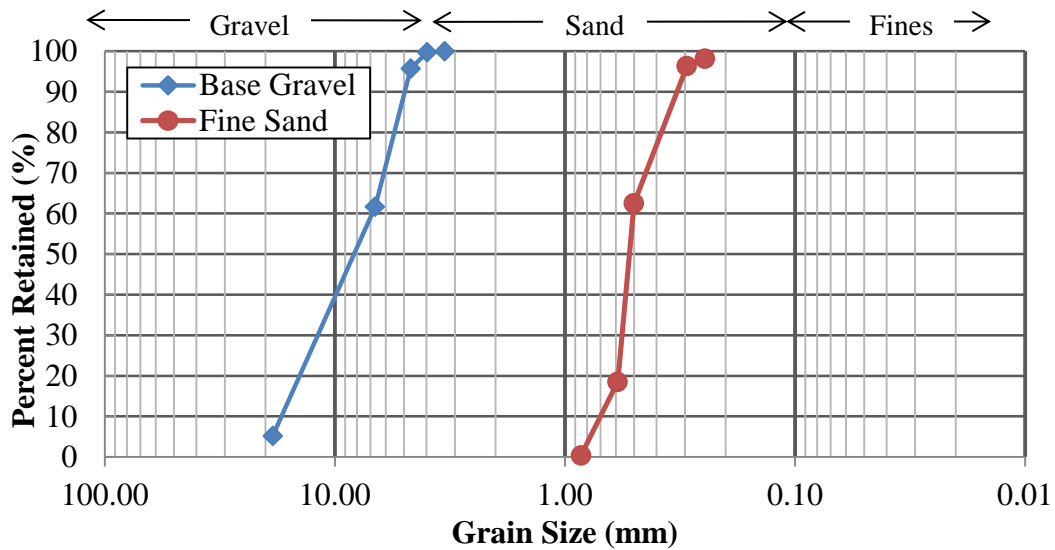


Figure 33. Grain size distribution for base gravel and fine sand fill.

8.2 Moisture Content of Fine Sand

Table 19. Moisture content of fine sand fill material.

Sample	Wet Volume (mL)	Wet mass (g)	Dry mass (g)	Δ mass (g)	Volumetric water content (θ_v)
1	90	345.15	344.88	0.27	0.30%
2	69	199.34	199.18	0.16	0.23%
3	99	322.55	322.2	0.35	0.35%
Average:					0.30%

8.3 Porosity of Column Fill Material

Table 20. Porosity test data for base gravel and fine sand fill material.

Soil Type	Sample	Mass water (g)	Total Volume water + soil (mL)	Porosity (ϕ)
Fine sand	1	16.57	41.5	0.40
	2	29.97	73.0	0.41
	3	21.61	56.0	0.39
	Average			0.40
Gravel	1	89.89	208.0	0.43
	2	91.51	208.0	0.44
	3	87.31	209.0	0.42
	Average			0.43

8.4 Ambient Pressure in Hydraulics Laboratory

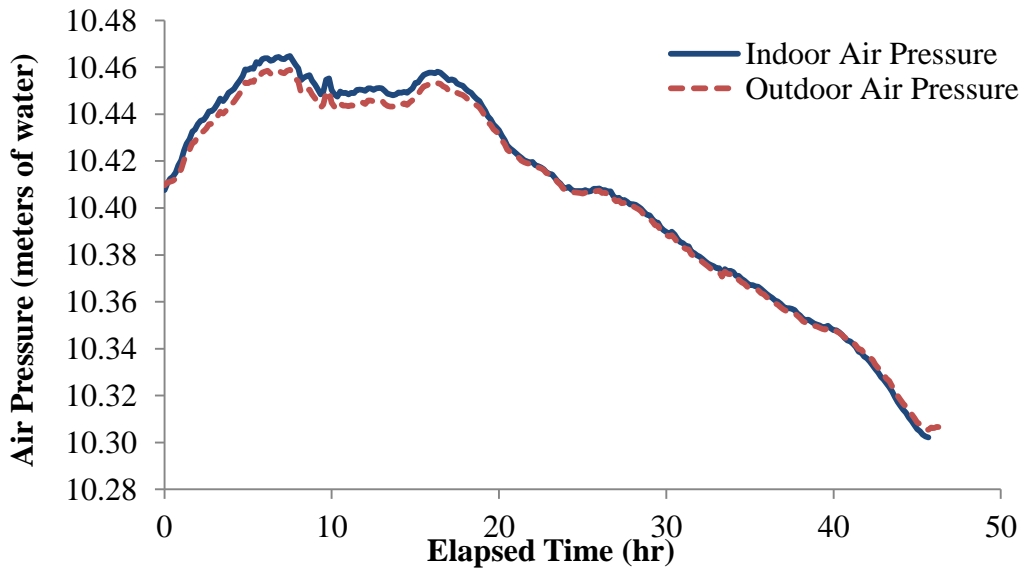


Figure 34. Outdoor air pressure versus indoor air pressure in the laboratory testing facility. Indoor air pressure closely follows outdoor air pressure, indicating pressure conditions in the laboratory are representative of pressure conditions observed in the field.

9. APPENDIX B: EXPERIMENTAL DATA FROM METHODS COMPARISONS

This appendix contains data from method comparison experiments conducted under ideal and windy test conditions. Section 9.1 lists all variables that were used to determine the imposed flux for each trial. Section 9.2 lists all gradient method data, including data used to determine the In-situ effective diffusion coefficient. Section 9.3 summarizes data from the chamber method and data collection settings for the LI-8100A. Finally, data from the trap method is presented in Section 9.4.

9.1 Summary of Imposed Fluxes

Table 21. Change in mass of CO₂ cylinder for imposed test fluxes.

Test	Calculated Flux ($\mu\text{mol}/\text{m}^2/\text{s}$)	Test Conditions	Change in CO ₂ mass (g)	Time (days)	Flux based on change in CO ₂ mass ($\mu\text{mol}/\text{m}^2/\text{s}$)
1	15.1 ± 0.4	Ideal	104.3	3.88	19.9
2	10.7 ± 0.2	Ideal	104.3	7.74	10.0
3	7.9 ± 0.2	Ideal	122.5	10.09	9.0
4	3.3 ± 0.1	Ideal	54.4	24.03	1.7
5	8.7 ± 0.2	No wind base case	90.7	9.65	7.0
6	8.6 ± 0.2	Low wind	72.6	9.19	5.8
7	8.5 ± 0.2	High wind	59.0	9.06	4.8

Table 22. Summary of imposed test fluxes

Test	Actual Calculated Flux ($\mu\text{mol}/\text{m}^2/\text{s}$)	Test Conditions	Characteristic	Average Value	Standard Deviation	Coefficient of Variation (%)	Sample Size
1	15.1 ± 0.4	Ideal	Volumetric flow rate (mL/min)	9.30	0.30	2.98	16
			Mass flow rate ($\mu\text{mol}/\text{s}$)	5.37	0.30	2.98	16
			Ambient temperature ($^{\circ}\text{C}$)	18.84	1.41	7.49	126
			Ambient pressure (atm)	0.830	9.03×10^{-3}	1.09	126
			Imposed CO_2 flux ($\mu\text{mol}/\text{m}^2/\text{s}$)	15.1	0.4	2.98	-
2	10.7 ± 0.2	Ideal	Volumetric flow rate (mL/min)	6.64	0.15	2.21	20
			Mass flow rate ($\mu\text{mol}/\text{s}$)	3.80	0.15	2.21	20
			Ambient temperature ($^{\circ}\text{C}$)	21.56	1.64	7.63	187
			Ambient pressure (atm)	0.830	8.19×10^{-4}	0.10	187
			Imposed CO_2 flux ($\mu\text{mol}/\text{m}^2/\text{s}$)	10.7	0.2	2.21	-
3	7.9 ± 0.2	Ideal	Volumetric flow rate (mL/min)	4.94	0.10	2.11	21
			Mass flow rate ($\mu\text{mol}/\text{s}$)	2.82	0.10	2.11	21
			Ambient temperature ($^{\circ}\text{C}$)	22.52	0.84	3.75	243
			Ambient pressure (atm)	0.831	3.46×10^{-3}	0.42	243
			Imposed CO_2 flux ($\mu\text{mol}/\text{m}^2/\text{s}$)	7.9	0.2	2.11	-
4	3.3 ± 0.1	Ideal	Volumetric flow rate (mL/min)	2.04	0.04	2.12	25
			Mass flow rate ($\mu\text{mol}/\text{s}$)	1.18	0.04	2.12	25
			Ambient temperature ($^{\circ}\text{C}$)	21.05	1.30	6.16	578
			Ambient pressure (atm)	0.831	5.22×10^{-3}	0.63	577
			Imposed CO_2 flux ($\mu\text{mol}/\text{m}^2/\text{s}$)	3.3	0.1	2.12	-
5	8.7 ± 0.2	No wind base condition	Volumetric flow rate (mL/min)	5.27	0.13	2.48	11
			Mass flow rate ($\mu\text{mol}/\text{s}$)	3.06	0.08	2.48	11
			Ambient temperature ($^{\circ}\text{C}$)	16.46	1.10	6.67	232
			Ambient pressure (atm)	0.834	6.47×10^{-3}	0.78	232
			Imposed CO_2 flux ($\mu\text{mol}/\text{m}^2/\text{s}$)	8.7	0.2	2.48	-

Test	Actual Calculated Flux ($\mu\text{mol}/\text{m}^2/\text{s}$)	Test Conditions	Characteristic	Average Value	Standard Deviation	Coefficient of Variation (%)	Sample Size
6	8.6 ± 0.2	Low wind	Volumetric flow rate (mL/min)	5.28	0.10	1.84	20
			Mass flow rate ($\mu\text{mol}/\text{s}$)	3.05	0.06	1.84	20
			Ambient temperature ($^{\circ}\text{C}$)	20.66	1.02	4.92	223
			Ambient pressure (atm)	0.835	3.30×10^{-3}	0.39	223
			Imposed CO_2 flux ($\mu\text{mol}/\text{m}^2/\text{s}$)	8.6	0.2	1.84	-
7	8.5 ± 0.2	High wind	Volumetric flow rate (mL/min)	5.23	0.15	2.78	13
			Mass flow rate ($\mu\text{mol}/\text{s}$)	3.02	0.08	2.78	13
			Ambient temperature ($^{\circ}\text{C}$)	19.65	1.66	8.43	224
			Ambient pressure (atm)	0.833	3.76×10^{-3}	0.45	224
			Imposed CO_2 flux ($\mu\text{mol}/\text{m}^2/\text{s}$)	8.5	0.2	2.78	-

9.2 Summary of Gradient Data

Table 23. Summary of soil gas sample data used with gradient method.

Imposed Flux ($\mu\text{mol}/\text{m}^2/\text{s}$)	Test Conditions	Sampling Event	Sample Port Location	Average Percent CO_2 (%)	CO_2 Concentration ($\mu\text{mol}/\text{m}^3$)	Depth from $z=0$ (m)
15.1 ± 0.4	Ideal	1	Gradient 1	0.81	2.82×10^5	1.29
			Gradient 2	2.88	9.99×10^5	1.03
			Gradient 3	5.25	1.82×10^6	0.69
			Gradient 4	7.65	2.65×10^6	0.41
			Gradient 5	9.48	3.29×10^6	0.13
			LBC	11.08	3.84×10^6	0.00
		2	Gradient 1	0.84	2.92×10^5	1.29
			Gradient 2	3.09	1.07×10^6	1.03
			Gradient 3	5.59	1.94×10^6	0.69
			Gradient 4	8.15	2.82×10^6	0.41
			Gradient 5	10.28	3.56×10^6	0.13
			LBC	11.75	4.07×10^6	0.00
		3	Gradient 1	0.86	2.99×10^5	1.29
			Gradient 2	3.07	1.06×10^6	1.03
			Gradient 3	5.47	1.90×10^6	0.69
			Gradient 4	8.07	2.80×10^6	0.41
			Gradient 5	10.22	3.54×10^6	0.13
			LBC	11.64	4.04×10^6	0.00
10.7 ± 0.2	Ideal	1	Gradient 1	0.76	2.61×10^5	1.29
			Gradient 2	2.20	7.56×10^5	1.03
			Gradient 3	3.66	1.26×10^6	0.69
			Gradient 4	5.43	1.86×10^6	0.41
			Gradient 5	6.59	2.26×10^6	0.13
			LBC	7.72	2.65×10^6	0.00
		2	Gradient 1	0.68	2.32×10^5	1.29
			Gradient 2	2.20	7.55×10^5	1.03
			Gradient 3	3.92	1.35×10^6	0.69
			Gradient 4	5.29	1.81×10^6	0.41
			Gradient 5	6.97	2.39×10^6	0.13
			LBC	8.36	2.87×10^6	0.00
		3	Gradient 1	0.62	2.13×10^5	1.29
			Gradient 2	2.17	7.46×10^5	1.03
			Gradient 3	3.90	1.34×10^6	0.69
			Gradient 4	5.55	1.90×10^6	0.41
			Gradient 5	6.95	2.39×10^6	0.13
			LBC	8.09	2.78×10^6	0.00

Flux ($\mu\text{mol}/\text{m}^2/\text{s}$)	Test Conditions	Sampling Event	Sample Port Location	Average Percent CO ₂ (%)	CO ₂ Concentration ($\mu\text{mol}/\text{m}^3$)	Depth from z=0 (m)
7.9 ± 0.2	Ideal	1	Gradient 1	0.54	1.86 x 10 ⁵	1.29
			Gradient 2	1.55	5.30 x 10 ⁵	1.03
			Gradient 3	2.71	9.28 x 10 ⁵	0.69
			Gradient 4	3.90	1.34 x 10 ⁶	0.41
			Gradient 5	4.92	1.68 x 10 ⁶	0.13
			LBC	5.52	1.89 x 10 ⁶	0.00
		2	Gradient 1	0.38	1.29 x 10 ⁵	1.29
			Gradient 2	1.41	4.82 x 10 ⁵	1.03
			Gradient 3	2.58	8.85 x 10 ⁵	0.69
			Gradient 4	3.87	1.33 x 10 ⁶	0.41
			Gradient 5	4.84	1.66 x 10 ⁶	0.13
			LBC	5.67	1.94 x 10 ⁶	0.00
		3	Gradient 1	0.36	1.24 x 10 ⁵	1.29
			Gradient 2	1.38	4.72 x 10 ⁵	1.03
			Gradient 3	2.54	8.69 x 10 ⁵	0.69
			Gradient 4	3.73	1.28 x 10 ⁶	0.41
			Gradient 5	4.74	1.62 x 10 ⁶	0.13
			LBC	5.50	1.88 x 10 ⁶	0.00
3.3 ± 0.1	Ideal	1	Gradient 1	ND	-	1.29
			Gradient 2	0.67	2.29 x 10 ⁵	1.03
			Gradient 3	1.14	3.92 x 10 ⁵	0.69
			Gradient 4	1.63	5.62 x 10 ⁵	0.41
			Gradient 5	2.06	7.08 x 10 ⁵	0.13
			LBC	2.38	8.18 x 10 ⁵	0.00
		2	Gradient 1	ND	-	1.29
			Gradient 2	0.66	2.29 x 10 ⁵	1.03
			Gradient 3	1.14	3.93 x 10 ⁵	0.69
			Gradient 4	1.64	5.65 x 10 ⁵	0.41
			Gradient 5	2.00	6.88 x 10 ⁵	0.13
			LBC	2.26	7.80 x 10 ⁵	0.00
		3	Gradient 1	ND	-	1.29
			Gradient 2	0.65	2.24 x 10 ⁵	1.03
			Gradient 3	1.11	3.81 x 10 ⁵	0.69
			Gradient 4	1.59	5.47 x 10 ⁵	0.41
			Gradient 5	1.99	6.86 x 10 ⁵	0.13
			LBC	2.29	7.89 x 10 ⁵	0.00

ND = non-detectable concentration

Flux ($\mu\text{mol}/\text{m}^2/\text{s}$)	Test Conditions	Sampling Event	Sample Port Location	Average Percent CO_2 (%)	CO_2 Concentration ($\mu\text{mol}/\text{m}^3$)	Depth from z=0 (m)
8.7 ± 0.2	No wind base condition	1	Gradient 1	0.39	1.36×10^5	1.29
			Gradient 2	1.59	5.58×10^5	1.03
			Gradient 3	2.92	1.03×10^6	0.69
			Gradient 4	4.36	1.53×10^6	0.41
			Gradient 5	5.64	1.98×10^6	0.13
			LBC	6.52	2.29×10^6	0.00
		2	Gradient 1	0.38	1.34×10^5	1.29
			Gradient 2	1.58	5.56×10^5	1.03
			Gradient 3	2.93	1.03×10^6	0.69
			Gradient 4	4.34	1.52×10^6	0.41
			Gradient 5	5.53	1.94×10^6	0.13
			LBC	6.41	2.25×10^6	0.00
		3	Gradient 1	0.38	1.34×10^5	1.29
			Gradient 2	1.56	5.46×10^5	1.03
			Gradient 3	2.92	1.02×10^6	0.69
			Gradient 4	4.40	1.54×10^6	0.41
			Gradient 5	5.50	1.93×10^6	0.13
			LBC	6.47	2.27×10^6	0.00
8.6 ± 0.2	Low wind	1	Gradient 1	ND	-	1.29
			Gradient 2	1.25	4.32×10^5	1.03
			Gradient 3	2.59	8.95×10^5	0.69
			Gradient 4	3.95	1.37×10^6	0.41
			Gradient 5	5.00	1.73×10^6	0.13
			LBC	5.81	2.01×10^6	0.00
		2	Gradient 1	0.14	4.92×10^4	1.29
			Gradient 2	1.19	4.12×10^5	1.03
			Gradient 3	2.40	8.32×10^5	0.69
			Gradient 4	3.71	1.28×10^6	0.41
			Gradient 5	4.57	1.58×10^6	0.13
			LBC	5.35	1.85×10^6	0.00
		3	Gradient 1	0.13	4.43×10^4	1.29
			Gradient 2	1.21	4.18×10^5	1.03
			Gradient 3	2.64	9.13×10^5	0.69
			Gradient 4	3.82	1.32×10^6	0.41
			Gradient 5	4.91	1.70×10^6	0.13
			LBC	5.83	2.02×10^6	0.00

ND = non-detectable concentrations

Flux ($\mu\text{mol}/\text{m}^2/\text{s}$)	Test Conditions	Sampling Event	Sample Port Location	Average Percent CO_2 (%)	CO_2 Concentration ($\mu\text{mol}/\text{m}^3$)	Depth from z=0 (m)
8.5 ± 0.2	High wind	1	Gradient 1	ND	-	1.29
			Gradient 2	1.01	3.49×10^5	1.03
			Gradient 3	2.36	8.18×10^5	0.69
			Gradient 4	3.95	1.37×10^6	0.41
			Gradient 5	5.01	1.74×10^6	0.13
			LBC	6.22	2.15×10^6	0.00
		2	Gradient 1	ND	-	1.29
			Gradient 2	1.08	3.74×10^5	1.03
			Gradient 3	2.29	7.94×10^5	0.69
			Gradient 4	3.55	1.23×10^6	0.41
			Gradient 5	4.76	1.65×10^6	0.13
			LBC	5.48	1.90×10^6	0.00
		3	Gradient 1	ND	-	1.29
			Gradient 2	0.96	3.34×10^5	1.03
			Gradient 3	2.24	7.76×10^5	0.69
			Gradient 4	3.60	1.25×10^6	0.41
			Gradient 5	4.66	1.62×10^6	0.13
			LBC	5.47	1.90×10^6	0.00

ND = non-detectable concentrations

Table 24. Summary of triplicate results for gradient method.

Method for Estimating Effective Diffusion Coefficient	Imposed Flux ($\mu\text{mol}/\text{m}^2/\text{s}$)	Measured Flux ($\mu\text{mol}/\text{m}^2/\text{s}$)
Millington	15.1 ± 0.4	13.0
		13.8
		13.7
	10.7 ± 0.2	9.0
		9.7
		9.4
	7.9 ± 0.2	6.4
		6.6
		6.4
	3.3 ± 0.1	2.7
		2.6
		2.6
	No wind base condition 8.7 ± 0.2	7.8
		7.6
		7.7
	Low wind 8.6 ± 0.2	6.8
		6.3
		6.8
High wind 8.5 ± 0.2	7.3	
	6.4	
	6.4	
In-situ	15.1 ± 0.4	9.5
		10.1
		10.0
	10.7 ± 0.2	6.6
		7.1
		6.9
	7.9 ± 0.2	4.7
		4.8
		4.7
	3.3 ± 0.1	2.0
		1.9
		1.9
	No wind base condition 8.7 ± 0.2	5.7
		5.6
		5.6
	Low wind 8.6 ± 0.2	5.0
		4.6
		5.0
High wind 8.5 ± 0.2	5.3	
	4.7	
	4.7	

9.2.1 In-Situ Effective Diffusion Coefficient Data

Percent CH₄ was determined using calibration data from Figure 40 in Section 9.2.3.

Table 25. In-situ effective diffusion data.

Sample Port Location	Depth from z=0 (m)	Injection Volume (mL)	Extraction Volume (mL)	Time of sample (min)	Injection %CH ₄ (%)	Extraction %CH ₄ (%)	Fraction of tracer recovered, η	Corresponding β	D _{eff, CO2} (cm ² /s)
Gradient 1	1.29	100	100	15	80.00	0.25	3.075 x 10 ⁻³	2.580 x 10 ⁻²	5.011 x 10 ⁻²
		100	100	30	78.80	ND	-	-	-
Gradient 2	1.03	100	100	15	80.00	0.39	4.821 x 10 ⁻³	3.500 x 10 ⁻²	3.694 x 10 ⁻²
		100	100	30	78.95	0.14	1.791 x 10 ⁻³	1.793 x 10 ⁻²	3.605 x 10 ⁻²
		100	100	60	80.00	0.03	4.244 x 10 ⁻⁴	6.800 x 10 ⁻³	4.753 x 10 ⁻²
Gradient 3	0.69	100	100	15	77.22	0.38	4.899 x 10 ⁻³	3.350 x 10 ⁻²	3.663 x 10 ⁻²
		100	100	30	80.00	0.17	2.126 x 10 ⁻³	2.020 x 10 ⁻²	3.169 x 10 ⁻²
		100	100	60	80.00	0.06	7.657 x 10 ⁻⁴	1.020 x 10 ⁻²	3.200 x 10 ⁻²
Gradient 4	0.41	100	100	15	80.00	0.30	3.744 x 10 ⁻³	2.950 x 10 ⁻²	4.383 x 10 ⁻²
		100	100	30	80.00	0.15	1.908 x 10 ⁻³	1.870 x 10 ⁻²	3.457 x 10 ⁻²
		100	100	60	80.00	0.12	1.478 x 10 ⁻³	1.580 x 10 ⁻²	2.046 x 10 ⁻²
Gradient 5	0.13	100	100	15	79.67	0.38	4.769 x 10 ⁻³	3.470 x 10 ⁻²	3.726 x 10 ⁻²
		100	100	30	80.00	0.25	3.080 x 10 ⁻³	2.585 x 10 ⁻²	2.501 x 10 ⁻²
		100	100	60	79.98	0.17	2.113 x 10 ⁻³	2.005 x 10 ⁻²	1.612 x 10 ⁻²
Average								3.448 x 10⁻²	
Standard Deviation								9.447 x 10 ⁻³	

ND = non-detectable concentration

9.2.3 Gas Chromatography Calibration Curves

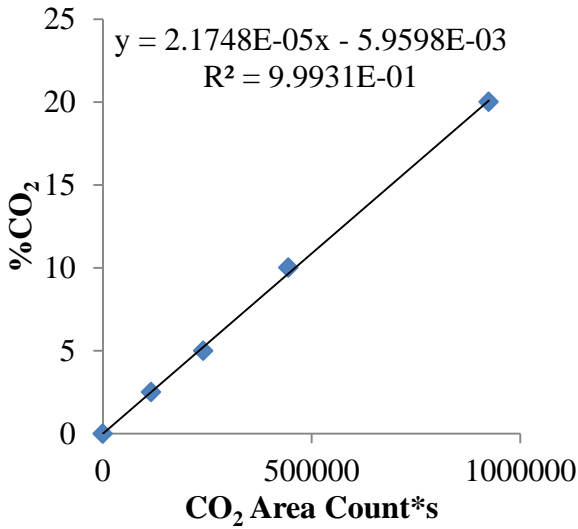


Figure 35. GC-TCD calibration curve for test #1, imposed flux 15.1 $\mu\text{mol}/\text{m}^2/\text{s}$.

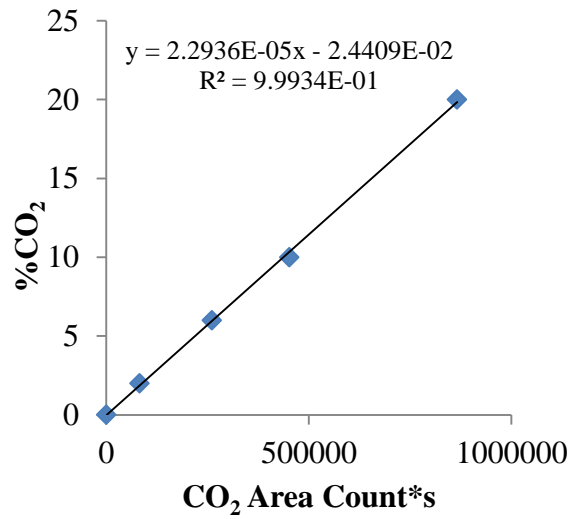


Figure 36. GC-TCD calibration curve for test #2, imposed flux 10.7 $\mu\text{mol}/\text{m}^2/\text{s}$.

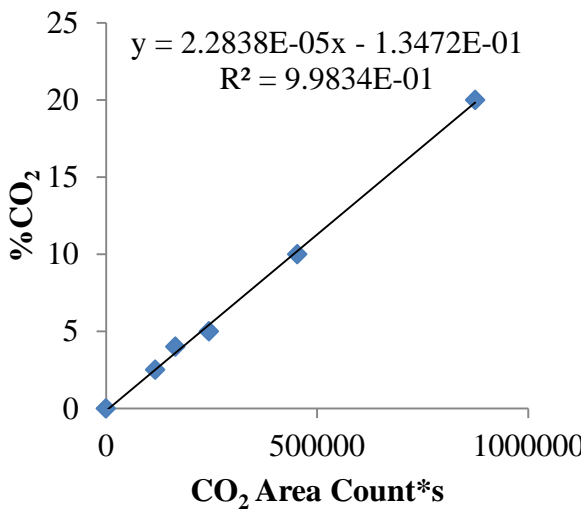


Figure 37. GC-TCD calibration curve for test #3, imposed flux 7.9 $\mu\text{mol}/\text{m}^2/\text{s}$.

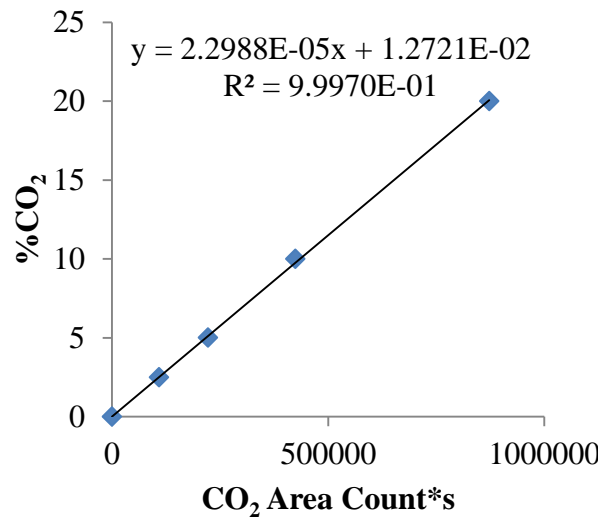


Figure 38. GC-TCD calibration curve for test #4, imposed flux 3.3 $\mu\text{mol}/\text{m}^2/\text{s}$.

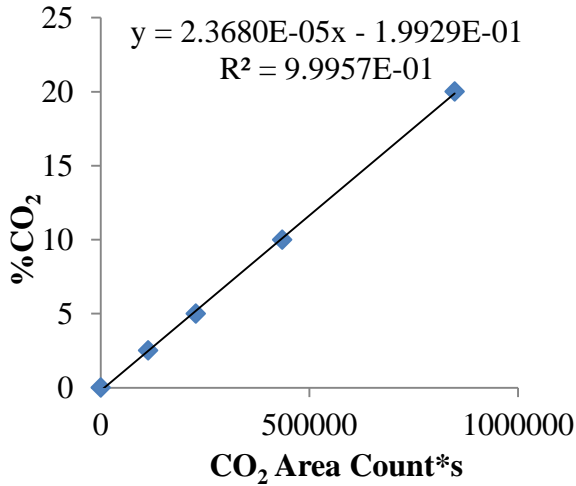


Figure 39. GC-TCD calibration curve for imposed wind tests.

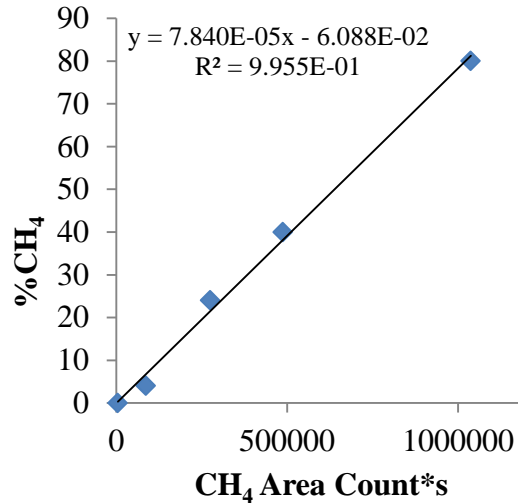


Figure 40. GC-TCD calibration curve for CH₄ used with In-situ effective diffusion test

9.2.4 Integrity of Gas Sampling Syringes

The purpose of this section is to determine the ability of plastic BD syringes capped with a Luer Lock[®] fitting to maintain the integrity of extracted soil gas samples over a time span of several hours. This is an important test that ensures soil gas samples withdrawn from the column are not altered during the 2 hour period required to analyze samples on the gas chromatograph by means of leaks and diffusion through the plastic walls.

Two BD syringes with Luer Lock[®] fittings (60 mL and 10 mL) were filled with a gas mixture containing 80% CH₄ and 20% N₂. Samples were periodically taken from the syringes over the course of 24 hours through rubber stoppers and analyzed on the GC-TCD for CH₄ concentration using calibration data from Figure 41. CH₄ was chosen because of the high concentration

gradient that exists between the gas sample and atmosphere, which would maximize any diffusive leaks present.

As shown in Figure 41, both syringes maintained the gas sample integrity for 24 hours, indicating this type of syringe setup is adequate to use for the gradient method gas samples.

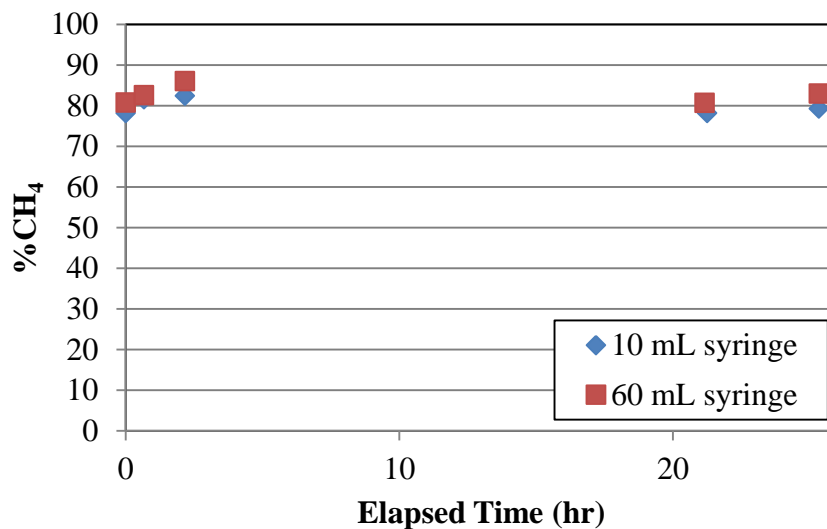


Figure 41. Results from syringe integrity test. Both sizes of syringes maintained the initial CH₄ concentration for 24+ hrs.

9.3 Summary of Chamber Method Data

Table 26. Data from LI-8100-104 Long-Term Survey Chamber.

Imposed Flux ($\mu\text{mol}/\text{m}^2/\text{s}$)	Test Conditions	Curve Fit Type	Mean Calculated Flux ($\mu\text{mol}/\text{m}^2/\text{s}$)	Standard Deviation ($\mu\text{mol}/\text{m}^2/\text{s}$)	Coefficient of Variation (%)	Sample Size
15.1 ± 0.4	Ideal	Linear	15.7	0.4	2.5	149
		Exponential	17.9	2.3	12.7	149
10.7 ± 0.2	Ideal	Linear	10.8	0.3	3.1	336
		Exponential	12.4	1.5	12.3	336
7.9 ± 0.2	Ideal	Linear	7.8	0.2	3.1	385
		Exponential	8.9	1.2	13.1	385
3.3 ± 0.1	Ideal	Linear	2.2	0.1	4.4	814
		Exponential	2.5	0.4	17.0	814
8.7 ± 0.2	No wind base condition	Linear	8.2	0.3	3.3	462
		Exponential	8.8	1.0	11.8	462
8.6 ± 0.2	Low wind	Linear	4.5	0.2	5.1	439
		Exponential	4.7	0.4	8.7	439
8.5 ± 0.2	High wind	Linear	1.8	0.2	9.5	444
		Exponential	1.9	0.2	10.4	444

*Results from the highest flux ($15.2 \mu\text{mol}/\text{m}^2/\text{s}$) are from a separate trial than the gradient and trap methods due to a failure with the LI-COR instrument during the sampling event

Table 27. Data collection settings for LI-8100-104 Long-Term Survey Chamber.

Parameter	Setting
Observation Length	01:30 min
Pre-purge	00:20 min
Post-purge	00:20 min
Deadband	00:20 min
Time interval for flux calculations	00:20 – 00:40 min
Chamber offset	4.0-4.5 cm (depending on trial)
Repeat sequence	Every 30 min for duration of flux trial

9.4 Summary of Trap Method Data

Table 28. Results of gravimetric analysis for trap method

Imposed Flux ($\mu\text{mol}/\text{m}^2/\text{s}$)	Test Conditions	Trap Element Position	Column Location	Total Measured %CO ₂ (g/g)	Standard Deviation of triplicate analysis (%)	Coefficient of Variation of triplicate analysis (%)	Blank Corrected %CO ₂ (g/g)	Deployment Time (days)	Measured CO ₂ Flux ($\mu\text{mol}/\text{m}^2/\text{s}$)
15.1 ± 0.4	Ideal	Top	TB	2.12	0.43	20.14	0.00	5.20	0.0
			A	4.86	0.38	7.85	2.75	5.20	7.9
			B	5.00	1.05	21.04	2.88	5.20	8.2
			C	4.86	0.87	17.99	2.74	5.20	7.8
			Background	4.50	0.10	2.15	2.35	5.20	6.7
		Bottom	TB	1.67	0.54	7.90	0.00	5.20	0.0
			A	7.11	0.76	10.71	5.44	5.20	15.8
			B	6.80	0.29	4.32	5.12	5.20	14.9
			C	7.46	0.93	12.51	5.78	5.20	16.8
			Background	1.90	0.84	45.12	0.18	5.20	6.7
10.7 ± 0.2	Ideal	Top	TB	2.13	0.49	22.80	0.00	7.75	0.0
			A	5.86	0.42	7.21	3.73	7.75	7.1
			B	5.91	0.60	10.09	3.78	7.75	7.2
			C	5.85	0.72	12.25	3.72	7.75	7.1
			Background	5.24	0.15	2.80	3.11	7.75	5.9
		Bottom	TB	2.26	1.09	48.07	0.00	7.75	0.0
			A	6.98	0.31	4.50	4.72	7.75	9.1
			B	7.60	1.11	14.57	5.34	7.75	10.2
			C	7.92	0.50	6.27	5.66	7.75	10.8
			Background	1.86	0.30	16.32	0.00 ^a	7.75	0.0 ^a
7.9 ± 0.2	Ideal	Top	TB	1.98	0.02	0.86	0.00	10.09	0.0
			A	7.01	0.88	12.60	5.03	10.09	7.3
			B	6.65	0.62	9.30	4.67	10.09	6.8
			C	6.53	0.31	4.80	4.55	10.09	6.6
			Background	6.03	1.61	26.79	4.04	10.09	5.9
		Bottom	TB	2.19	0.35	15.87	0.00	10.09	0.0
			A	7.85	0.89	11.38	5.66	10.09	8.3
			B	6.83	1.13	16.55	4.63	10.09	6.7
			C	6.78	1.22	17.97	4.59	10.09	6.7
			Background	1.58	0.41	28.15	0.00 ^a	10.09	0.0 ^a

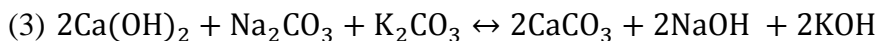
^a Negative values reported as 0.

Imposed Flux ($\mu\text{mol}/\text{m}^2/\text{s}$)	Test Conditions	Trap Element Position	Column Location	Total Measured %CO ₂ (g/g)	Standard Deviation of triplicate analysis (%)	Coefficient of Variation of triplicate analysis (%)	Blank Corrected %CO ₂ (g/g)	Deployment Time (days)	Measured CO ₂ Flux ($\mu\text{mol}/\text{m}^2/\text{s}$)
3.3 ± 0.1	Ideal	Top	TB	2.06	0.64	31.24	0.00	24.03	0.0
			A	10.42	0.13	1.27	8.37	24.03	5.3
			B	9.84	0.06	0.60	7.79	24.03	4.9
			C	9.77	0.24	2.45	7.71	24.03	4.9
			Background	10.10	0.23	2.32	8.04	24.03	5.1
		Bottom	TB	2.38	0.60	25.14	0.00	24.03	0.0
			A	7.47	0.41	5.43	5.10	24.30	3.2
			B	7.55	0.13	1.67	5.18	24.03	3.2
		C	7.82	0.36	4.55	5.45	24.03	3.4	
		Background	3.08	0.24	7.86	0.70	24.03	0.4	
8.7 ± 0.2	No wind base condition	Top	TB	2.02	0.30	14.76	0.00	9.65	0.0
			Column	6.20	0.05	0.86	4.18	9.65	6.4
		Bottom	TB	2.10	0.28	13.53	0.00	9.65	0.0
			Column	7.10	0.52	7.26	5.01	9.65	7.4
8.6 ± 0.2	Low wind	Top	TB	1.52	0.31	20.42	0.00	9.25	0.0
			Column	9.76	0.72	7.34	3.92	9.25	13.8
		Bottom	TB	2.24	0.94	41.76	0.00	9.25	0.0
			Column	10.45	0.09	0.82	3.94	9.25	13.8
8.5 ± 0.2	High wind	Top	TB	2.05	0.42	20.56	0.00	9.31	0.0
			Column	10.31	0.65	6.34	8.26	9.31	13.6
		Bottom	TB	2.18	0.23	10.56	0.00	9.31	0.0
			Column	13.42	0.33	2.46	11.24	9.31	18.9

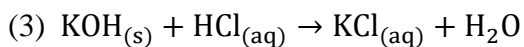
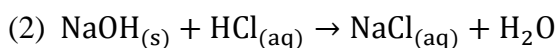
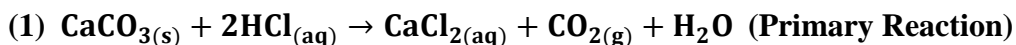
9.4.1 Chemistry of Gravimetric Acid Analysis

Per manufacturer specified values, Sodasorb[®] consists primarily of calcium hydroxides (50-100%). The remaining mass consists of sodium (0-1%) and potassium hydroxides (2-5%). The sorption/desorption reactions of CO₂ with the Sodasorb[®] sorbent material are described by the following chemical reactions:

Sorption Reactions (In order):



Desorption Reactions (Simultaneous):



10. APPENDIX C: EXPERIMENTAL DATA FROM TRAP MODIFICATION STUDIES

Imposed Flux ($\mu\text{mol}/\text{m}^2/\text{s}$)	Modification	Trap Element Position	Column Location	Total Measured %CO ₂ (g/g)	Standard Deviation of triplicate analysis (%)	Coefficient of Variation of triplicate analysis (%)	Blank Corrected %CO ₂ (g/g)	Deployment Time (days)	Measured CO ₂ Flux ($\mu\text{mol}/\text{m}^2/\text{s}$)
Mass of Absorbent in Bottom Element									
10.5 ± 0.4	50.0 g bottom absorbent	Top	TB	1.53	0.36	23.25	0.0	8.04	0.0
			A	6.04	0.50	8.27	4.51	8.04	8.4
			B	6.18	0.43	7.02	4.65	8.04	8.7
		Bottom	C	5.70	0.26	4.59	4.17	8.04	7.7
			TB	1.63	0.66	40.51	0.0	8.04	0.0
			A	5.65	0.22	3.89	4.02	8.04	7.6
			B	5.48	0.38	7.02	3.85	8.04	7.2
C	5.48	0.26	4.76	3.85	8.04	7.2			
10.5 ± 0.4	100.0 g bottom absorbent	Top	TB	1.93	0.50	25.86	0.00	16.00	0.0
			A	11.06	2.05	18.51	9.13	16.00	8.7
			B	10.43	0.40	3.87	8.50	16.00	9.6
		Bottom	C	9.88	0.64	6.49	7.95	16.00	7.5
			TB	1.59	0.34	21.59	0.0	16.00	0.0
			A	6.28	1.18	18.72	4.69	16.00	8.8
			B	6.92	1.81	26.20	5.33	16.00	10.0
C	5.66	0.11	1.92	4.07	16.00	7.7			
CO₂ Breakthrough to Top Element									
Refer to Table 12 in Section 5.3.2.									
Height of Bottom Element from Soil Surface									
10.5 ± 0.4	Headspace height 2.0 cm	Top	TB	1.33	0.23	17.51	0.00	8.11	0.0
			Column	6.78	0.78	11.45	5.45	8.11	9.9
		Bottom	TB	1.79	0.28	15.85	0.00	8.11	0.0
			Column	8.68	0.74	8.53	6.89	8.11	12.8
	Headspace height 15.5 cm	Top	TB	1.7	0.82	48.2	0.00	8.01	0.0
			Column	6.0	0.53	8.9	4.4	8.01	8.0
		Bottom	TB	1.9	0.70	36.8	0.00	8.01	0.0
			Column	6.6	0.07	1.1	4.7	8.01	8.7
	Headspace height 20.0 cm	Top	TB	1.53	0.36	23.25	0.00	8.04	0.0
			Column	5.70	0.26	4.59	4.17	8.04	7.7
		Bottom	TB	1.63	0.66	40.51	0.00	8.04	0.0
			Column	5.48	0.26	4.76	3.85	8.04	7.3

11. APPENDIX D: SAMPLE CALCULATIONS

11.1 Porosity and Moisture Content of Fill Material

Porosity:

Sample calculation from fine sand, sample #1:

$$\text{Porosity } (\phi) = \frac{\text{volume voids}}{\text{volume total}} = \frac{\text{water weight/water density}}{\text{volume total}} \quad (51)$$

$$\phi_{\text{fine sand}} = \frac{16.57 \text{ g water}}{41.5 \text{ mL soil}} = \frac{16.57 \text{ g water}/1 \frac{\text{g}}{\text{mL}}}{41.5 \text{ mL soil}} = 0.40 \quad (52)$$

Moisture Content:

Sample calculation from fine sand, sample #1:

$$\text{Volumetric Water Content } (\theta_v) = \frac{\text{Volume water}}{\text{Volume total}} \quad (53)$$

$$\theta_v = \frac{0.27 \text{ g water}/1 \frac{\text{g}}{\text{mL}}}{90 \text{ mL soil}} = \frac{0.27 \text{ mL water}}{90 \text{ mL soil}} = 0.003 = 0.30\% \quad (54)$$

11.2 Open System Imposed Flux Calculation

Sample calculation from test 2, imposed flux $10.7 \pm 0.2 \mu\text{mol}/\text{m}^2/\text{s}$:

The mean CO_2 (ρ_{CO_2}) density is determined using mean temperature (T) and pressure (P) data collected over the duration of the imposed flux. R is the universal gas constant, defined as $8.205 \times 10^{-5} \text{ m}^3 \cdot \text{atm}/\text{mol}/^\circ\text{K}$.

$$\rho_{\text{CO}_2} = \frac{P}{R * T} \quad (55)$$

$$\rho_{\text{CO}_2} = \frac{0.83 \text{ atm}}{\left(\frac{8.205 \times 10^{-5} \text{ m}^3 \text{ atm}}{\text{mol K}}\right) * 294.7\text{K}} = 34.09 \frac{\text{mol}}{\text{m}^3} = 0.034 \frac{\text{mol}}{\text{L}} \quad (56)$$

Using the mean volumetric flow rate (Q) from the mass flow meter and mean CO_2 density, a mean mass flow rate (M) is calculated.

$$M = Q * \rho_{\text{CO}_2} \quad (57)$$

$$M = 6.64 \frac{\text{mL}}{\text{min}} * \frac{1\text{L}}{1000 \text{ mL}} * 0.034 \frac{\text{mol}}{\text{L}} * \frac{1\text{min}}{60 \text{ sec}} * \frac{10^6 \mu\text{mol}}{1\text{mol}} = 3.80 \frac{\mu\text{mol}}{\text{s}} \quad (58)$$

Flux of CO_2 (J_{CO_2}) through the column is calculated by dividing the mean mass flow rate by the column cross-sectional area (A), defined as $3.56 \times 10^{-1} \text{ m}^2$.

$$J_{\text{CO}_2} = \frac{M}{A} \quad (59)$$

$$J_{\text{CO}_2} = \frac{3.80 \frac{\mu\text{mol}}{\text{s}}}{3.56 \times 10^{-1} \text{ m}^2} = 10.7 \frac{\mu\text{mol}}{\text{m}^2 * \text{s}} \quad (60)$$

Standard deviation of the mean flux is calculated by taking the standard deviation of the volumetric flow rate (Q) and following the same process.

$$\pm M = 0.15 \frac{\text{mL}}{\text{min}} * \frac{1\text{L}}{1000 \text{ mL}} * 0.034 \frac{\text{mol}}{\text{L}} * \frac{1\text{min}}{60 \text{ sec}} * \frac{10^6 \mu\text{mol}}{1\text{mol}} = \pm 0.08 \frac{\mu\text{mol}}{\text{s}} \quad (61)$$

$$\pm J_{\text{CO}_2} = \frac{\pm 0.08 \frac{\mu\text{mol}}{\text{s}}}{3.56 \times 10^{-1} \text{ m}^2} = \pm 0.2 \frac{\mu\text{mol}}{\text{m}^2 * \text{s}} \quad (62)$$

11.3 Percent CO₂ to CO₂ Flux (Gradient Analysis)

Sample calculation from test 2, imposed flux $10.7 \pm 0.2 \mu\text{mol}/\text{m}^2/\text{s}$, CGM sampling event #1:

Concentration of CO₂ is first converted to parts per million (ppm) and a dimensionless volume/volume quantity (CO₂').

$$\text{CO}_2(\text{ppm}) = \frac{10,000\text{ppm}}{1\%} * \% \text{CO}_2 \quad (63)$$

$$\text{CO}_2(\text{ppm}) = \frac{10,000\text{ppm}}{1\%} * 0.76\% = 7600 \text{ ppm} \quad (64)$$

$$\text{CO}_2' = \frac{7600 \text{ m}^3 \text{CO}_2}{10^6 \text{ m}^3 \text{air}} = 7.60 \times 10^{-3} \quad (65)$$

CO₂ concentration is then converted to a mass/volume basis using the Ideal Gas Law, mean temperature (T) and pressure (P) values from the duration of the imposed flux, and the universal gas constant (R).

$$\text{CO}_2 = \text{CO}_2' * \frac{P}{RT} \quad (66)$$

$$\text{CO}_2 = \frac{7.60 \times 10^{-3} \text{m}^3 \text{CO}_2}{\text{m}^3 \text{air}} * \frac{0.83 \text{ atm}}{\frac{8.205 \times 10^{-5} \text{ m}^3 \text{atm}}{\text{mol K}} * 294.7 \text{K}} * \frac{10^6 \mu\text{mol}}{\text{mol}} = 2.61 \times 10^5 \frac{\mu\text{mol}}{\text{m}^3} \quad (67)$$

11.4 Mass CO₂ to Efflux CO₂ (Trap Analysis)

Three aliquots per trap element were analyzed using gravimetric analysis. For each aliquot, percent CO₂ was determined by taking the change in mass before and after hydrochloric acid (HCl) was added to desorb calcium carbonate (CaCO₃):

$$g_{\text{CO}_2(\text{aliquot})} = \text{Initial mass of sorbent} + \text{mass HCl added} - \text{final weight of sorbent} \quad (68)$$

$$\% \text{CO}_2(\text{aliquot}) = \frac{g_{\text{CO}_2(\text{aliquot})}}{\text{total mass aliquot}} \quad (69)$$

The background corrected %CO₂ is calculated by subtracting the %CO₂ of the travel blank from the %CO₂ in the aliquot. Total mass of CO₂ is then calculated by multiplying the corrected %CO₂ by the total sorbent mass:

$$\text{Background corrected \%CO}_2 = \% \text{CO}_2(\text{aliquot}) - \% \text{CO}_2(\text{travel blank}) \quad (70)$$

$$\text{Total g CO}_2 \text{ for trap element} = \text{Background corrected \%CO}_2 * \text{Dry mass total sorbent} \quad (71)$$

Efflux of CO₂ (J_{CO₂}) is calculated by dividing the total mass of CO₂ captured by the trap element by the deployment duration (t) and cross-sectional area (A) of the CO₂ Trap.

$$J_{\text{CO}_2} = \text{Total g CO}_2 * \frac{\text{mol CO}_2}{\text{g CO}_2} * \frac{10^6 \mu\text{mol}}{\text{mol}} * \frac{1}{\text{t}} * \frac{1}{\text{A}} \quad (72)$$

Sample calculations are from test 2, imposed flux 10.7 ± 0.2 μmol/m²/s, trap A, bottom sorbent element:

$$g_{\text{CO}_2} = 121.11\text{g} + 42.12\text{g} - 162.87\text{g} = 0.36\text{g} \quad (73)$$

$$\%CO_2(\text{aliquot}) = \frac{0.36 \text{ g } CO_2}{5.03 \text{ g sample}} * 100 = 6.98\% \quad (74)$$

$$\text{Background corrected } \%CO_2 = 6.98\% - 2.26\% = 4.72\% \quad (75)$$

$$\text{Total g } CO_2 \text{ in trap element} = 4.72\% * 45.93 \text{ g} = 2.17\text{g} \quad (76)$$

$$J_{CO_2} = 2.17\text{g} * \frac{\text{mol } CO_2}{44 \text{ g}} * \frac{1}{7.75 \text{ days}} * \frac{1}{8.11 * 10^{-3} \text{ m}^2} = 9.07 \frac{\mu\text{mol}}{\text{m}^2 * \text{s}} \quad (77)$$

The mass flux can be converted to a volumetric flux using the molecular weight (MW) and density (ρ) of a representative hydrocarbon.

$$J_{\text{hydrocarbon}} = J_{CO_2} * \frac{MW_{\text{hydrocarbon}}}{\rho_{\text{hydrocarbon}}} \quad (78)$$

Using Eqn 72 and decane as the representative hydrocarbon, the following volumetric loss rate is obtained:

$$J_{\text{decane}} = 9.07 \frac{\mu\text{mol}}{\text{m}^2 * \text{s}} * 142.3 \frac{\text{g}}{\text{mol}} * \frac{\text{mol}}{10^6 \mu\text{mol}} * \frac{\text{m}^3}{730 \text{ kg}} * \frac{\text{gal}}{3.785 * 10^{-3} \text{ m}^3} * \frac{\text{kg}}{1000 \text{ g}} \quad (79)$$

$$* \frac{\text{m}^2}{2.47 * 10^{-4} \text{ acre}} * \frac{3.156 * 10^7 \text{ s}}{\text{yr}}$$

$$J_{\text{decane}} = 5965 \frac{\text{gal}}{\text{acre} * \text{yr}} \quad (80)$$

12. APPENDIX E: STATISTICS

12.1 Confidence Intervals for Individual Methods vs Ideal Line (1:1)

Table 29. Confidence intervals (CI) for individual methods based on best fit linear regression of average values.

Method	Sample Size	Factor	Lower CI	Upper CI	Significantly different from 1:1 line (slope=1, intercept=0)?	Conclusion
Gradient (Millington)	4	Slope	0.810	1.043	No	Not significantly different from 1:1 line
	4	Intercept	-1.768	0.607	No	
Gradient (In-situ)	4	Slope	0.591	0.762	Yes	Significantly different from 1:1 line
	4	Intercept	-1.281	0.459	No	
Chamber (linear)	4	Slope	1.005	1.251	Yes	Significantly different from 1:1 line
	4	Intercept	-2.573	-0.059	Yes	
Chamber (exponential)	4	Slope	1.141	1.438	Yes	Significantly different from 1:1 line
	4	Intercept	-3.055	-0.022	Yes	
Trap	4	Slope	0.678	1.431	No	Not significantly different from 1:1 line
	4	Intercept	-4.488	3.192	No	

12.2 Method Comparison ANOVA Results

An ANOVA F-test was run on the average values for each method to determine if there were significant differences between the slopes of all methods. The P-value was 3.686×10^{-5} , indicating that there is a statistically significant difference among the slopes at a 95% confidence level.

The results of pairwise ANOVA testing between each individual method are summarized in Table 30. P-values less than 0.05 indicate there is a statistically significant difference between slopes of the methods. P-values greater than 0.05 indicate there is no statistically significant difference between slopes of the methods being compared. Interactions where no significant differences exist are indicated in bold.

Table 30. P-values for pairwise comparison of slopes between individual methods. Interactions where no significant differences exist are indicated in bold.

	Gradient: Millington	Gradient: In- Situ	Chamber: Linear	Chamber: Exponential	Traps
Gradient: Millington	-	3.504×10^{-3}	1.188×10^{-2}	2.488×10^{-4}	8.031×10^{-2}
Gradient: In-Situ	3.504×10^{-3}	-	4.298×10^{-5}	2.938×10^{-6}	1.870×10^{-4}
Chamber: Linear	1.188×10^{-2}	4.298×10^{-5}	-	3.484×10^{-2}	2.981×10^{-1}
Chamber: Exponential	2.488×10^{-4}	2.938×10^{-6}	3.484×10^{-2}	-	5.466×10^{-3}
Traps	8.031×10^{-2}	1.870×10^{-4}	2.981×10^{-1}	5.466×10^{-3}	-